Adaptive Beamforming and Autocalibration for Swath Sonars

Tor Inge Birkenes Lønmo

Thesis submitted for the degree of Philosophiae Doctor

Series of dissertations submitted to the
Faculty of Mathematics and Natural Sciences, University of Oslo
No. 2243

ISSN 1501-7710

Cover: Hanne Baadsgaard Utigard.
Print production: Reprosentralen, University of Oslo.

Preface

This thesis has been submitted to the Faculty of Mathematics and Natural Sciences at the University of Oslo as a part of the requirements for the degree Philosophiae Doctor (Ph.D.). The work was carried out at the Digital Signal Processing and Image Analysis group at the Department of Informatics, University of Oslo. During 2016 I was fortunate enough to stay 6 months at the Center for Coastal and Ocean Mapping/Joint Hydrographic Center, which is part of the University of New Hampshire. This work has been supervised by Professor Andreas Austeng and Adjunct Professor Roy Edgar Hansen. This thesis has been funded by Kongsberg Maritime AS and the Norwegian Research Council (Project 241275).

Acknowledgment

I would like to start by thanking my supervisors Professor Andreas Austeng, Adjunct Associate Professor Roy Edgar Hansen, and Dr. Ing. Frank Tichy. Their support has made this work possible. Andreas has been a source of motivation and patience. His guidance has helped me through many challenges. My meetings with Roy and Andreas have been thought-provoking, educational, and never dull. Their review of my work has greatly enhanced my learning and the resulting quality. I really appreciate the work we have done together and the support I have received to navigate the academic world.

Kongsberg Maritime AS including colleagues in Horten and around the world have been an essential part of this thesis. It has been a privilege to work, travel, and learn with their support. Their long experience has kick-started my project, enabled the essential data collection, and provided much constructive feedback. In addition, their contacts have enabled valuable opportunities. Special thanks to Bente Borgundvåg Berg, for always being exceptionally helpful.

I express my gratitude to everyone at the Center of Coastal and Ocean Mapping (CCOM) at the University of New Hampshire for making my stay enjoyable and extremely valuable. I particularly thank Anthony Lyons, John Hughes Clarke, Tom Weber, Glen Rice, Giuseppe Masetti, and Val Schmidt.

I thank the Digital Signal Processing and Image Analysis (DSB) group which I have been a part of for a pleasant and supportive working environment. I thank my family for the support through the last five years. Special thanks to my wife Nina. Your love and enthusiastic support has made this possible and much more enjoyable.

Abstract

Accurate knowledge of the seabed is of vital importance for many human endeavors. Applications range from safe navigation to climate change models. Swath sonars are a key tool for efficient and high-resolution mapping of the seabed. This thesis aims to improve the quality of swath sonars by improving the beamformer, which is a key part of current signal processing. We explore two methods: Adaptive beamforming and autocalibration.

Adaptive beamforming improves the beamforming process by adapting the beamforming to the received signal. We investigate how the adaptive Capon and Low Complexity Adaptive (LCA) beamformers can improve swath sonar beamforming on both simulated and field data, and their effect on the water column image and bathymetry. The Capon beamformer is well-tested and can give high performance, but has a high computational load and may have robustness issues. LCA is a recently developed and related adaptive beamformer which may be more robust and faster, with similar performance in many ways.

We find that both beamformers improve resolution, edge definition and sidelobe level in the water column, and give more accurate amplitude detections. This leads to better defined features, better separation of features from the background, and sometimes detection of features not visible with the conventional delay and sum (DAS) beamformer. Capon has better resolution, somewhat better edge definition, and somewhat higher sidelobe level than LCA. We also find that an adaptive beamformer may improve interference rejection for phase detection, but generally reduces accuracy in the current configuration. This seems to be a side effect of the improved edge definition, and the effect can be reduced by reconfiguring the beamformers.

Autocalibration estimates calibration errors without external reference sources. The errors, which particularly limit the sidelobe level, may then be compensated for. We model the errors by a complex factor per element and estimate them using data available during normal surveys. The method is based on the Generalized Interferometric Array Response. On simulated data, we are able to lower the sidelobe level below 50 dB. On field data, the sidelobe level is generally reduced, but the effect is much smaller. However, some sidelobes are unchanged and new sidelobes occasionally appear. We suggest that the reduced performance in the field is due to an insufficient calibration model.

List of included publications

Paper I Lønmo, T. I. B., Austeng, A., & Hansen, R. E. (2015b). Low Complexity Adaptive Beamforming Applied to Sonar Imaging (Invited). In J. S. Papadakis & L. Bjørnø (Eds.), *Proceedings of the 3rd International Conference and Exhibition on Underwater Acoustics* (pp. 653–658). Crete, Greece. url: http://www.uaconferences.org/docs/Past_proceedings/UACE2015_Proceedings.pdf

Paper II Lønmo, T. I. B., Austeng, A., & Hansen, R. E. (2015a). Interference rejection by Low Complexity Adaptive Beamforming. In *Proceedings of the Institute of Acoustics* (Vol. 37). Institute of Acoustics, Bath, United Kingdom. url: http://www.proceedings.com/27961.html

Paper III Lønmo, T. I. B., Austeng, A., & Hansen, R. E. (2019b). Improving Swath Sonar Water Column Imagery and Bathymetry with Adaptive Beamforming. *IEEE Journal of Oceanic Engineering*. Early access. doi:10.1109/JOE.2019.2926863

Paper IV Lønmo, T. I. B., Austeng, A., & Hansen, R. E. (2019c). On Interferometric Phase Detections for Swath Sonars with Adaptive Beamformers. *IEEE Journal of Oceanic Engineering*, in review, submitted October 31st.

Paper V Lønmo, T. I. B., Austeng, A., & Hansen, R. E. (2019a). Data Driven Autocalibration for Swath Sonars. *IEEE Journal of Oceanic Engineering*, in review, comments received November 1st.

Related work

Paper VI Lønmo, T. I. B., & Lyons, A. (2016). Effect of low complexity adaptive beamforming on seafloor backscatter statistics. In *The Journal of the Acoustical Society of America* (Vol. 140, p. 3287). Presented at the 172nd Meeting of the Acoustical Society of America. doi:10.1121/1.4970447

Paper VII Lønmo, T. I. B., & Weber, T. C. (2017). Improving seep detection by swath sonars with adaptive beamforming. In *The Journal of the Acoustical Society of America* (Vol. 141, p. 4005). Presented at 173rd Meeting of the Acoustical Society of America. doi:10.1121/1.4989190

Paper VIII Blachet, A., Lønmo, T. I. B., Austeng, A., Prieur, F., Hunter, A. J., & Hansen, R. E. (2017). Sonar data simulation with application to multi-beam echo sounders. In *Proceedings of 4th Underwater Acoustics Conference and Exhibition*, Skiathos, Greece. url: http://www.uaconferences.org/index.php/component/contentbuilder/details/9/36/uace2017-sonar-data-simulation-with-application-to-multi-beam-echo-sounders?Itemid=410

Paper IX Lønmo, T. I. B., Austeng, A., & Hansen, R. E. (2017). Phase Detections with Low Complexity Adaptive Beamforming on Swath Sonars. In *2017 Underwater Acoustic Signal Processing Workshop* (p. 16). url: http://www.uasp.org/abstractbooks/uasp2017abstracts.pdf

Contents

Preface iii

Acknowledgement iii

Abstract i

List of included papers iii

1 Introduction 1

1.1 Motivation 1

1.2 Aims & claims 2

2 Background 5

2.1 Fundamentals of swath sonars 5

2.2 Beamforming 7

2.2.1 DAS beamforming 8

2.2.2 Capon beamforming 9

2.2.3 Low Complexity Adaptive beamforming 10

2.2.4 Comparison of beamformer properties 11

2.2.5 Previous use of adaptive signal processing in swath sonars 13

2.3 Bottom detection 14

2.3.1 Amplitude detection 14

2.3.2 Phase detections 15

2.4 Calibration 17

2.5 Swath sonar simulations 19

3 Summary of publications **21**
Paper I 22
Paper II 22
Paper III 23
Paper IV 24
Paper V 25

4 Summary and discussion **27**
4.1 Autocalibrated adaptive beamforming 31

5 Further work **35**

Bibliography **37**

Included publications **45**

Paper I

Lønmo, T. I. B., Austeng, A., & Hansen, R. E. (2015b). Low Complexity Adaptive Beamforming Applied to Sonar Imaging (Invited). In J. S. Papadakis & L. Bjørnø (Eds.), *Proceedings of the 3rd International Conference and Exhibition on Underwater Acoustics* (pp. 653–658). Crete, Greece. url: http://www.uaconferences.org/docs/Past_proceedings/UACE2015_Proceedings.pdf **47**

Paper II

Lønmo, T. I. B., Austeng, A., & Hansen, R. E. (2015a). Interference rejection by Low Complexity Adaptive Beamforming. In *Proceedings of the Institute of Acoustics* (Vol. 37). Institute of Acoustics, Bath, United Kingdom. url: http://www.proceedings.com/27961.html **57**

Paper III

Lønmo, T. I. B., Austeng, A., & Hansen, R. E. (2019b). Improving Swath Sonar Water Column Imagery and Bathymetry with Adaptive Beamforming. *IEEE Journal of Oceanic Engineering*. Early access. doi:10.1109/JOE.2019.2926863 **71**

Paper IV

Lønmo, T. I. B., Austeng, A., & Hansen, R. E. (2019c). On Interferometric Phase Detections for Swath Sonars with Adaptive Beamformers. *IEEE Journal of Oceanic Engineering*, in review, submitted October 31st. **107**

Paper V

Lønmo, T. I. B., Austeng, A., & Hansen, R. E. (2019a). Data Driven Autocalibration for Swath Sonars. *IEEE Journal of Oceanic Engineering*, in review, comments received November 1st. **135**

Chapter 1

Introduction

1.1 Motivation[1]

Accurate knowledge of the seabed is of vital importance for many human endeavors. Historically, the use has sometimes been straightforward, as the creation of maps for safe navigation, sometimes fundamental, like when contributing to the development of plate tectonics. As our influence of the planet and use of the sea expands, the need for accurate maps of the seabed grows. At a local scale, applications include habitat mapping or preparation for building operations. At a global scale seabed maps are used to create ocean circulation models, which are central for modeling the climate.

Currently, under 20 % of the ocean is mapped with modern survey equipment. Global depth maps are based on satellite altimetry, which has much lower resolution than current echosounders. The Nippon Foundation–GEBCO Seabed 2030 Project (Mayer et al., 2018) aims to map the ocean deeper than 200 m with swath sonars within the coming decade. Currently 15 % coverage is achieved (Seabed 2030 Project, 2019). Surveying at a massive scale will be required to cover the rest. Much of this data will be collected by swath sonars, which is a key tool for efficient and high-resolution mapping. Improving the quality of swath sonars is therefore of great interest, both for mapping surveys and for other uses of swath sonars.[2]

One way to improve swath sonars is by improving the swath sonar signal processing, where the delay-and-sum (DAS) beamformer is a core component

[1] The motivation is heavily based on (Mayer et al., 2018; Wölfl et al., 2019).

[2] See Wölfl et al., 2019 for more examples.

(de Moustier, 1988; Lurton, 2010, Ch. 8.3.2). Improvements to the beamformer may improve all swath sonar data products, since they are all derived from the beamformed data. High-resolution alternatives to the DAS beamformer has existed for decades (Krim & Viberg, 1996) and the potential for use on swath sonar has been noted (de Moustier, 1993; Lurton, 2010, Ch. 5.4.9-10). However, they have not been widely used in swath sonars, partially due to high computational load and robustness concerns (Lurton, 2010, Ch. 5.4.10). The continuous improvements in processing power, in addition to the development of new robust and efficient techniques (Synnevåg, Austeng, & Holm, 2011), mitigate these concerns and warrant new attempts.

1.2 Aims & claims

The aim of this thesis is to improve the quality of swath sonar data products through improving the receive beamforming, preferably using methods that are relatively easy to implement. We have approached this in two ways, through adaptive beamformers and calibration. The results have been evaluated on how they affect the bathymetry, since it is the main data product of swath sonars, and the water column image, both since it is useful to explain the bathymetric results and due to its use as a separate data product. We have developed a simulator to do controlled experiments and more easily explore particular cases. We consider a swath sonar operating around 300 kHz, largely due to data availability.

The main emphasis of this thesis is adaptive beamforming, which is treated in **Paper I-IV**. We have studied the relatively new Low Complexity Adaptive (LCA) beamformer, due to its robustness and low computational demands. We also consider the Capon beamformer, since it is well-studied, has high performance, and LCA is strongly related to it.

Paper I examines how the LCA beamformer affects the water column image and bottom detections for a smooth seafloor. It also introduces the use of Field II to simulate swath sonar time series data. We find that LCA appears to reduce the mainlobe width and sidelobe level, and improves most bottom detections. In a similar way, **Paper II** examines the effect of the LCA beamformer for a more complicated scene with a wreck. LCA again appears to reduce the mainlobe width and sidelobe level, both effects improve amplitude detections.

Paper III extends the results with the Capon beamformer, extensive simulations, and further field examples. A key result is that reducing the mainlobe for

DAS causes two effects which are uncoupled with the adaptive beamformers: resolution and edge definition. LCA mainly improves edge definition, while Capon improves both. We show that edge definition is a key property for improving the amplitude detections over large parts of the seafloor. We also find that the improvement in sidelobe level is better for LCA than for Capon, and significantly lower for our field data than for our simulated data.

Paper IV analyzes the effect of the LCA and Capon beamformers on phase detections. Motivated by field examples that indicate lower phase detection accuracy, we use simulations and properties of the adaptive beamformers to understand the effects. We show that an adaptive beamformer may improve phase detection accuracy with interference, but in the configurations from **Paper III** they tend to reduce the accuracy in general. We show indications that better overall performance may be possible with adapted configurations.

Paper V studies a method for autocalibration, motivated by the limited sidelobe level improvements for field data in **Paper III**. We estimate phase and amplitude errors for each element through the coherence based "Generalized Interferometric Array Response" (GIAR) method, and correct for them before the DAS beamformer. This works very well on simulated data and gives some improvements on field data. We find indications that an extended error model may be needed to improve the field results.

Chapter 2 gives a brief background for the methods we use and describes previous work. The included publications are summarized in Chapter 3 and discussed in Chapter 4. Chapter 5 gives suggestions for further work, followed by the included papers.

Chapter 2

Background

This chapter provides background material for the research in this thesis. Parts of the material has been adapted from the included publications. This has been done to make it easier to read the thesis independently of the publications, while keeping the description of the content unified.

2.1 Fundamentals of swath sonars

This section briefly describes the most relevant features of swath sonars for this thesis. See for example Lurton, 2010, Ch 8.3 or de Moustier, 1988, 1993 for a more thorough treatment.

The core of a swath sonar is a linear transmitter array mounted along-track and a linear receiver array mounted across-track on a boat. The transmitter emits sound in a fan which is narrow along-track and wide across-track. This ensonifies a across-track line, or thin strip, as illustrated by Figure 2.1. The receiver separates the reflected sound into different beams, which contain the sound arriving from small across-track angular regions. These beams are then used to estimate the quantities of interest, for example the seafloor depth across the ensonified line. As the boat moves forward a broad strip, typically around four times the water depth (Mayer et al., 2018), is mapped. For full coverage of the seabed the boat continues back and forth in a lawn mower pattern.

A swath sonar provides mainly three data products: Bathymetry, backscatter and the water column image. As mentioned in the introduction, bathymetry has a wide application area (Wölfl et al., 2019). Backscatter has been of growing interest recently (Lamarche & Lurton, 2017), and a key use is to characterize the seabed

Figure 2.1: Illustration of swath sonar transmit sector. The bright sector illustrates region covered by the transmitted sound. The white line across the seafloor illustrates the region of the seafloor which is ensonified and mapped by the echosounder during this transmission. Illustration courtesy of Kongsberg Maritime AS.

type. The water column image is a more recent addition to swath sonars. It is used both for bathymetric quality control and exploring the water column itself (Clarke, 2006, 2017).

Swath sonar signal processing includes many steps (Lurton, 2010, Ch. 8.3.2). The most important ones for this thesis are shown in Figure 2.2. Since this thesis focuses on the beamformer, we have ensured that our processing chain includes the processing steps important for comparing beamformers. We ignore many factors that are less important when comparing beamformers but need to be accounted for in active swath sonars, like the sound speed profile and vessel motion (Clarke, 2003; Hare, 1995). In addition, we mostly ignore advanced features like beam stabilization and multi-sector transmission.

As stated in Section 1.2 we have considered swath sonars based around 300 kHz. The theory presented below is in principle unchanged if frequency, array size and related parameters are scaled correspondingly, so the results should in principle also apply for swath sonars at other frequencies. However, differences in noise or other characteristics may require adaptions.

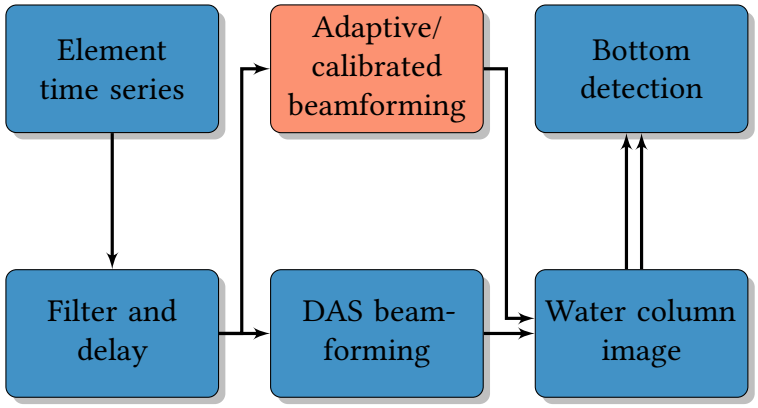

Figure 2.2: Overview standard and modified processing chain. We replace the DAS beamformer with either an adaptive beamformer or a calibrated DAS beamformer. The alternative beamformers use the same data as the DAS beamformer, and the results from each beamformer are processed in the same way. This ensures that differences can be attributed to the beamformers. Figure adapted from **Paper III**.

2.2 Beamforming

The main task of the beamformer is to enhance a signal from an angle of interest, the steering angle, compared to everything else. It is useful to divide "everything

else" into interference, signals from other directions, and noise. This is conventionally done by the DAS beamformer. It is fast, robust, and easily adaptable to different systems and situations. It is also optimal for some situations. However, a trade-off between desired qualities must be made to provide decent performance across all cases.

Adaptive beamformers essentially use the received signal to find an (supposedly) optimal configuration for each situation. When it works well, this avoid DAS's trade-off and improve performance. However, adaptive beamformers may be less robust and degrade performance if the situation is not well known or estimated. Through this thesis we have tried to exploit the advantages and limit the problems, and evaluated the results.

We use two adaptive beamformers: The Capon and the Low Complexity Adaptive (LCA) beamformer. The essentials of these and DAS are described below. The effect of calibration errors on the beamformers is further described in Section 2.4.

2.2.1 DAS beamforming

"DAS beamforming algorithmically steers the array by delaying the signal from each element such that the signal from the steering direction (far field) or point (near field) add coherently, while others sum incoherently. The delays may be approximated by phase rotation for narrow band signals and small enough steering angles (Johnson & Dudgeon, 1993). The DAS beamformer is typically weighted (also called shaded or tapered) to better suppress interfering signals by lowering the sidelobe level. This reduces resolution and edge definition due to a wider mainlobe (Harris, 1978). The resulting beam time series $b^{(\theta)}(t)$ steered toward the angle θ is given by

$$b^{(\theta)}(t) = \mathbf{w}^H \mathbf{s}^{(\theta)}(t) = \begin{bmatrix} w_1 \\ w_2 \\ \vdots \\ w_{N_{\text{El}}} \end{bmatrix}^H \begin{bmatrix} s_1^{(\theta)}(t) \\ s_2^{(\theta)}(t) \\ \vdots \\ s_{N_{\text{El}}}^{(\theta)}(t) \end{bmatrix}, \tag{2.1}$$

where N_{El} is the number of elements, w_i is the weight for element i and $s_i^{(\theta)}$ is the signal from element i at time t, after it has been delayed toward θ, and $\bullet^H$ indicates the complex conjugate transpose. The steering angle θ is 0 toward nadir

and is equal to the incidence angle for a horizontal seafloor. DAS's advantages are speed, simplicity and robustness.

Paper III, slightly adapted.

We have used a several differently weighted DAS beamformers in our research. Most weights are from the Kaiser class (Harris, 1978), where the β parameter controls the sidelobe-mainlobe trade-off. The weights are uniform when $\beta = 0$, increasing β widens the mainlobe and lowers the sidelobes and the white noise gain (WNG).

2.2.2 Capon beamforming

The adaptive Capon beamformer (Van Trees, 2002, Ch. 6; Krim & Viberg, 1996) is known for having better resolution and interference rejection capabilities than the standard DAS beamformer. The key difference between an adaptive beamformer as Capon, and DAS is that the weights $\mathbf{w}^{(\theta)}_{Capon}(t)$ now depend on the received signal. This allows for enhanced performance by dynamically adjusting the beampattern to the present signal conditions.

Capon selects the weights by minimizing the variance of the beamformed signal without distorting signals from the steering direction. For pre-delayed signals this can be expressed as:

$$\mathbf{w}^{(\theta)}_{Capon}(t) = \arg\min_{\mathbf{w}} E\left|\mathbf{w}^H \mathbf{s}^{(\theta)}(t)\right|^2 \tag{2.2}$$

$$= \arg\min_{\mathbf{w}} \mathbf{w}^H R^{(\theta)}(t)\mathbf{w}, \tag{2.3}$$

$$\text{under the constraint that } \sum_{i=1}^{N_{\text{El}}} w_i = 1, \tag{2.4}$$

where $R^{(\theta)}(t) = E\left(\mathbf{s}^{(\theta)}(t)\mathbf{s}^{(\theta)}(t)^H\right)$ is the steered covariance matrix (Krolik & Swingler, 1989). The beam time series can then be obtained by (2.1).

Capon's main drawbacks compared to DAS are potentially lower robustness (Cox, Zeskind, & Owen, 1987) and higher computational demands (Lurton, 2010, Ch. 5.4.10). The main sources of the robustness problems are signal model mismatch and difficulties with estimating the covariance matrix R.

To ensure sufficient robustness we use spatial smoothing (Lo, 2004; Shan, Wax, & Kailath, 1985; Synnevåg, Austeng, & Holm, 2009) over $N_{\text{El}}/2$ elements,

forward-backward averaging (Lo, 2004; Rao & Hari, 1990; Rønhovde, Yang, Taxt, & Holm, 1999) and diagonal loading (Carlson, 1988; Cox, 1973) equal to 5 % of the mean signal energy. The signal statistics may change quickly for our case, so we do not use time averaging (Llort-Pujol, Sintes, Chonavel, Morrison, & Daniel, 2012; Rønhovde et al., 1999). Based on earlier work (Austeng et al., 2008; Buskenes, Hansen, & Austeng, 2017; Synnevåg, Austeng, & Holm, 2007) we consider this to be a relatively robust set of parameters that will work well for our application.

Paper III, slightly adapted.

2.2.3 Low Complexity Adaptive beamforming

LCA (Buskenes et al., 2017; Synnevåg et al., 2011) is a relatively new adaptive beamformer, first used in medical ultrasound. With a small weight set, LCA can give a large part of the improvement from Capon without important drawbacks (Buskenes et al., 2017; Synnevåg et al., 2011). It can be viewed as a hybrid between Capon and DAS. LCA, as Capon, minimizes the variance and obeys the distortionless constraint. The difference is that while Capon can select almost any weight, LCA is restricted to a pre-selected weight set $\mathcal{W} = \{\mathbf{w}^1, \mathbf{w}^2, \ldots, \mathbf{w}^{N_{\text{LCA}}}\}$, where N_{LCA} is the number of weights in the set. LCA beamforming may also be interpreted as selecting the apparently best beam value from differently weighted DAS beamformers according to the Capon optimality criteria.

The LCA weight set contains standard DAS weights and *microsteered* (Synnevåg et al., 2011) weights. Microsteered weights mimic certain asymmetric beampatterns used by the Capon beamformer, which particularly improves the edge definition (Synnevåg et al., 2011). Microsteering requires that small, additional, delays are applied after beam steering. We apply them by phase rotation.

The pre-selected weight set makes LCA inherently more robust than Capon. As an example, the limited weight set prevents signal cancellation (Synnevåg et al., 2011), which is potentially detrimental for Capon (Van Trees, 2002). This reduces the need for additional constraints on LCA (Synnevåg et al., 2011). In this paper we use LCA without any of the modifications applied to Capon. The LCA weight is selected by:

$$\hat{\mathbf{w}}_{LCA}^{(\theta)}(t) = \underset{\mathbf{w}\in\mathcal{W}}{\arg\min} \left|\mathbf{w}^H \mathbf{s}^{(\theta)}(t)\right|^2. \tag{2.5}$$

Paper III

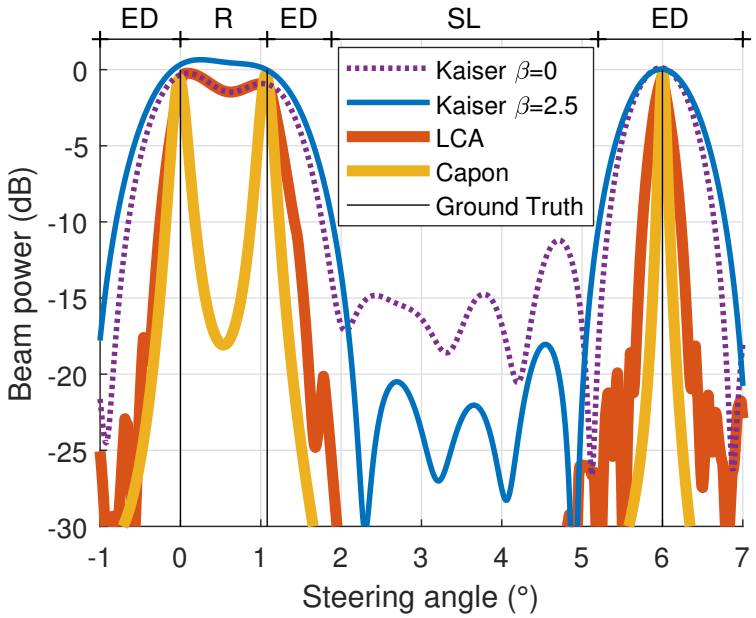

Figure 2.3: Beamformer steered response for a simplified scenario with 3 equal strength sources and 10 dB SNR. The text above indicates which beamformer property that is most important in each region. R: Resolution, ED: Edge Definition, SL: Sidelobe Level. Figure from **Paper III**.

LCA's performance naturally depends on the weight set in use. Our preferred variant has evolved during this thesis. The included publications describe the weight set used in each case.

2.2.4 Comparison of beamformer properties

Paper III introduced three properties central for our analysis of beamformer performance: Resolution, edge definition and sidelobe level. This section describes the properties and how the beamformers affect them.

> Figure 2.3 shows how the DAS, LCA and Capon beamformers work in a simplified case with three equal strength sources and 10 dB SNR. There are one isolated and two closely spaced sources, their directions are shown by the black vertical lines.
>
> Resolution is the ability to separate closely spaced sources. It is illustrated by the region marked "R" in Figure 2.3. Capon easily resolves the two points, Kaiser

$\beta = 0$ DAS and LCA barely resolve the points, while Kaiser $\beta = 2.5$ DAS does not resolve them.

Edge definition describes the steepness of the steered response at the sides of an isolated point or object. For the DAS beamformer, resolution and edge definition are both determined by the mainlobe width. For adaptive beamformers, the two concepts are uncoupled, as the regions marked "ED" in Figure 2.3 show. We see that although LCA has the same resolution as the best-case ($\beta = 0$) DAS, the edge definition is almost as good as Capon's.

A convenient way to describe the edge definition and resolution improvements is that the adaptive beamformers reduce the *effective beamwidth*. For our purposes the effective beamwidth has essentially the same role for the adaptive beamformers as the beamwidth for DAS, for example in determining amplitude detection accuracy. It is important to note that the effective beamwidth varies across the scene.

Sidelobe level describes how strongly the beamformer suppresses signals from directions different from the steering direction and is illustrated in the sidelobe region marked "SL" in Figure 2.3. The sidelobe level of the weighted ($\beta = 2.5$) DAS beamformer is lower than the unweighted ($\beta = 0$), illustrating the trade-off with DAS weighting. The adaptive beamformers have much lower sidelobe levels than both DAS beamformers, in addition to the edge definition and resolution improvements described above.

Real transducers have errors which make the actual signal model different from the one presented earlier. This affects the beamformers, and properties above, to a different degree. For DAS, the mainlobe is very robust against such errors, while the sidelobes are more sensitive (Steinberg, 1976, Ch. 13). In practice, model mismatch effectively limits the lowest attainable sidelobe level.

LCA selects one of a set of DAS beamformers, therefore LCA's sensitivity is linked to DAS's. Resolution and edge definition improvements are linked to the mainlobe of the underlying DAS beamformers, and should therefore be less sensitive to model mismatch than the sidelobe level. Model mismatch can be detrimental for the Capon beamformer if not properly accounted for (Cox, 1973; J. Li, Stoica, & Wang, 2003).

As this example shows, adaptive beamformers may avoid the trade-off inherent to DAS and may improve all properties simultaneously.

Paper III

2.2.5 Previous use of adaptive signal processing in swath sonars

Using adaptive beamforming for swath sonars is not a new idea, however computational constraints and robustness concerns have prevented adoption until now (Lurton, 2010, Ch. 5.4.9-10). Below I briefly describe some earlier efforts in more detail, and how they compare to our work.

Alexandrou and de Moustier (1988) discuss an adaptive noise canceling method that removes some sidelobes in their experiments. The method requires additional post processing of the beams after identifying which beams are causing the sidelobe interference. This identification is challenging, and the method is also complicated to initialize. The method also does not affect resolution or edge definition, which our selected methods may do.

Pantzartzis, de Moustier, and Alexandrou (1993) and Rønhovde et al. (1999) consider various adaptive methods and the results indicate that they may achieve improved performance. However, the Capon beamformer is barely covered and the range of examples is sparse.

Llort-Pujol et al. (Llort-Pujol, 2007; Llort-Pujol et al., 2012; Llort-Pujol, Sintes, & Lurton, 2005, 2008) mainly focused on MUSIC and advanced phase detection methods. They also considered the Capon beamformer, but did not achieve satisfactory performance with realistic data (Llort-Pujol, 2007, Ch. C.4.2).

Mitchley and Sears (2014) consider the use of Capon and other high-resolution methods for swath sonars, targeted toward mining applications. They compare a wide range of methods for estimating the covariance matrix, and how the high-resolution methods improve the ability to resolve a simulated sinusoidal seafloor with large amplitude waves. However, they do not consider phase detections, even at high angles, or validate the results on field data. Amplitude detection accuracy is averaged over the whole seafloor, not viewed as a function over angle.

None of the works described above appear to utilize diagonal loading when using Capon. This is a significant omission since diagonal loading may greatly improve the performance of the Capon beamformer, especially with few samples in the covariance matrix estimate (Van Trees, 2002, Ch. 7.3.3). An examination of a properly configured Capon beamformer for swath sonar, and its effect on the water column image and the commonly used bottom detectors therefore seem to be missing from the literature. In addition, LCA has not been considered for swath sonar. The robustness and lower computational demand may make it an attractive alternative, and therefore interesting to consider.

2.3 Bottom detection

Bottom detectors transform the beamformed data to bathymetry This can be done in many ways (Lurton, 2010, Ch. 8.3.3). Here I describe the most relevant details of the two most common methods, which are the ones we have used. This is the amplitude detector, which essentially estimates the instant with strongest echo for each beam, and the phase detector, which estimates the arrival angle for each instant.

The detectors have different strengths and weaknesses, and together provide accurate bathymetry across the swath. The following segment from **Paper III** describes how they typically are used.

> Commonly, amplitude detections are used near specular directions and phase detections are used at higher incidence angles. Amplitude detections are also used when the phase detector fails. For example, if there are multiple targets at the same slant range, either within the beam or in a sidelobe that is not sufficiently suppressed.
>
> The location of the transition angle, where the system switches between phase and amplitude detections, varies depending on system, signal-to-noise ratio (SNR), scene, detector configuration and transition criteria (Hare, Godin, & Mayer, 1995; Llort-Pujol et al., 2012; Lurton & Augustin, 2010). It may be as low as $\pm 10^\circ$ (Clarke, 2018), or as high as 45° (Lurton & Augustin, 2010).
>
> ***Paper III***

2.3.1 Amplitude detection

We have used two amplitude detection methods through our work. **Paper I** and **Paper II** use the maximum amplitude detection method (Lurton & Augustin, 2010, Ch. 8.3.3), while **Paper III** uses a center of gravity (barycenter) detector. This section describes the latter method.

> The barycenter detector is based on the envelope between the -10 dB points around the peak (Lurton & Augustin, 2010), and use a Hamming (Harris, 1978) shaped averaging filter with same length as the transmitted pulse for selecting the -10 dB points.
>
> For a given swath sonar configuration, the amplitude detection accuracy is determined by the envelope length after processing (Lurton & Augustin, 2010).

The envelope length is determined by effective pulse length, beamwidth and seabed geometry (Lurton, 2010, Ch. 8.3.3.2). The typical regimes for a flat seafloor are illustrated in Figure 2.4. A reduced beamwidth improves amplitude detections, especially at high incidence angles.

Low sidelobe levels are important to avoid false detections with the amplitude detector, which may happen when an echo in a sidelobe is stronger than the seafloor echo. Typical cases where this may be a problem is for strong specular echoes or with large differences in scattering strength across the seafloor (Lurton, 2010, Ch. 8.3.3).

Paper III, slightly adapted.

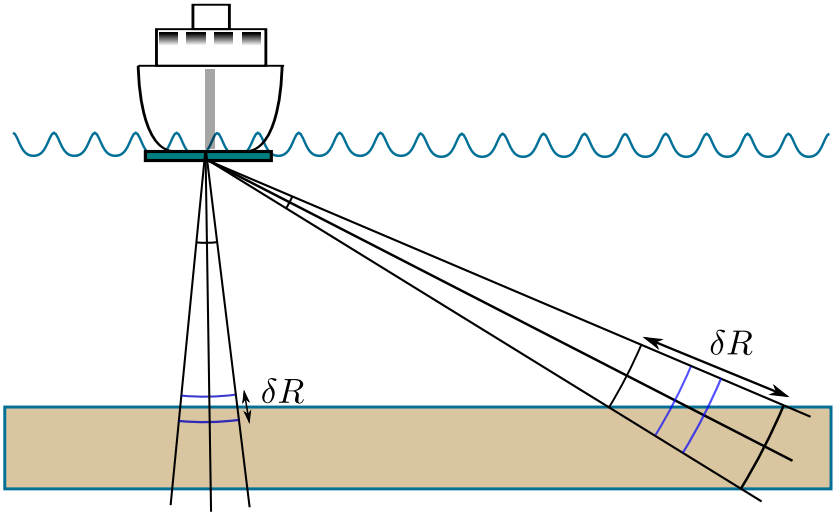

Figure 2.4: Illustration of pulse- (left) and beam-determined (right) regimes for received envelope length (not to scale). Blue arcs show the effective edges of the pulse (after processing) at a given instant, δR shows the distance corresponding to the received envelope length. At vertical incidence the whole beamwidth is illuminated approximately simultaneously, and the pulse length determines δR. At high incidence angles the pulse length is short compared to the footprint, and the time needed for the pulse to travel across the beam footprint determines δR. Figure from **Paper III**.

2.3.2 Phase detections

There exist multiple variants of phase detections. For swath sonars, they rely on the phase difference between the beamformed signals on two subarrays of the

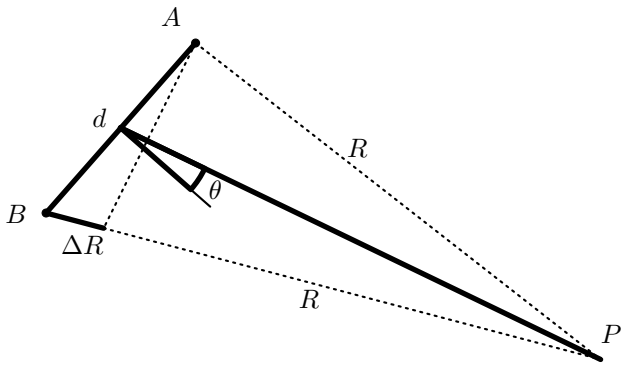

Figure 2.5: Sketch of phase detection geometry. A and B are the receiver locations with baseline d. P is the signal location with distance R from A and angle θ relative to the interferometer normal. ΔR is the range difference between P and B and P and A. For swath sonars A and B represent the centers of two subarrays of the receiving array. For far field signals ΔR is approximated by $d \sin\theta$. Figure from **Paper IV**.

receiving array (Lurton & Augustin, 2010).

> This phase difference indicates the difference in arrival time between two receivers for a narrowband signal (Lurton, 2010, Ch. 5.4.8). Based on a known receiver geometry, like in Figure 2.5, the delay can be related to a range difference, and therefore arrival angle. When the signal originates from the far field, the phase difference $\Delta\Phi$ is related to the arrival angle θ by $\Delta\Phi = 2\pi\Delta R/\lambda \approx 2\pi d \sin\theta/\lambda$, where λ is the wavelength.
>
> ***Paper IV***, slightly adapted.

The phase difference can be used for bottom detection in multiple ways Lurton, 2010; Schmidt, Weber, and Lurton, 2014. In **Paper IV** we focus on properties of the underlying phase difference instead of focusing on any particular method, mainly because this is necessary to understand the observed effects. The following segment from **Paper IV** describes the important factors for good phase detections and relates them to the beamformers.

> Regardless of method there are three central factors for determining the detection accuracy Lurton and Augustin, 2010: Phase ramp steepness, phase difference variance $\sigma^2_{\Delta\Phi}$ and the number of samples used for the detection. The number of samples scale the variance for a single sample detection, so it is

not relevant when comparing beamformers. In Section 3.2 we show that the steepness of the phase ramp is independent of the beamformer under fairly general conditions. The key for comparing beamformer effect on phase detections is therefore to understand how they affect $\sigma^2_{\Delta\Phi}$.

Without interference, the phase difference variance $\sigma^2_{\Delta\Phi}$ basically depend on SNR Lurton and Augustin, 2010. The relation is approximately

$$\sigma^2_{\Delta\Phi} = \frac{2.5712 + \ln \mathrm{SNR}}{\mathrm{SNR}}, \tag{2.6}$$

where SNR is the power-SNR measured at the interferometer input Lurton and Augustin, 2010.

We have implicitly assumed a single dominating signal in the description above. However, strong interference can corrupt the phase difference. Either by increasing the variance such that the detections become unusable, or by dominating the phase difference such that detections are misplaced Lurton and Augustin, 2010; Pereira and Clarke, 2015. Subarray beamforming is supposed to prevent this Lurton, 2010, Ch. 8.3.3.3.

This means that the beamformer has two, partially conflicting, tasks: Maximizing the SNR and minimizing interference. In current swath sonars this is generally done by the DAS beamformer Lurton, 2010, Ch 8.3.2. If another beamformer can do this better, phase detections should improve.

Paper IV

2.4 Calibration

Calibration means to estimate and compensate for differences between the ideal and actual signal model, to improve performance. Through our research we found indications that performance may be limited by such effects. We therefore developed and tested a calibration procedure. The following segment describes why calibration may be necessary, consequences and benefits, and possible alternatives.

The sidelobe level of the DAS beamformer can be set almost arbitrarily low by weighting the beamformer (Harris, 1978). In practice, it is limited. The achieved sidelobe level for swath sonars is typically no lower than 25 to 30 dB (Clarke, 2006; Lurton, 2010, Ch. 5.4.6.3). This limit is caused by errors like element displacement,

amplitude and phase mismatch, mutual coupling and non-linearities (Litva & Lo, 1996, Ch. 4.1; Steinberg, 1976, Ch. 13; Butler & Sherman, 2016, Ch. 7, 12; Krim & Viberg, 1996; Viberg, Lanne, & Lundgren, 2009). To achieve lower levels, calibration is necessary.

Calibration may also be helpful for using adaptive beamformers with swath sonars, as the adaptive beamformers are more sensitive to calibration errors (Krim & Viberg, 1996; Lønmo et al., 2019b; Van Trees, 2002, Ch 6.6). We have recently shown that adaptive beamformers may improve swath sonar performance (Lønmo et al., 2015a, 2015b, 2019b), and calibration may increase that benefit (Lønmo et al., 2019b).

Most swath sonar calibration methods are targeted at system parameters like mounting angles and beampattern. The patch test handles integration and mounting parameters (Clarke, 2003; Guériot, Chèdru, Daniel, & Maillard, 2000). Other methods are used to measure the overall beampattern and calibrate the backscatter level (Foote et al., 2005; Lamarche & Lurton, 2017). Although important for their purposes, the corrections are applied after beamforming. Since sidelobes are determined in the beamforming step, such calibration methods cannot improve the sidelobe level. Other calibration methods are therefore needed.

There exist a range of possible methods for element calibration (Krim & Viberg, 1996; Y. Li & Er, 2006; Qiong, Long, & Zhongfu, 2003; Van Trees, 2002, Ch. 8.11), with variable assumptions and error models. In principle, calibration could be performed routinely in a tank. On the other hand, tank calibration would not account for changed calibration values due to changes in the local environment, for example acoustical interference from the ship-mount (Lanzoni & Weber, 2012) or changed material properties due temperature or pressure (Butler & Sherman, 2016, Ch. 2.9 and 5; Lurton & Lamarche, 2015, Ch. 4.2.2). Calibration values for backscatter may drift over time (Lurton & Lamarche, 2015, Ch. 5.2), so the same may be expected for element calibration. Environmental effects are also not included if calibrating via internal reference signals (Pocwiardowski, Yufit, Maillard, & Eriksen, 2006). A field calibration method which includes the whole system is therefore desirable, preferably a method without the need for additional equipment like reference sources.

Calibration without known source locations is known as autocalibration or self-calibration (Viberg et al., 2009, Ch. 3). Autocalibration exists for general arrays (Qiong et al., 2003; Viberg et al., 2009, Ch. 3.4; Van Trees, 2002, Ch. 8.11.5) or for particular applications (Cervenka, 2015; Farquharson, Lopez-Dekker, &

Frasier, 2013; Ng, Er, & Kot, 1994).

Paper V, slightly adapted.

We chose to autocalibrate with a method based on the Generalized Interferometric Array Response (GIAR) for two reasons. Firstly, because it is the directly proposed for swath sonars Cervenka, 2015, with Cervenka outlined how GIAR could be used for autocalibration, with an example indicating meaningful results. Secondly, because it seemed like the theoretically best suited method among the ones we reviewed. We estimated a complex calibration value per channel, as done in Cervenka, 2015. A detailed description of GIAR and our calibration method can be found in **Paper V**. Below, I briefly comment on the choice of method.

The typical received signal for swath sonar is different from many related applications, which appeared to invalidate many calibration techniques. One example is that the assumption behind shear-averaging autofocus used in synthetic aperture sonar break down if a strong target is present Callow, 2003, Ch. 7.7.1. Another example is that some phase aberration techniques from medical ultrasound require signals from a limited angular region, enabled by focused transmission Flax and O'Donnell, 1988. Neither of these methods are well suited for a swath sonar where the signal is typically dominated by two strong signals which are widely spaced in angle and have limited angular extent. In contrast, the GIAR method essentially look for samples dominated by a point-like signal from the steering direction. Since GIAR usually can sufficiently suppress the second signal, when steered toward the first, such samples are often available.

2.5 Swath sonar simulations

Swath sonar simulations has been an essential part of our work. We have both used them independently, to explore problems and test explanations, and with field data, to understand and extend the results. We have used similar simulator configuration through all our papers. The following is a representative example, from **Paper III**.

Our simulation program is built around Field II (Jensen, 1996; Jensen & Svendsen, 1992), a point-based simulator well regarded in the medical ultrasound community. Field II can provide element time series for a given set of scatterers and transmit and receive arrays.

We model the seafloor segments as a collection of points with uniform directivity and Gaussian scattering strength. The points are initially distributed on a grid to ensure an even coverage of every resolution cell. Random position changes on the order of a wavelength are added to the point scatterers to emulate a rough seafloor. This assumes a seafloor that is rough compared to the wavelength. The point density is chosen to get fully developed speckle. We have not adjusted the absolute scattering strength to physically meaningful levels since only relative values are important for our analysis.

We model a swath sonar with the standard Mill's cross geometry (Lurton, 2010, Ch. 8.3.2). For faster simulations we replace a long transmit-array with a single element and model the transmit beampattern by limiting the along-track extent of the seafloor to $0.7°$. We transmit a 100 μs Hanning (Harris, 1978) shaped pulse with center frequency of 300 kHz. We add Gaussian noise to the simulated element data before doing receiver processing. The element SNR ranges from roughly 20 dB at nadir to around -5 dB at $40°$. We have only seen minor changes in accuracy when adjusting the noise level, and therefore use a constant value. These and the remaining parameters are summarized in Table 2.1. The parameters were chosen based on (Lurton, 2010) and historical survey data.

Paper III

Table 2.1: Simulation parameters for **Paper III**.

Parameter	Value
Center frequency	300 kHz
Pulse length	100 μs
Pulse type	CW
Pulse shaping	Hanning (Harris, 1978)
Sound speed	1500 m/s
Depth	$\approx$ 40 m
Number of elements	128
Element spacing	$\lambda/2$
Attenuation	65 dB/km
Element SNR	$\approx$ -5 to 20 dB
Simulation region	$0.7° \times 120°$

Chapter 3

Summary of publications

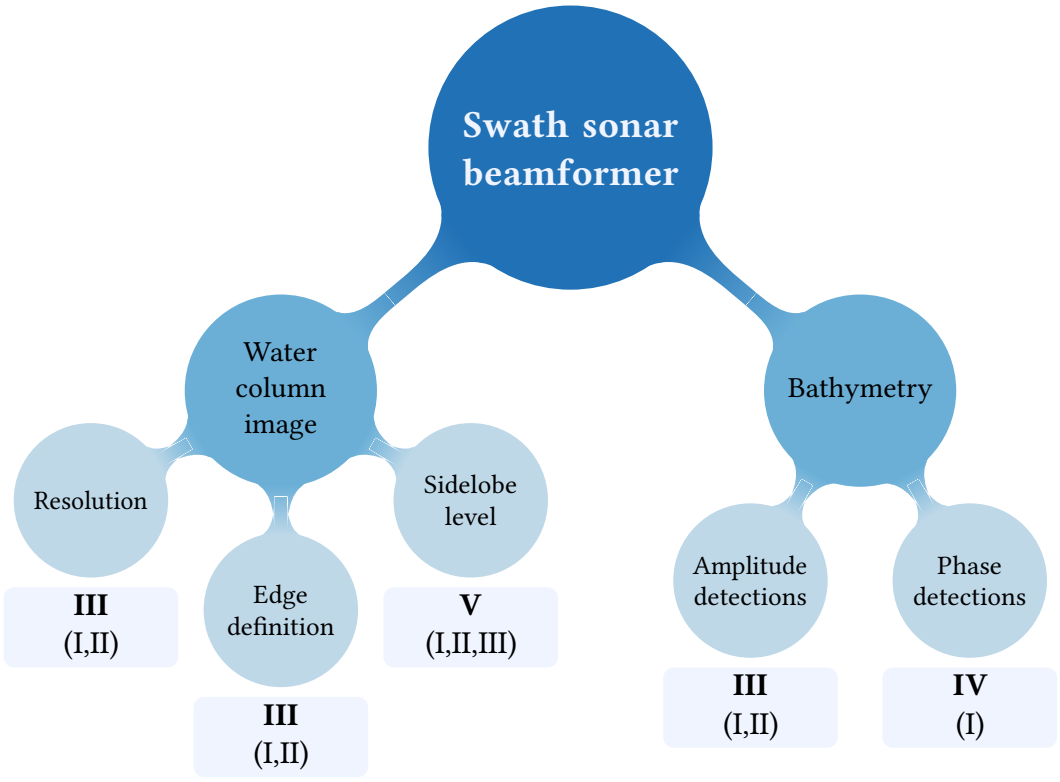

Figure 3.1: Illustration of swath sonar data products and how they are covered by the papers. The bold roman numerals indicate which paper covers the topic above best. The numerals in parenthesis list other papers that also cover the topic.

This chapter summarizes the motivation, methods and results for the included publications. Figure 3.1 shows a quick overview of what the papers cover.

Paper I

> Lønmo, T. I. B., Austeng, A., & Hansen, R. E. (2015b). Low Complexity Adaptive Beamforming Applied to Sonar Imaging (Invited). In J. S. Papadakis & L. Bjørnø (Eds.), *Proceedings of the 3rd International Conference and Exhibition on Underwater Acoustics* (pp. 653–658). Crete, Greece. url: http://www.uaconferences.org/docs/Past_proceedings/UACE2015_Proceedings.pdf

Paper I examines the effect of the LCA beamformer on the water column image and bottom detection for smooth seafloors. It also introduces the use of Field II as a swath sonar simulator. The water column image and amplitude and phase bottom detections are qualitatively evaluated for small and large angles, both in a simulated and a field example. Amplitude detection is done by the maximum amplitude instant, and phase detection by finding the zero phase difference instant. We use the original LCA weight set used by Synnevåg et al. (2011). LCA is compared with two DAS beamformers, one uniformly weighted and one with Kaiser weights with $\beta = 3$.

We show that the mainlobe appears narrower for LCA than both DAS beamformers. This effect is larger at the highest angles. The sidelobes also appear lower with LCA, especially in the simulations. The mainlobe improvements leads to amplitude detections that follows the seafloor more closely. In particular, strong points on the seafloor often dominate the detection for several close beams with DAS, while this is not the case for LCA. Phase detections appear more accurate with LCA than DAS on the field data, but seem to be somewhat worse on the simulated data.

Paper II

> Lønmo, T. I. B., Austeng, A., & Hansen, R. E. (2015a). Interference rejection by Low Complexity Adaptive Beamforming. In *Proceedings of the Institute of Acoustics* (Vol. 37). Institute of Acoustics, Bath, United Kingdom. url: http://www.proceedings.com/27961.html

Paper II further examines the effect of the LCA beamformer by investigating the water column image and amplitude bottom detections for a field example with a wreck. The performance is qualitatively evaluated via the water column

image with detections and a scatterplot of all detections on the wreck. We do amplitude detection via the maximum amplitude instant and use the LCA weight set from Synnevåg et al. (2011) without the inverted weights. LCA is compared with two DAS beamformers, one uniformly weighted and one Kaiser weighted with $\beta = 3$.

As in **Paper I**, we show that both mainlobe and sidelobes seem to improve with LCA, and this leads to improved amplitude detections. Uniformly weighted DAS shows high sidelobes which cause false detections not present for LCA and Kaiser weighted DAS. Kaiser weighted DAS broadens features in the water column which cause the detector to miss details revealed by DAS and LCA. LCA seems to have the best performance in both cases, and also generally has the apparent best detections along the seafloor.

Paper III

> Lønmo, T. I. B., Austeng, A., & Hansen, R. E. (2019b). Improving Swath Sonar Water Column Imagery and Bathymetry with Adaptive Beamforming. *IEEE Journal of Oceanic Engineering*. Early access. doi:10.1109/JOE.2019.2926863

Paper III extends the water column and amplitude detection results from **Paper I** and **Paper II** with a larger set of simulated and field examples, quantification of amplitude detection accuracy and the addition of the Capon beamformer. It describes three key properties for understanding the performance of the beamformers: Edge definition, resolution and sidelobe level.

We show the average water column image and detection statistics for three simulated cases: A flat seafloor with steps and two sinusoidal seafloors, one with large low frequency waves, and one with small high frequency waves. In addition, we show a cross section at a step from the first case and a sun-illuminated view of all detections in the last case. We include two field examples, one over a wreck and one over a flat seafloor with a boulder. For the boulder example amplitude detections are shown on the water column image and visualized with a sun-illuminated view. LCA and Capon are compared with a DAS beamformer weighted with Kaiser $\beta = 2.5$ weights. We use a custom weight set for LCA and a center-of-gravity amplitude detector.

We show that the adaptive beamformers improve all three quality metrics. On simulated data, the sidelobe level and edge definition are much better for both

LCA and Capon. Resolution is also improved for both, but significantly more with Capon. Particularly the improved edge definition, determined by microsteering for LCA, leads to lower depth error for the amplitude detections across large parts of the swath. LCA and Capon often have similar performance, although Capon is better in cases where resolution or particularly high edge definition is important. The improvements compared to DAS increase as the incidence angle grows. We show that these improvements allow LCA and Capon to resolve the high frequency waves, which are mostly hidden for DAS.

We find that the field examples are consistent with the results from the simulations. The extent of the seafloor and many features in the water column is reduced to more realistic sizes. The amplitude detections appear to track the seafloor better, and seem less noisy. The improvement in sidelobe level is smaller than for the simulated data, with somewhat better results for LCA than for Capon. We suggest that the sidelobe level is degraded more in the field than resolution and edge definition since the sidelobe level is more sensitive to calibration errors.

Paper IV

> Lønmo, T. I. B., Austeng, A., & Hansen, R. E. (2019c). On Interferometric Phase Detections for Swath Sonars with Adaptive Beamformers. *IEEE Journal of Oceanic Engineering*, in review, submitted October 31st.

Paper IV studies if the adaptive beamformers also improve phase detections. Field examples illustrate observations which suggest degraded performance. We use simulations to quantify the performance and explain the observed effects by investigating how the adaptive beamformers affect the phase difference. We mainly use the LCA and Capon configurations from **Paper III**, and compare them with uniformly weighted DAS.

We show that LCA and Capon generally preserve the expected phase difference, but increase the variance. Increased phase difference variance leads to lower depth accuracy. The effect is larger away from the beam direction. We find that the use of low WNG weights is a cause of this. This reduces the signal to noise ratio (SNR) and consequently increases the phase difference variance. These weight choices improve the edge definition and are therefore beneficial for the water column image and amplitude detections. For LCA, microsteering is linked to much of the degradation.

We also show that an adaptive beamformer may prevent missed detections in case of strong interference. Capon demonstrates a low phase difference variance in a case where no detection is possible for DAS. Adjusting LCA by removing the microsteered weights gives phase difference variance near DAS without interference and also improves performance with interference. We conclude that improved phase detections with adaptive beamformers may be possible. However, to achieve that, the adaptive beamformers, the bottom detection method, or both, need to be modified.

Paper V

> Lønmo, T. I. B., Austeng, A., & Hansen, R. E. (2019a). Data Driven Autocalibration for Swath Sonars. *IEEE Journal of Oceanic Engineering*, in review, comments received November 1st.

Paper V studies if data from normal swath sonar operation can be used to estimate phase and amplitude errors via the GIAR, and if correcting for them improve the sidelobe level of the DAS beamformer. This is motivated by the limited sidelobe level improvement in **Paper III**. We show the effect of amplitude and phase errors on the water column image, particularly the sidelobe level, and how it improves after calibrating. The water column image, cross sections, and calibration errors are shown for simulated data and two field examples. We also show the effect of grouping the calibration samples across-track and along-track on the estimation error.

We find that GIAR autocalibration reliably estimates calibration errors using data from normal operation. The standard deviation of the calibration estimate seems to consistently improve as $1/\sqrt{N_{\text{El}}}$, reducing the sidelobe level to near ideal levels on the simulated data. The estimate of the calibration error appears unbiased for phase, and slightly biased for amplitude. The amplitude bias induces a small extra weighting, not likely to significantly influence the sidelobe level. Our results also suggest that GIAR autocalibration works in low SNR situations, although the fraction of data usable for calibration is reduced.

We show that GIAR calibration also improves the sidelobe level in the field. However, the scale of the improvements is lower, and the results are mixed. The sidelobe level is lowered over large areas, removing artefacts from the water column image and allowing for better separation between features and the back-

ground. However, the sidelobe level is sometimes unchanged and occasionally higher.

We also show that the estimation error increases greatly when switching from across-track to along-track grouping when using field data, while it is relatively unchanged with simulated data. Together with the reduced sidelobe improvements in the field compared to the simulations, this suggests that the amplitude and phase calibration model is insufficient, at least for the swath sonars we tested.

Chapter 4

Summary and discussion

This chapter summarizes the main contributions of this thesis and briefly discusses aspects relevant for use on a general swath sonar. Finally, I illustrate the total improvement of this thesis on the water column image by demonstrating autocalibrated adaptive beamforming.

The main contributions of this thesis to swath sonar signal processing are:

- Demonstrate working configurations for the adaptive LCA and Capon beamformer, and showing how they can improve the water column image and amplitude detections on simulated and field data.
- Characterizing the DAS, Capon, and LCA beamformers in terms of resolution, edge definition, and sidelobe level.
- Demonstrating the usefulness of the beamformer characteristics for analyzing performance, improving adaptive beamformer configuration, and transferring experience from simulations to the field.
- Demonstrate that and discuss why the adaptive beamformers preserve the expected phase difference used in phase detections, but typically increase the phase difference variance.
- Demonstrate that an adaptive beamformer may improve interference rejection for phase detection, and that the increased phase difference variance can be reduced by reconfiguration.
- Demonstrate that the demands of different data products differ, which suggest different optimal adaptive beamformers for each data product.

- Demonstrate that swath sonar beamforming can be improved via GIAR autocalibration on field data collected during normal operation.
- Identifying that the phase and amplitude error calibration model may be insufficient.
- Introduce and demonstrate the usefulness of Field II as a swath sonar simulator.

Swath sonars exist in a range of different configurations, and are used in widely different scenarios. This thesis has only considered a very limited subset. A key remaining question is how these results will transfer to other systems and scenarios. A related question is if autocalibration and adaptive beamforming support modern features like multi-sector and multi-swath transmission. My discussion of these questions below is also based on all my experience of using adaptive beamformers and autocalibration on swath sonars through this work. This includes examples from more systems, modes, and sectors than what is included in the publications.

I have observed similar improvements as in the publications when using data from different sectors, modes, and transducers. Therefore, I expect similar improvements when using the methods from this thesis on a comparable system with multi-sector and/or multi-swath enabled, for all frequency modes. Capon is a broadband method, and both Capon and LCA were used on a much higher fractional bandwidth pulse in (Synnevåg et al., 2011). Therefore, this should also apply to FM modes.

In principle, the proposed methods are largely frequency independent,[1] so a first approximation is that changing to a system with another operating frequency should not change the results. In practice, I expect that this will effectively change features that may affect performance. For example, the relative importance of noise sources will change, which may change the typical structure of the covariance matrix. Therefore, I think that larger differences are more likely when switching to systems with different operation frequencies.

Predicting performance in new scenarios can in many cases be done via the beamformers properties resolution, edge definition, and sidelobe performance as described in **Paper III**. As long as the received signal is dominated by signals from relatively few angles, I think this will be accurate in most cases. The difference in beamformer properties may also be used to help decide if LCA

[1] Assuming frequency, array size, and other parameters are scaled correspondingly.

performance is good enough or if it is worth the extra effort to implements Capon. In addition, the properties may guide modifications of the adaptive beamformers for further improvements. For example, if better edge definition is needed, increase microsteering for LCA.

This applies for scenarios like the ones shown in the paper, which briefly described are scenarios where the signal predominantly arrives from a few small angular regions at each instant and, most significantly, fairly high SNR. The low SNR performance is important since it determines the achievable swath width, which can greatly affect mapping efficiency. Autocalibration may improve SNR, however the improvement would be relatively small with the scale of our calibration errors. Therefore, it is more important to know the low SNR performance of the adaptive beamformers. The reduced SNR observed in **Paper IV** is the most related result from the published work. This would suggest lower performance of the adaptive beamformers. However, this result may not be relevant since Capon can perform better in cases with lower SNR (Van Trees, 2002, Ch. 7.3). Therefore, I think further research is needed to make reliable predictions for the low SNR case.

Another open question is the effect of adaptive beamforming on backscatter. The processing is dependent on properties of the DAS beamformer, like beamwidth, which is not well defined for adaptive beamformers. This means that backscatter processing likely must be modified when using adaptive beamformers. Preliminary results from **Paper VI** indicate that LCA may slightly lower the mean power and change the backscatter distribution. Larger and better controlled studies, which also include Capon, are needed before adaptive beamformers may be used for backscatter.

I would also like to note that it might be reasonable to use autocalibration more widely than the adaptive beamformers in the current state. The benefit of autocalibration is lower than from adaptive beamforming, however the potential downsides are also much lower since the induced changes are relatively small. If the current improvements seem attractive, I expect autocalibration can be applied broadly with low risk.

To increase the benefit of autocalibration a better error model is needed. There exist many causes for calibration errors (Steinberg, 1976, Ch. 13; Litva & Lo, 1996, Ch. 4.1; Viberg et al., 2009), which leads to different error models. When designing a calibration procedure, we need a calibration model that is simple enough to allow efficient estimation and compensation, but sufficiently complex to capture enough of the calibration errors to provide useful improvements. The simplest

extension of the current model may be to add mutual coupling. Mutual coupling may be the simplest extension, since it essentially extends the calibration model from a diagonal matrix to a full matrix, or at least a matrix with more non-zero elements. Our calibration method can estimate and compensate for errors with coupling with few changes. Another natural extension is to include position errors. This is more complicated and will significantly increase the computational demand, since the beam delay depends on the element positions and must be included in the optimization loop. Position errors can also not be completely compensated for, and the perturbed array shape may change the ideal sidelobe level. However, these methods are relatively simple compared to other options, like non-linear effects, and may improve performance.

Through all our research we have used the Field II simulations. The controlled experiments and ease of configuration that the simulator provides has been essential for our work. Similar simulators exist (Etter, 2013, Ch. 10.7), however, none appeared available to us at the start of this project. The introduction of Field II, which is freely available, for swath sonar simulation may therefore also be valuable for other researchers. The general value is increased by Antoine Blachet who has reworked the simulator and integrated it with the UltraSound ToolBox (USTB) (Rodriguez-Molares et al., 2017). These developments have been presented in **Paper VIII** and (Blachet et al., 2019). The latter shows that the simulator can generate data which are representative of a real case and provide a fully functional example.

In short, this thesis has demonstrated that adaptive beamformers can improve several aspects of the swath sonar data products. We have also shown that different configurations are likely needed for different data products. In the current state adaptive beamforming needs to be a supplement to, not a replacement of, the DAS beamformer. Autocalibration may likely improve DAS beamforming in a broader set of cases. In addition, the next section shows that autocalibration further increase the improvements of adaptive beamforming. Assuming that the improvements we found in this thesis are realized, applying these methods across a huge initiative like Seabed2030 would lead to large benefits. It seems unlikely that most of the areas mapped in Seabed2030 would be resurveyed rapidly, therefore the application of adaptive beamformers and autocalibration could bring a net benefit for a long time.

4.1 Autocalibrated adaptive beamforming

Our work has sought to improve the swath sonar beamformer through adaptive beamforming and autocalibration. The methods are intended to work best together. However, this has not been examined by the included papers. I therefore show a brief example of autocalibrated adaptive beamforming here.

Figure 4.1 shows autocalibrated adaptive beamforming on one of the field examples from **Paper V**. It shows Kaiser weighted DAS with $\beta = 2.5$ as the baseline,[2] uncalibrated LCA, calibrated LCA, and calibrated Capon. The latter two illustrate, in a sense, the total improvement of the water column image from this thesis.

As in the included papers the adaptive beamformers show smaller features in the water column image and lower sidelobes. The main additional effect of calibration is further reduction of the sidelobes. Several remaining streaks of sidelobes are removed when LCA is calibrated in Figure 4.1. This shows that adaptive beamforming and autocalibration can be combined for further benefits.

[2] **Paper V** used $\beta = 5$. I use $\beta = 2.5$ here since this gives a more reasonable mainlobe-sidelobe trade-off.

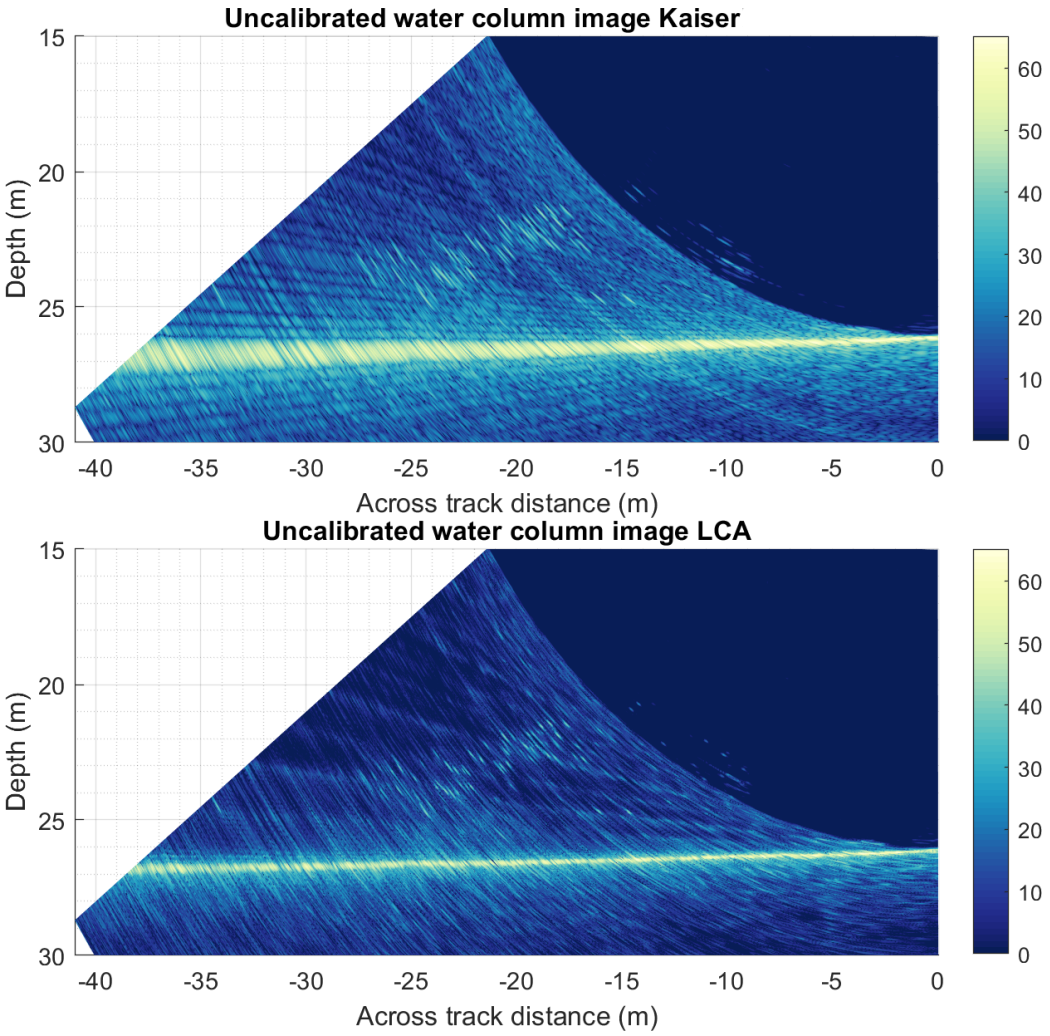

Figure 4.1: (Part 1 of 2) Autocalibrated adaptive beamforming example on field data. (Top) Uncalibrated Kaiser $\beta = 2.5$ weighted DAS. (Bottom) Uncalibrated LCA configured as in **Paper III**.

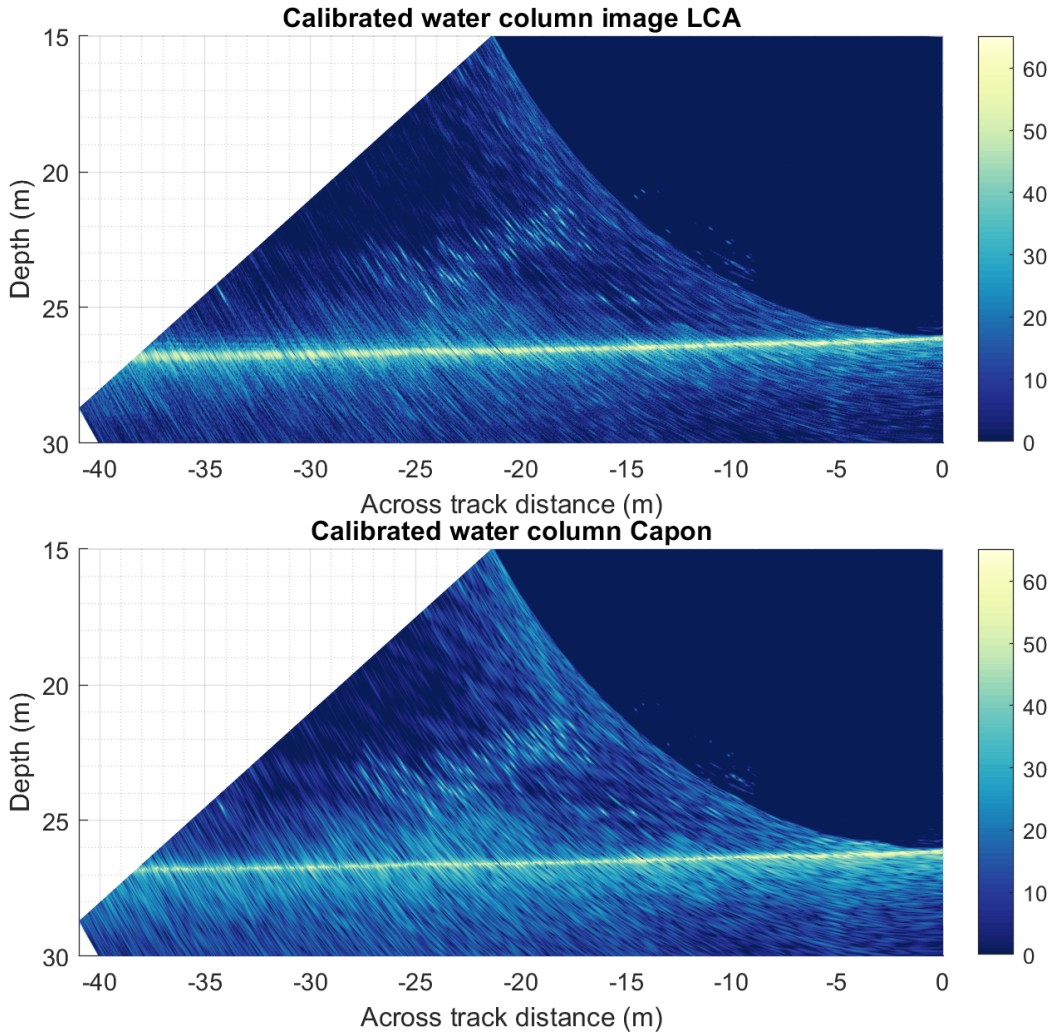

Figure 4.1: (Part 2 of 2) Autocalibrated adaptive beamforming example on field data. (Top) Calibrated LCA configured as in **Paper III**. (Bottom) Calibrated Capon configured as in **Paper III**.

Chapter 5

Further work

Further work is needed to validate these results and improve remaining data products. Some relevant research tasks are:

- **Validate improvements with users of swath sonars**
  Some examples are: Acquire data from areas with known features at the resolution limit and check if they are better resolved with adaptive beamformers. Perform full motion compensation and other corrections such that amplitude detection improvements may be verified through a patch test.

- **Check robustness and performance in remaining cases**
  Particularly with low SNR.

- **Extend improvements to other systems and modes**
  Both check performance for systems in other frequency ranges, and validate that the adaptive beamformers support FM, multi-sector, and multi-swath modes.

- **Adapt and optimize LCA and Capon configurations**
  Develop new configurations suitable for phase detections, and investigate optimal configurations for the water column image and amplitude detections.

- **Investigate how LCA and Capon affect backscatter**
  Backscatter is a data product of high and growing interest. It is important to check if adaptive beamformers is incompatible with existing backscatter processing and how to account for this, if needed.

- **Evaluate autocalibration with an extended error model**
  Using a calibration model which can account for the apparent across-track difference in calibration values.

- **Investigate if autocalibration is more effective for aging transducers**
  We investigated new transducers. Errors and benefits may be higher for older arrays which show effects of aging.

In a wider perspective, this thesis also illustrates the benefits of collecting even more data during swath sonar surveys. During my time at the Center for Coastal and Ocean Mapping at the University of New Hampshire I became familiar with the principle "Map once, use many times". One realization of this is that backscatter and water column imagery may be logged even if bathymetry is the feature of interest for the particular survey. This is relatively inexpensive compared to a new survey, and enables further use of the data later. The next step is to also log element data, before beamforming. This would enable past surveys to benefit from improved beamforming methods, like the ones examined in this thesis. This would likely increase the amount of data logged by an order of magnitude. The increased data rate will be challenging to handle, but should be manageable with current technology. If this is applied to all new surveys across a large project like Seabed2030, imagine the benefits of gradually being able to discover new features as signal processing improves.

Bibliography

Alexandrou, D., & de Moustier, C. (1988). Adaptive noise canceling applied to Sea Beam sidelobe interference rejection. *IEEE Journal of Oceanic Engineering*, *13*(2), 70–76. doi:10.1109/48.556

Austeng, A., Bjastad, T., Synnevåg, J.-F., Masoy, S.-E., Torp, H., & Holm, S. (2008). Sensitivity of minimum variance beamforming to tissue aberrations. In *IEEE Ultrasonics Symposium 2008*. doi:10.1109/ultsym.2008.0258

Blachet, A., Lønmo, T. I. B., Austeng, A., Prieur, F., Hunter, A. J., & Hansen, R. E. (2017). Sonar data simulation with application to multi-beam echo sounders. In *Proceedings of 4th Underwater Acoustics Conference and Exhibition*, Skiathos, Greece. url: http://www.uaconferences.org/index.php/component/contentbuilder/details/9/36/uace2017-sonar-data-simulation-with-application-to-multi-beam-echo-sounders?Itemid=410

Blachet, A., Plets, R., Sacchetti, F., Hunter, A. J., Austeng, A., & Hansen, R. E. (2019). MBES data simulation: Assessment by direct comparison with a high-resolution multi-settings wreck survey. In *Proceedings of 5th Underwater Acoustics Conference and Exhibition*, Hersonissos, Greece. url: http://www.uaconferences.org/index.php/component/contentbuilder/details/22/179/uace2019-mbes-data-simulation-assessment-by-direct-comparison-with-a-high-resolution-multi-settings-wreck-survey#

Buskenes, J. I., Hansen, R. E., & Austeng, A. (2017). Low Complexity Adaptive Sonar Imaging. *IEEE Journal of Oceanic Engineering*, *42*(1). doi:10.1109/JOE.2016.2565038

Butler, J. L., & Sherman, C. H. (2016). *Transducers and Arrays for Underwater Sound* (2.). doi:10.1007/978-3-319-39044-4

Callow, H. J. (2003). *Signal processing for synthetic aperture sonar image enhancement* (Doctoral dissertation, University of Canterbury). url: https://ir.canterbury.ac.nz/handle/10092/4000

Carlson, B. (1988). Covariance matrix estimation errors and diagonal loading in adaptive arrays. *IEEE Transactions on Aerospace and Electronic Systems*, *24*(4), 397–401. doi:10.1109/7.7181

Cervenka, P. (2015). New Processing Schemes for Multi-Beam Echo-Sounders Based on the Generalized Interferometric Array Response (Invited). In J. S. Papadakis & L. Bjørnø (Eds.), *Proceedings of 3rd International Conference and Exhibition on Underwater Acoustics* (pp. 635–640). Crete, Greece. url: http://www.uaconferences.org/docs/Past_proceedings/UACE2015_Proceedings.pdf

Clarke, J. E. H. (2003). Dynamic Motion and Residuals in Swath and Sonar Data: Ironing out the Creases. *International Hydrographic Review*, *4*(1), 6–23. url: https://journals.lib.unb.ca/index.php/ihr/article/view/20600

Clarke, J. E. H. (2006). Applications of multibeam water column imaging for hydrographic survey. *The Hydrographic Journal*, *120*, 3–15. url: http://www.omg.unb.ca/omg/papers/HJ_water_column_JHC.pdf

Clarke, J. E. H. (2017). Coherent refraction "noise" in multibeam data due to oceanographic turbulence. In *Proceedings of the U.S. Hydrographic Conference 2017*, Galveston, Texas, USA.

Clarke, J. E. H. (2018). The Impact of Acoustic Imaging Geometry on the Fidelity of Seabed Bathymetric Models. *Geosciences*, *8*(4), 109. doi:10.3390/geosciences8040109

Cox, H. (1973). Resolving power and sensitivity to mismatch of optimum array processors. *The Journal of the Acoustical Society of America*, *54*(3), 771–785. doi:10.1121/1.1913659

Cox, H., Zeskind, R. M., & Owen, M. M. (1987). Robust adaptive beamforming. *IEEE Transactions on Acoustics, Speech and Signal Processing*, *35*(10), 1365–1376. doi:10.1109/TASSP.1987.1165054

de Moustier, C. (1988). State of the art in swath bathymetry survey systems. *The International Hydrographic Review*, *65*(2).

de Moustier, C. (1993). Signal Processing for Swath Bathymetry and Concurrent Seafloor Acoustic Imaging. In J. M. F. Moura & I. M. G. Lourtie (Eds.), *Acoustic Signal Processing for Ocean Exploration* (Vol. 388, pp. 329–354). doi:10.1007/978-94-011-1604-6_33

Etter, P. C. (2013, February 21). *Underwater Acoustic Modeling and Simulation* (4th ed.). CRC PR INC.

Farquharson, G., Lopez-Dekker, P., & Frasier, S. (2013). Contrast-Based Phase Calibration for Remote Sensing Systems With Digital Beamforming Anten-

nas. *IEEE Transactions on Geoscience and Remote Sensing*, *51*(3), 1744–1754. doi:10.1109/TGRS.2012.2205695

Flax, S., & O'Donnell, M. (1988). Phase-aberration correction using signals from point reflectors and diffuse scatterers: basic principles. *IEEE Transactions on Ultrasonics, Ferroelectrics and Frequency Control*, *35*(6), 758–767. doi:10.1109/58.9333

Foote, K. G., Chu, D., Hammar, T. R., Baldwin, K. C., Mayer, L. A., Hufnagle, L. C., Jr., & Jech, J. M. (2005). Protocols for calibrating multibeam sonar. *The Journal of the Acoustical Society of America*, *117*(4), 2013–2027. doi:10.1121/1.1869073

Guériot, D., Chèdru, J., Daniel, S., & Maillard, E. (2000). The patch test: a comprehensive calibration tool for multibeam echosounders. In *Proceedings of OEANS 2000 MTS/IEEE Conference and Exhibition* (Vol. 3, 1655–1661 vol.3). doi:10.1109/OCEANS.2000.882178

Hare, R. (1995). Depth and Position Error Budgets for Multibeam Echosounding. *The International Hydrographic Review*, *72*(2), 37–69.

Hare, R., Godin, A., & Mayer, L. (1995). *Accuracy estimation of Canadian Swath (multibeam) and Sweep (multi-transducer) sounding systems*. Canadian Hydrographic Service.

Harris, F. (1978). On the use of windows for harmonic analysis with the discrete Fourier transform. *Proceedings of the IEEE*, *66*(1), 51–83. doi:10.1109/PROC.1978.10837

Jensen, J. A. (1996). Field: A Program for Simulating Ultrasound Systems. In *Medical & Biological Engineering & Computing* (Vol. 34, pp. 351–353). url: http://field-ii.dk/documents/jaj_nbc_1996.pdf

Jensen, J. A., & Svendsen, N. B. (1992). Calculation of pressure fields from arbitrarily shaped, apodized, and excited ultrasound transducers. *IEEE Transactions on Ultrasonics, Ferroelectrics, and Frequency Control*, *39*(2), 262–267. doi:10.1109/58.139123

Johnson, D. H., & Dudgeon, D. E. (1993). *Array signal processing: Concepts and techniques*. Prentice Hall.

Krim, H., & Viberg, M. (1996). Two decades of array signal processing research: the parametric approach. *IEEE Signal Processing Magazine*, *13*(4), 67–94. doi:10.1109/79.526899

Krolik, J., & Swingler, D. (1989). Multiple broad-band source location using steered covariance matrices. *IEEE Transactions on Acoustics, Speech, and Signal Processing*, *37*(10), 1481–1494. doi:10.1109/29.35386

Lamarche, G., & Lurton, X. (2017). Recommendations for improved and coherent acquisition and processing of backscatter data from seafloor-mapping sonars. *Marine Geophysical Research*, *39*(1-2), 5–22. doi:10.1007/s11001-017-9315-6

Lanzoni, J. C., & Weber, T. C. (2012). Calibration of multibeam echo sounders: a comparison between two methodologies. In *European Conference on Underwater Acoustics*. doi:10.1121/1.4772734

Li, J., Stoica, P., & Wang, Z. (2003). On robust Capon beamforming and diagonal loading. *IEEE Transactions on Signal Processing*, *51*(7), 1702–1715. doi:10.1109/TSP.2003.812831

Li, Y., & Er, M. H. (2006). Theoretical analyses of gain and phase error calibration with optimal implementation for linear equispaced array. *IEEE Transactions on Signal Processing*, *54*(2), 712–723. doi:10.1109/TSP.2005.861892

Litva, J., & Lo, T. K.-Y. (1996). *Digital Beamforming in Wireless Communications*. Artech House.

Llort-Pujol, G. (2007). *Improvement of the spatial resolution for multibeam echosounders* (Doctoral dissertation, Télécom Bretagne). url: https://portail.telecom-bretagne.eu/publi/public/fic_download.jsp?id=4814

Llort-Pujol, G., Sintes, C., Chonavel, T., Morrison, A. T., & Daniel, S. (2012). Advanced Interferometric Techniques for High-Resolution Bathymetry. *Marine Technology Society Journal*, *46*(2), 9–31. doi:10.4031/mtsj.46.2.4

Llort-Pujol, G., Sintes, C., & Lurton, X. (2005). High-resolution interferometry for multibeam echosounders. In *Europe Oceans 2005* (Vol. 1, pp. 345–349). doi:10.1109/OCEANSE.2005.1511738

Llort-Pujol, G., Sintes, C., & Lurton, X. (2008). Improving spatial resolution of interferometric bathymetry in multibeam echosounders. *The Journal of the Acoustical Society of America*, *123*(5), 3952–3952. doi:10.1121/1.2936066

Lo, K. (2004). Adaptive Array Processing for Wide-Band Active Sonars. *IEEE Journal of Oceanic Engineering*, *29*(3), 837–846. doi:10.1109/joe.2004.833096

Lønmo, T. I. B., Austeng, A., & Hansen, R. E. (2015a). Interference rejection by Low Complexity Adaptive Beamforming. In *Proceedings of the Institute of Acoustics* (Vol. 37). Institute of Acoustics, Bath, United Kingdom. url: http://www.proceedings.com/27961.html

Lønmo, T. I. B., Austeng, A., & Hansen, R. E. (2015b). Low Complexity Adaptive Beamforming Applied to Sonar Imaging (Invited). In J. S. Papadakis & L. Bjørnø (Eds.), *Proceedings of the 3rd International Conference and Exhibition*

on Underwater Acoustics (pp. 653–658). Crete, Greece. url: http://www.uaconferences.org/docs/Past_proceedings/UACE2015_Proceedings.pdf

Lønmo, T. I. B., Austeng, A., & Hansen, R. E. (2017). Phase Detections with Low Complexity Adaptive Beamforming on Swath Sonars. In *2017 Underwater Acoustic Signal Processing Workshop* (p. 16). url: http://www.uasp.org/abstractbooks/uasp2017abstracts.pdf

Lønmo, T. I. B., Austeng, A., & Hansen, R. E. (2019a). Data Driven Autocalibration for Swath Sonars. *IEEE Journal of Oceanic Engineering*, in review, comments received November 1st.

Lønmo, T. I. B., Austeng, A., & Hansen, R. E. (2019b). Improving Swath Sonar Water Column Imagery and Bathymetry with Adaptive Beamforming. *IEEE Journal of Oceanic Engineering*. Early access. doi:10.1109/JOE.2019.2926863

Lønmo, T. I. B., Austeng, A., & Hansen, R. E. (2019c). On Interferometric Phase Detections for Swath Sonars with Adaptive Beamformers. *IEEE Journal of Oceanic Engineering*, in review, submitted October 31st.

Lønmo, T. I. B., & Lyons, A. (2016). Effect of low complexity adaptive beamforming on seafloor backscatter statistics. In *The Journal of the Acoustical Society of America* (Vol. 140, p. 3287). Presented at the 172nd Meeting of the Acoustical Society of America. doi:10.1121/1.4970447

Lønmo, T. I. B., & Weber, T. C. (2017). Improving seep detection by swath sonars with adaptive beamforming. In *The Journal of the Acoustical Society of America* (Vol. 141, p. 4005). Presented at 173rd Meeting of the Acoustical Society of America. doi:10.1121/1.4989190

Lurton, X. (2010). *An Introduction to Underwater Acoustics: Principles and Applications* (2nd ed.). Springer-Verlag Berlin Heidelberg.

Lurton, X., & Augustin, J.-M. (2010). A Measurement Quality Factor for Swath Bathymetry Sounders. *IEEE Journal of Oceanic Engineering*, *35*(4), 852–862. doi:10.1109/JOE.2010.2064391

Lurton, X., & Lamarche, G. (Eds.). (2015). *Backscatter measurements by seafloor-mapping sonars: Guidelines and Recommendations*. GeoHab Backscatter Working Group. url: http://geohab.org/wp-content/uploads/2013/02/BWSG-REPORT-MAY2015.pdf

Mayer, L., Jakobsson, M., Allen, G., Dorschel, B., Falconer, R., Ferrini, V., … Weatherall, P. (2018). The Nippon Foundation—GEBCO Seabed 2030 Project: The Quest to See the World's Oceans Completely Mapped by 2030. *Geosciences*, *8*(2), 63. doi:10.3390/geosciences8020063

Mitchley, M., & Sears, M. (2014). Searching for seafloor massive sulfides: A quantitative review of high-resolution methods in deep sea sonar bathymetry for mining applications. *Marine Geophysical Research*, *35*(2), 157–174. doi:10.1007/s11001-014-9219-7

Ng, B. P., Er, M. H., & Kot, C. (1994). Array gain/phase calibration techniques for adaptive beamforming and direction finding. *IEE Proceedings - Radar, Sonar and Navigation*, *141*(1), 25–29. doi:10.1049/ip-rsn:19949538

Pantzartzis, D., de Moustier, C., & Alexandrou, D. (1993). Application of high-resolution beamforming to multibeam swath bathymetry. In *Proc. OCEANS '93* (Vol. 2, pp. 77–82). doi:10.1109/OCEANS.1993.326070

Pereira, D. L. d. S., & Clarke, J. E. H. (2015). Improving shallow water multibeam target detection at low grazing angles. In *U.S. Hydrographic Conference 2015*, National Harbor, Maryland U.S.A. url: http://www.omg.unb.ca/omg/papers/DouglasPereira_and_JHC_USHC2015_Paper.pdf

Pocwiardowski, P., Yufit, G., Maillard, E., & Eriksen, P. (2006). Method for Large Sonar Calibration and Backscattering Strength Estimation. In *OCEANS 2006*. doi:10.1109/oceans.2006.307056

Qiong, L., Long, G., & Zhongfu, Y. (2003). An overview of self-calibration in sensor array processing. In *Proceedings of 6th International Symposium on Antennas, Propagation and EM Theory (ISAPE'03)* (pp. 279–282). doi:10.1109/ISAPE.2003.1276682

Rao, B. D., & Hari, K. V. S. (1990). Effect of spatial smoothing on the performance of MUSIC and the minimum-norm method. *IEE Proceedings (F-Radar and Signal Processing)*, *137*(6), 449–458. doi:10.1049/ip-f-2.1990.0065

Rodriguez-Molares, A., Rindal, O. M. H., Bernard, O., Nair, A., Bell, M. A. L., Liebgott, H., … Lovstakken, L. (2017). The UltraSound ToolBox. In *2017 IEEE International Ultrasonics Symposium (IUS)*. doi:10.1109/ultsym.2017.8092389

Rønhovde, A., Yang, L., Taxt, T., & Holm, S. (1999). High-resolution beamforming for multibeam echo sounders using raw EM3000 data. In *OCEANS '99 MTS/IEEE. Riding the Crest into the 21st Century* (Vol. 2, pp. 923–930). doi:10.1109/OCEANS.1999.804997

Schmidt, V., Weber, T. C., & Lurton, X. (2014). A New Method for Generation of Soundings from Phase-Difference Measurements. In *Proceedings of the Canadian Hydrographic Conference 2014*. url: https://ccom.unh.edu/publications/new-method-generation-soundings-phase-difference-measurements

Seabed 2030 Project. (2019). International project to chart the world's ocean floor announces doubling of data available for definitive global map. Press release from The Nippon Foundation-GEBCO Seabed 2030 Project. Accessed Oct 30th, 2019. url: https://seabed2030.gebco.net/news/gebco_2019_release.html

Shan, T.-J., Wax, M., & Kailath, T. (1985). On spatial smoothing for direction-of-arrival estimation of coherent signals. *IEEE Transactions on Acoustics, Speech and Signal Processing*, *33*(4), 806–811. doi:10.1109/TASSP.1985.1164649

Steinberg, B. D. (1976). *Principles of aperture and array system design: Including random and adaptive arrays*. John Wiley & Sons.

Synnevåg, J.-F., Austeng, A., & Holm, S. (2007). Adaptive Beamforming Applied to Medical Ultrasound Imaging. *IEEE Transactions on Ultrasonics, Ferroelectrics, and Frequency Control*, *54*(8), 1606–1613. doi:10.1109/TUFFC.2007.431

Synnevåg, J.-F., Austeng, A., & Holm, S. (2009). Benefits of minimum-variance beamforming in medical ultrasound imaging. *IEEE Transactions on Ultrasonics, Ferroelectrics, and Frequency Control*, *56*(9), 1868–1879. doi:10.1109/TUFFC.2009.1263

Synnevåg, J.-F., Austeng, A., & Holm, S. (2011). A low-complexity data-dependent beamformer. *IEEE Transactions on Ultrasonics, Ferroelectrics and Frequency Control*, *58*(2), 281–289. doi:10.1109/TUFFC.2011.1805

Van Trees, H. L. (2002). *Optimum Array Processing*. Wiley-Interscience.

Viberg, M., Lanne, M., & Lundgren, A. (2009). Calibration in Array Processing. In *Classical and Modern Direction-of-Arrival Estimation* (pp. 93–124). Academic Press.

Wölfl, A.-C., Snaith, H., Amirebrahimi, S., Devey, C. W., Dorschel, B., Ferrini, V., … Wigley, R. (2019). Seafloor Mapping – The Challenge of a Truly Global Ocean Bathymetry. *Frontiers in Marine Science*, *6*. doi:10.3389/fmars.2019.00283

Included publications

The following chapters contain the publications included in this thesis. All publications have been typeset to fit the format of this thesis, while keeping the content as close to the originals as possible. Minor adaptions were necessary, and are described below.

Some figures have been split to accommodate the smaller page size in this thesis, and the captions have been slightly adapted accordingly. In addition, the citation style now match the rest of the thesis, instead of being numeric as in the originals. For the published papers I have used the last version I submitted, which means that edits by the publishers are not included. I have also omitted the biographies in the last three papers.

Paper I

Lønmo, T. I. B., Austeng, A., & Hansen, R. E. (2015b). Low Complexity Adaptive Beamforming Applied to Sonar Imaging (Invited). In J. S. Papadakis & L. Bjørnø (Eds.), *Proceedings of the 3rd International Conference and Exhibition on Underwater Acoustics* (pp. 653–658). Crete, Greece. url: http://www.uaconferences.org/docs/Past_proceedings/UACE2015_Proceedings.pdf

Low Complexity Adaptive Beamforming Applied to Sonar Imaging

Tor Inge Birkenes Lønmo, Andreas Austeng, and Roy Edgar Hansen.

Abstract

Modern sonars provide high-resolution acoustic imaging for a range of applications, including pipeline inspection, harbor surveys and seabed mapping. Central in the signal processing of the sonar data is the beamforming, where conventional (fixed) aperture tapering (or weighting) typically is used to set the equipment's resolution and robustness to appropriate values. This means that there are predefined weights, not necessary optimally chosen, that express a compromise between resolution and sensitivity to noise and interference.

In this work, we show how we can increase the resolution of bottom detections, without reducing the robustness, by applying Low Complexity Adaptive (LCA) beamforming. LCA can be viewed as a low computational cost version of the minimum variance distortionless response (MVDR) beamformer. It is easy to implement and improves the imaging process by adaptively choosing an appropriate weight for any point in time and space.

We apply LCA beamforming on measured and simulated data. The simulated data are generated by the freely available ultrasound simulator "Field II". The measured data was collected by a commercial echosounder.

LCA beamforming gives significant reduction of the mainlobe width and sidelobe level over conventional beamforming. LCA also gives clear improvements for amplitude detections, and phase detections on measured data. The phase detections on simulated data are partially worse. We expect to get the same improvement for both datasets after minor modifications of the LCA algorithm.

Keywords: *adaptive beamforming, underwater mapping, bathymetry, sonar*

1 Introduction

High-resolution acoustic methods bring advantages for many applications. One way to get increased resolution from existing equipment is with adaptive beamforming. In this work, we investigate if one adaptive method, Low Complexity Adaptive (LCA) beamforming, can improve the resolution of bottom detections.

LCA was first introduced by Synnevåg, Austeng and Holm (Synnevåg, Austeng, & Holm, 2011), and it can be viewed as a low complexity version of the Minimum Variance Distortionless Response (MVDR), also called Capon, beamformer (Van Trees, 2002). It has been used successfully on a vertical array in shallow water by Blomberg, Austeng, Hansen and Synnes (Blomberg., Austeng, Hansen, & Synnes, 2013), and on a sidescan sonar by Buskenes, Austeng and Nilsen (Buskenes, Austeng, & Nilsen, 2011).

The low complexity follows from using a discrete search space and only using one sample for its decision. This also reduces the signal suppression effects known to affect the MVDR beamformer when coherent signals are present.

To evaluate the performance, we apply LCA beamforming to simulated and measured data, and do bottom detection on the results. We compare this with the results we get with conventional and kaiser weighted delay-and-sum (DAS) beamforming. Bottom detection is done via both amplitude and phase.

2 Low Complexity Adaptive beamforming

The minimum variance distortionless response (MVDR) beamformer minimizes the variance of the beamformer output while passing signals from the steering direction through undistorted (Van Trees, 2002). It often needs to use diagonal loading and spatial smoothing to make it robust against errors in estimation of the covariance matrix and coherent signals. This reduces the resolution of the beamformer (Synnevåg, Austeng, & Holm, 2007). Solving for the MVDR weights also needs a matrix inversion, which may make the method too computationally expensive for some applications

Low Complexity Adaptive (LCA) beamforming uses the same optimization criteria but a discrete search space consisting of a predefined set of weights. In practice this means that we apply ordinary delay-and-sum beamforming for all weights and choose the minimum beam value. The discrete search space leads to a complexity of order $N_{\mathrm{El}} N_w$ instead of ${N_{\mathrm{El}}}^3$, where N_{El} is the number of elements and N_w is the number of weights in the search space. It also eliminates the need for spatial smoothing and diagonal loading, since the method does not have enough freedom to create signal suppression. This means that it is significantly faster and may perform better than MVDR (Blomberg. et al., 2013; Buskenes et al., 2011).

Weight selection is grounded in observation of how MVDR achieves its results. MVDR can for example use an asymmetric mainlobe, which gives sharper edges,

and low sidelobes in regions with strong signals. We use the weight set from Synnevåg et al. (Synnevåg et al., 2011), which includes both effects. The set consists of the following twelve weights: uniform weights, kaiser weights with $\beta = 2, 3, 4$, inverted kaiser weights for $\beta = 2, 4$, and kaiser weights with $\beta = 3$ steered to $1/2$, $3/4$, and 1 times the distance to first zero of the uniform window (in both directions). All the weights are normalized such that the sum of the weights equals one, to satisfy the distortionless constraint.

3 Data collection and simulation

We simulated a seabed mapping echosounder via the ultrasound simulation program Field II (Jensen, 1996; Jensen & Svendsen, 1992). It uses linear system theory to calculate the response from a distribution of point scatterers. The program simulates the elements by subdicing the array into rectangles (which may be smaller than an element) and uses a far field approximation for each rectangle.

The simulated receiver is a 300 kHz $\lambda/2$ line array with 128 elements. We transmit with one element and model the effect of transmission beampattern by restricting the bottom to a strip. The bottom is modeled by a collection of randomly distributed point scatterers. We use enough point scatterers to get fully developed speckle. Attenuation is set to 65 dB/km. White noise is added to the data before any receiver processing. We chose a noise level that was comparable to what we got in the measurements described below.

Field measurements were done by a commercial echosounder with geometry comparable to the simulated system. Both cases use a shaped single frequency pulse with center frequency 285 kHz.

4 Processing

We processed both datasets the same way, i.e. we used the same filters and beamforming algorithms. Beam steering was done via time delays.

For each beam, we performed bottom detection via amplitude and phase. Amplitude detection chooses the strongest sample in a beam, while phase detection finds the zero instant of the phase difference between the beams formed on two subarrays (Lurton, 2002). We used LCA independently on the two subarrays and used the amplitude detection instant as a starting point for phase detection.

5 Results and discussion

We applied DAS, weighted DAS, and LCA beamforming to simulated and measured data in two areas around the bottom. Fig. 1 and Fig. 2 show the resulting beam amplitudes and bottom detections. All plots have the same dynamic range of 70 dB, and are normalized to the strongest beam value across the three beams.

The most striking effect is that the main lobe width for LCA is narrower than for DAS. This causes the amplitude detections to lie closer to the bottom (presumed bottom in the measured case). For the two DAS cases strong speckle points at the bottom lead to an erroneous detection for neighbor beams. This effect essentially disappears with LCA. The reduction in main lobe width is largest for high angles.

The sidelobe region for LCA is also the lowest of the three methods. This is especially clear in Fig. 6.2(a).In this case, it does not affect the detections, but if the bottom has inhomogeneous backscatter-strength this may have a significant effect.

LCA is clearly better for phase detections for the measured data shown in Fig. 2. The detection sequence seems smoother and closer to the high amplitude area that indicates the presumed bottom.

A few detections deviate significantly from the others. In most of the cases we have investigated this is caused by the relatively simplistic phase detection algorithm we have used. A more sophisticated algorithm would improve or discard these detections. The other cases were for low angles in the simulated data, where there were no zero crossing in the right area. We do not pay closer attention to these in this study, since phase detection is known to perform worse for low angles.

For the simulated data at high angles, the LCA detection seems to have a bit higher variance than the detections from the two DAS methods, even after we disregard the outliers. We have not been able to track down the reason for this with certainty yet, but suspect it is connected to our LCA implementation. In general, the phase differences between the LCA subbeams are much more irregular than for the other methods. Our LCA implementation uses LCA independently on both subbeams, which means that different weighting may be selected. We expect that the phase will stabilize if LCA is forced to choose the same weighting for both subbeams. The selection can be done per sample, or by the most frequently selected weight in an area, as done by Buskenes et al. (Buskenes et al., 2011).

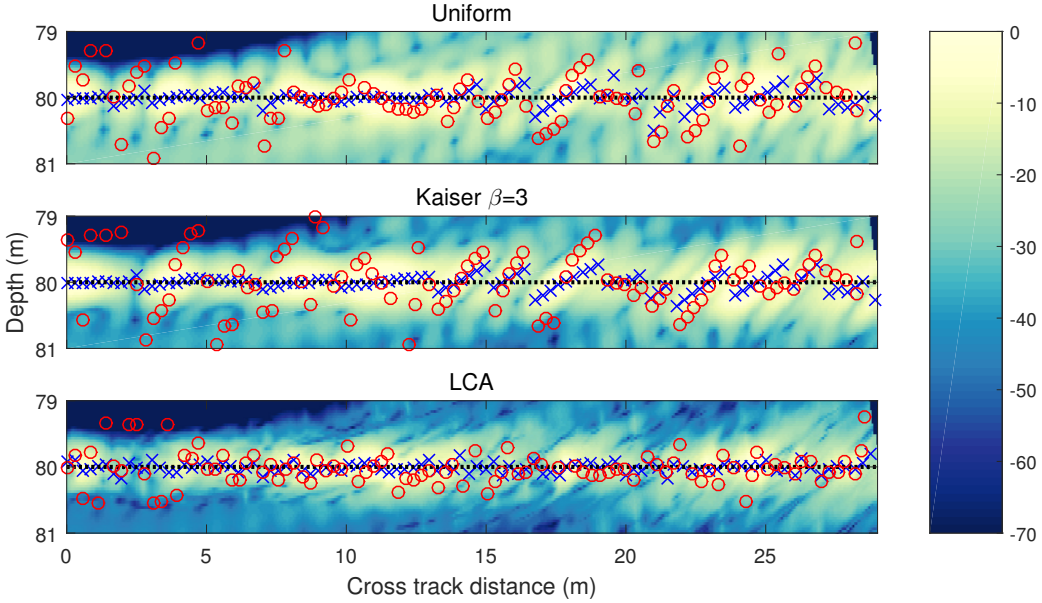

(a) Beam angles between 0 and 20 degrees.

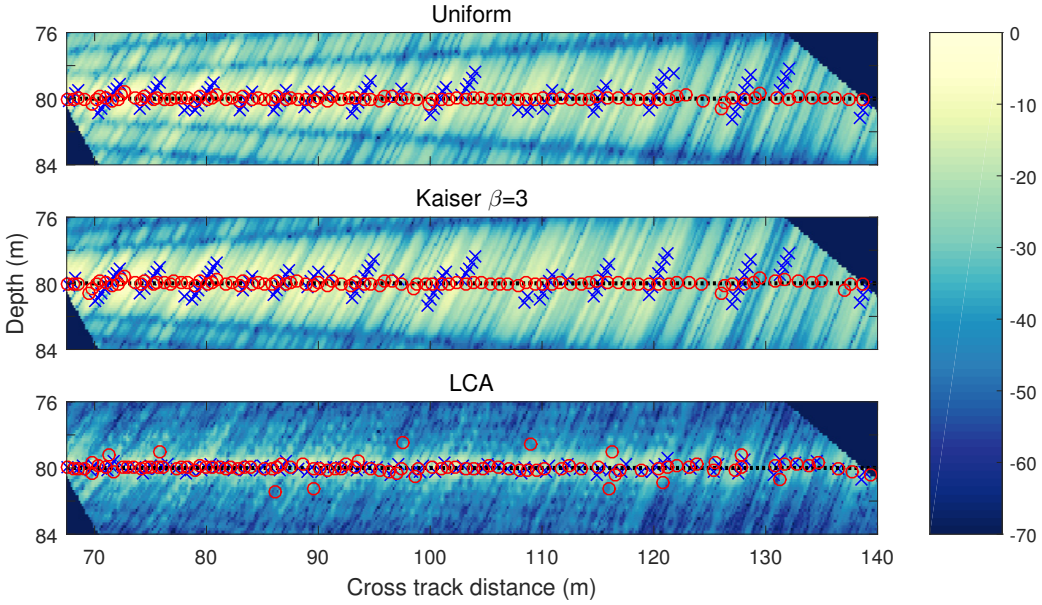

(b) Beam angles between 40 and 60 degrees.

Figure 1: Beam amplitude and bottom detections for different beamforming techniques on simulated data. Black dotted line shows actual bottom location. Blue crosses are amplitude detections, red circles are phase detections. The colormap represents relative power in dB.

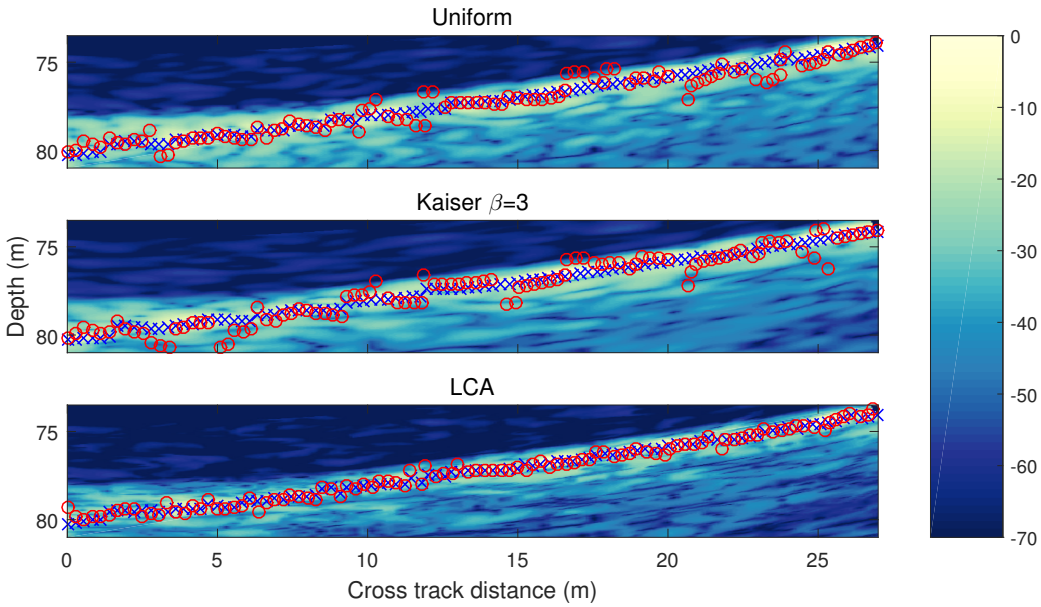

(a) Beam angles between 0 and 20 degrees.

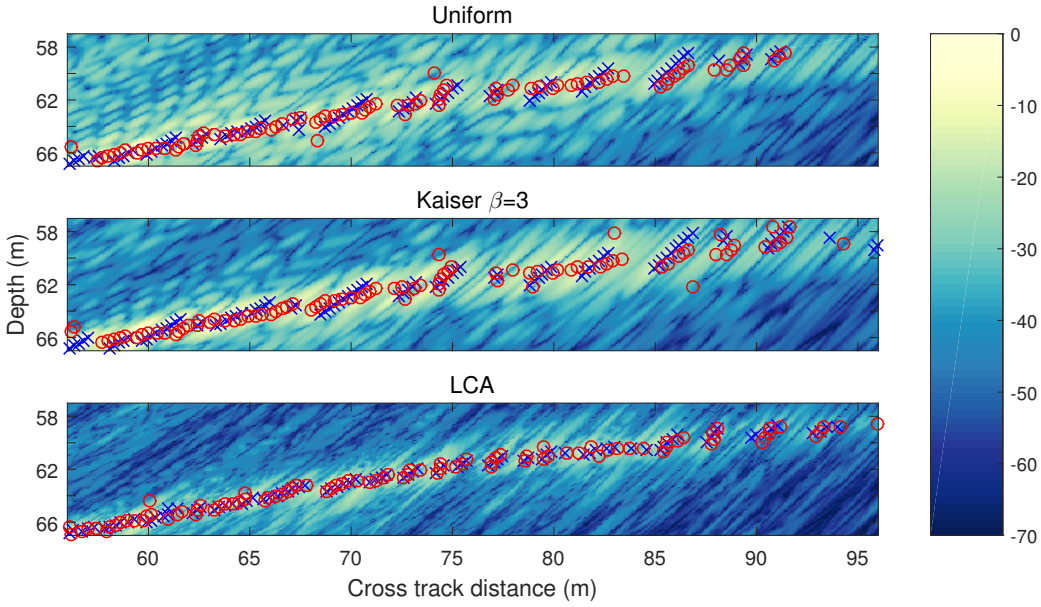

(b) Beam angles between 40 and 60 degrees.

Figure 2: Beam amplitude and bottom detections for different beamforming techniques on measured data. Blue crosses are amplitude detections, red circles are phase detections. The colormap represents relative power in dB.

6 Conclusions

We have seen that LCA produces water column plot with a narrower bottom region and less energy in the sidelobe region for both measured and simulated data. This leads to higher resolution for bottom detection via amplitude. The effect is larger at high angles.

LCA bottom detection is better than DAS for measured data, but partially worse for simulated data. We expect LCA to be better in both cases after an adjustment of the algorithm.

In total, LCA shows great potential to improve the resolution in seabed mapping applications. The complexity is also low enough that it is feasible to implement in a real time system.

7 Acknowledgments

We would like to thank Bente Borgundvåg Berg, Jan-Atle Storesund and Kjell Echholt Nilsen for their efforts. They have been vital for data collection and processing.

This work is sponsored by The Research Council of Norway.

The colormap is based on a map from www.ColorBrewer.org.

References

Blomberg., A. E. A., Austeng, A., Hansen, R., & Synnes, S. (2013). Improving Sonar Performance in Shallow Water Using Adaptive Beamforming. *IEEE Journal of Oceanic Engineering*, *38*(2), 297–307. doi:10.1109/JOE.2012.2226643

Buskenes, J. I., Austeng, A., & Nilsen, C.-I. C. (2011). A Low Complexity Adaptive Beamformer for Active Sonar Imaging. In J. S. Papadakis & L. Bjørnø (Eds.), *Proceedings of the 4rd International Conference & Exhibition on Underwater Acoustic Measurements: Technologies and Results* (pp. 281–286). Greece.

Jensen, J. A. (1996). Field: A Program for Simulating Ultrasound Systems. In *Medical & Biological Engineering & Computing* (Vol. 34, pp. 351–353). url: http://field-ii.dk/documents/jaj_nbc_1996.pdf

Jensen, J. A., & Svendsen, N. B. (1992). Calculation of pressure fields from arbitrarily shaped, apodized, and excited ultrasound transducers. *IEEE Transactions on Ultrasonics, Ferroelectrics, and Frequency Control*, *39*(2), 262–267. doi:10.1109/58.139123

Lurton, X. (2002). *An Introduction to Underwater Acoustics: Principles and Applications* (1st ed.). Springer. url: http://books.google.no/books?id=VTNRh3pyCyMC

Synnevåg, J.-F., Austeng, A., & Holm, S. (2007). Adaptive Beamforming Applied to Medical Ultrasound Imaging. *IEEE Transactions on Ultrasonics, Ferroelectrics, and Frequency Control*, *54*(8), 1606–1613. doi:10.1109/TUFFC.2007.431

Synnevåg, J.-F., Austeng, A., & Holm, S. (2011). A low-complexity data-dependent beamformer. *IEEE Transactions on Ultrasonics, Ferroelectrics and Frequency Control*, *58*(2), 281–289. doi:10.1109/TUFFC.2011.1805

Van Trees, H. L. (2002). *Optimum Array Processing*. Wiley-Interscience.

Paper II

Lønmo, T. I. B., Austeng, A., & Hansen, R. E. (2015a). Interference rejection by Low Complexity Adaptive Beamforming. In *Proceedings of the Institute of Acoustics* (Vol. 37). Institute of Acoustics, Bath, United Kingdom. url: http://www.proceedings.com/27961.html

Interference Rejection for Sonars via Low Complexity Adaptive Beamforming

Tor Inge Birkenes Lønmo, Andreas Austeng, and Roy Edgar Hansen.

1 Introduction

Accurate mapping of the seabed using active high frequency sonar is of importance in many applications, for example in inspection of underwater infrastructure and environmental seabed mapping. The delay-and-sum (DAS) beamformer is commonly used for beamforming. However, it suffers from high sidelobes, which make it susceptible to masking of weak signals when there are strong interfering signals present. This may cause serious problems as low quality data, loss of data, and range reduction.

Conventional aperture shading is used to mitigate this, with a trade-off against resolution. By adjusting the beampattern in real time, adaptive methods promise to provide increased sidelobe suppression while keeping or improving the resolution. This is done by adjusting the beam pattern to have low gain in the directions with interference and allowing large sidelobes in directions without signal.

In this work, we investigate the interference rejection capabilities of the Low Complexity Adaptive (LCA) beamformer, which is a computationally cheap version of the Minimum Variance Distortionless Response (MVDR) beamformer. It uses a discrete search space and bases its decision on a single sample. The discrete search space also make LCA resistant to signal suppression, which is a serious issue for MVDR in active applications.

In earlier work, we have shown that LCA outperforms the DAS beamformers for simulated and measured data over a flat seafloor(Lønmo, Austeng, & Hansen, 2015). This time we test LCA further by applying it to data collected by a high-resolution echosounder over the wreck of an oil tanker. The wreck has sharp edges and big differences in backscatter level, which are common challenges for the DAS beamformer. We investigate how LCA performs compared to the unweighted and a weighted DAS beamformer.

2 Low Complexity Adaptive beamforming

The adaptive Minimum Variance Distortionless Response (MVDR) beamformer minimizes the variance of the beamformer output while passing signals from the steering direction through undistorted (Van Trees, 2002). It may need to use diagonal loading and spatial smoothing to make it robust against errors in estimation of the covariance matrix and coherent signals. This reduces the resolution of the beamformer (Synnevåg, Austeng, & Holm, 2007). Solving for the MVDR weights also require inversion of the sample covariance matrix, which makes the method too computationally expensive for some applications.

Low Complexity Adaptive (LCA) beamforming(Synnevåg, Austeng, & Holm, 2011) uses the same optimization criteria but a discrete search space consisting of a predefined set of weights. In practice this means that we apply ordinary delay-and-sum beamforming for all weights and choose the minimum beam value. The discrete search space lets LCA avoid the need to estimate and invert the covariance matrix. It also eliminates the need for spatial smoothing and diagonal loading, since the method does not have enough freedom to create signal suppression. The computational complexity for LCA is therefore of order $N_{\text{El}}N_w$ instead of ${N_{\text{El}}}^3$, where N_{El} is the number of elements and N_w is the number of weights in the LCA weight set. This means that it is significantly faster and may perform better than MVDR (Blomberg., Austeng, Hansen, & Synnes, 2013; Buskenes, Austeng, & Nilsen, 2011).

MVDR uses a variety of effects to achieve its good results. We have chosen a weight set for LCA that captures the most important effects. MVDR can for example use an asymmetric mainlobe, which gives sharper edges, and low sidelobes in regions with strong signals(Synnevåg et al., 2011). Our set consists of the following ten weights: Uniform, kaiser with $\beta = 2, 3, 4$, and kaiser with $\beta = 3$ steered to $1/2$, $3/4$, and 1 times the distance to first zero of the uniform window (in both directions). This is a subset of the weight set from Synnevåg et al. (Synnevåg et al., 2011). We excluded two weights since they seemed to reduce the performance. All weights are normalized such that the sum of the weight equals one to satisfy the distortionless constraint.

3 Data collection and processing

We collected data with a high-resolution seabed mapping echosounder over the wreck of an oil tanker called Holmengraa, located outside Horten, Norway.

Holmengraa was a Norwegian 1500 dwt oil tanker. Allied airplanes sank it in 1944, while it was sailing under a German flag. The wreck is approximately 68 meters long and 9 meters wide, and lies in a slope at almost 80 meters depth. Figure 1 shows an interferometric SAS image of the wreck. The wreck has common challenging features as small and strong scatterers and sharp edges.

Our data were collected using a high-resolution seabed mapping echosounder. The echosounder uses a Mill's cross setup(Lurton, 2010) with two linear arrays: A transmitter with .5 degree opening along-track and a receiver with 1 degree opening angle across-track (for the used frequency). A tapered 285 kHz single frequency pulse was used. The data were collected on a calm and sunny day, without any rain or significant wind or waves.

For each channel in the received data, we do bandpass and matched filtering. Then we steer toward the wanted angle via time delay and do beamforming and bottom detection on the results. Later in this paper we compare different beamforming methods. The beamforming is then the only step to be changed, all the other processing steps stay the same.

Our processing is somewhat simplified since it assumes a homogeneous ocean and that all vessel movements are along track (no motion stabilization). Because of the calm data collection day and near vertical beams we expect these inaccuracies to be small and that they will not affect the conclusions from this study.

We do bottom detection via the maximum amplitude instant method, commonly used near vertical incidence(Lurton, 2010). The technique uses the maximum amplitude instant as the arrival time for the bottom echo. Using this instant, combined with beam direction and propagation speed, we can calculate the bottom location.

4 Results and discussion

We applied uniformly weighted (or unweighted) DAS, kaiser ($\beta = 3$) weighted DAS, and LCA beamforming to the echosounder data across Holmengraa. Unweighted and kaiser weighted DAS are selected to give two versions of the resolution-sidelobe tradeoff. Uniform DAS gives good resolution at the cost of high sidelobes, while kaiser DAS ($\beta = 3$) gives medium sidelobe level (24 dB) and reduced resolution.

Figure 2 show all detections across Holmengraa for the three methods. We have calculated beams for every 0.3 degrees. This is approximately a factor 3

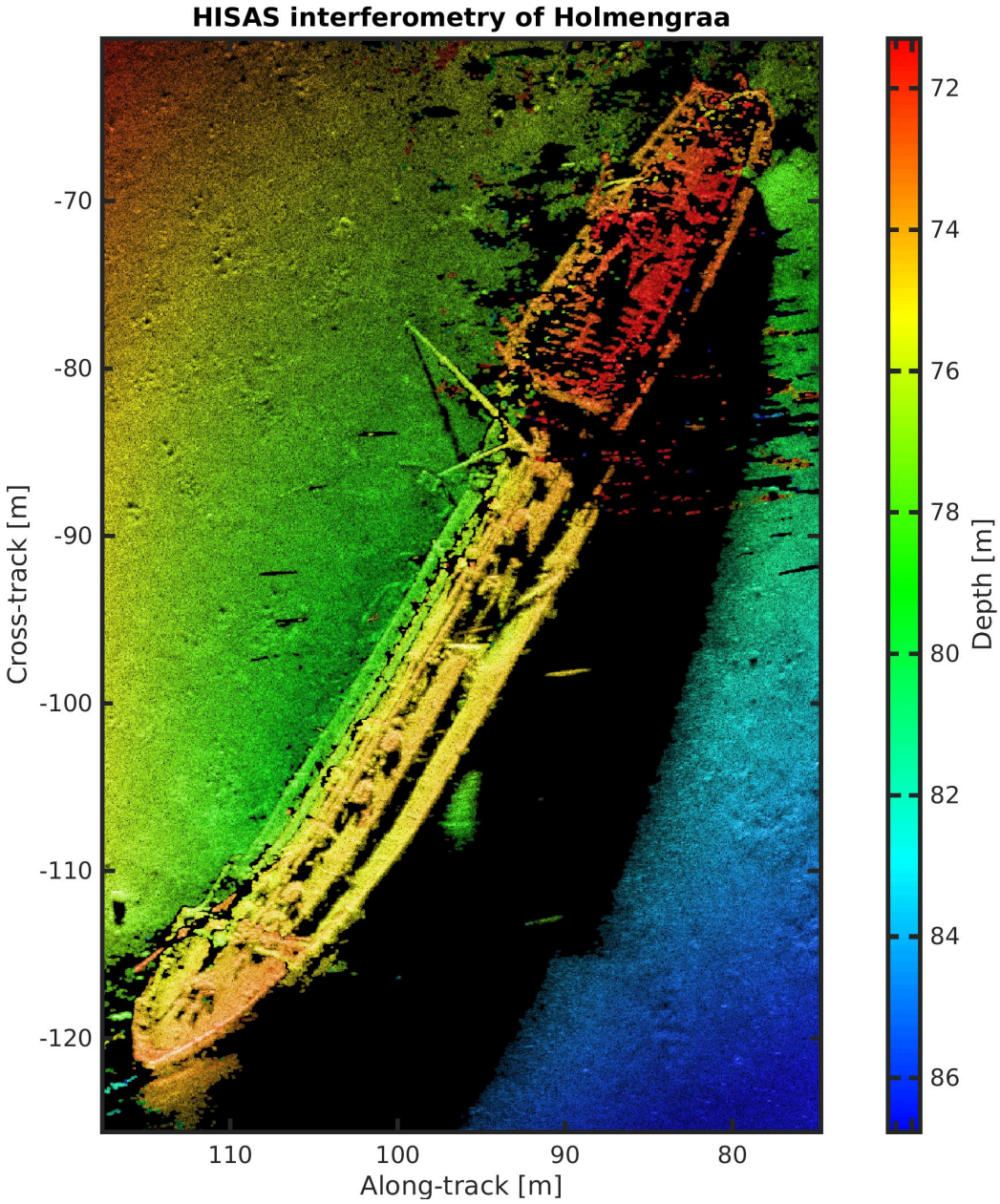

Figure 1: Interferometric SAS image of Holmengraa. Image by the Norwegian Defence Research Establishment (FFI).

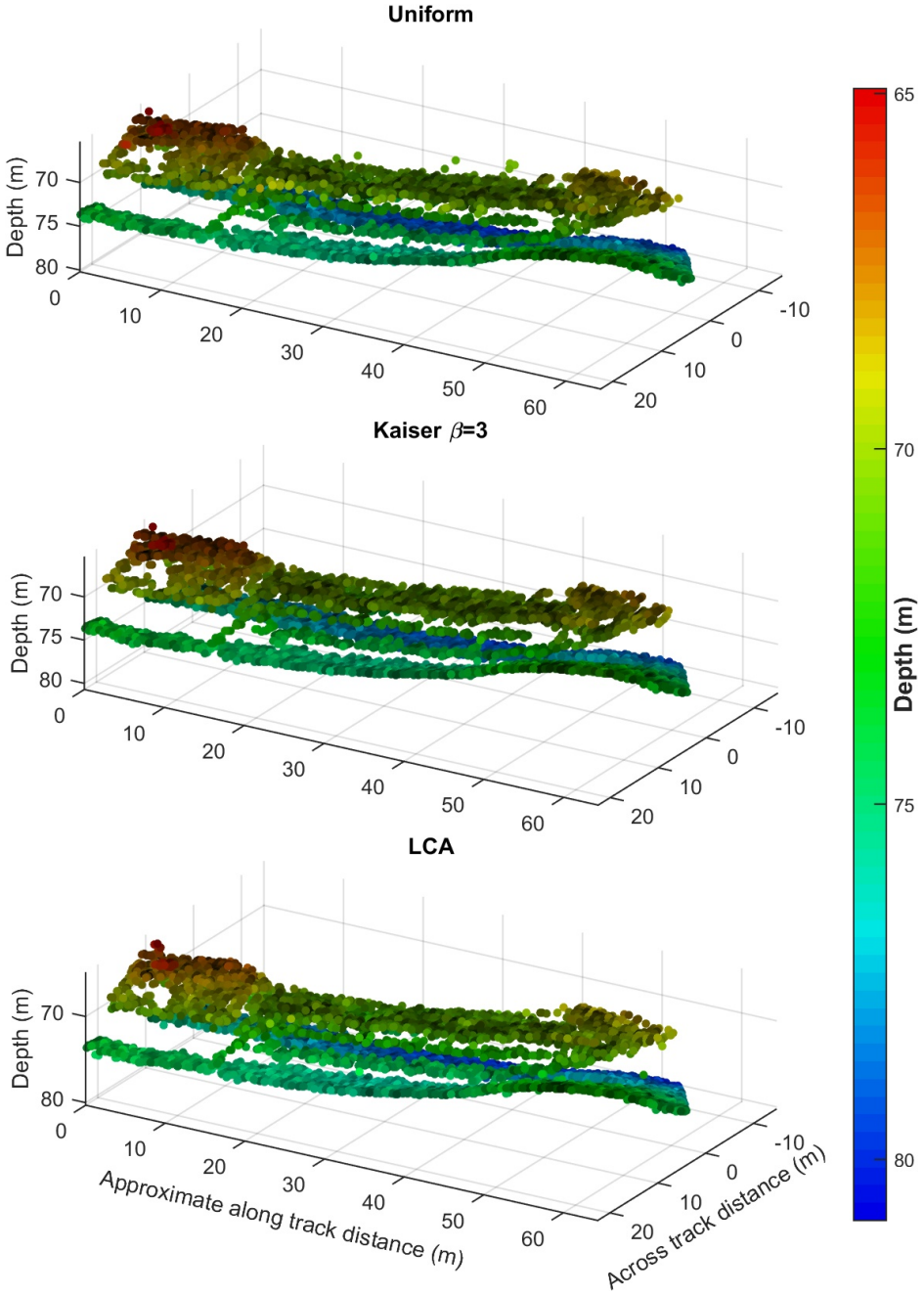

Figure 2: Scatterplot of amplitude detections from whole swath. Color indicate depth and brightness beam level for the detection instants. The along track distance has been approximated by moving each line according to the mean ping rate and vessel speed. Note that the average depth differ from Figure 1. This may be due to lack of tidal correction and/or transducer depth correction. Axis labels are the same in all three plots.

oversampling, which we have done since adaptive methods can achieve higher resolution than conventional methods.

The most apparent difference between the plots is that uniform weighted DAS have some outliers. Apart from the plots are very similar, but the keen eye may see a couple outliers for LCA that are not present for kaiser DAS. To explain the outliers and look closer on other effects we will examine three pings, shown in Figure 3, Figure 4 and Figure 5, in detail.

Figure 3 show a case with very strong backscatter from some areas. This give strong sidelobes for the uniform DAS beamformer, visible as light blue arcs at certain ranges. The sidelobes are stronger than the bottom echoes in this case, which causes misdetections and outliers in Figure 2. The distant misdetections are easy to identify, but the ones close to the right side of the wreck may be hard to identify.

By applying kaiser weighted beamforming we greatly reduce these sidelobes and consequently remove these misdetections. However, the widened mainlobe smear out the details and miss other features. For example, the hole at around 5 meters across track distance that were picked up by the uniform beamformer, is lost by the kaiser beamformer.

When using LCA we can get the best of both worlds. We get good sidelobe suppression, better than for the kaiser weighted DAS, while picking up the hole. LCA also gets significantly smaller extension, even when compared to uniform DAS, of what appears to be small sources at 2 meters across track distance and slightly above deck at 8 meters cross track distance (no detection on the latter for LCA). This enables the LCA detections to provide a better contour for the left side of the ship.

We see the same effects in Figure 4. There are strong sidelobe arcs for the uniform beams, which are lower or nonexistent for the kaiser and LCA beams. LCA seems to be able to resolve more details. Localized scatterers as the one to the top left of the deck have smaller extent for LCA. The LCA detections also give an more likely right edge for the wreck, while uniform and kaiser weighted DAS seem to be dominated by strong points in neighbor beams.

On the bottom to the left LCA seems to give a more probable shape for the seabottom than the other methods. The uniform and kaiser detections seem to lie in groups at constant range, indicating that neighbor beams are dominated by a strong center beam. To the far right we see a few outliers for LCA, more than for the kaiser weighted beams. The next figure has a clearer example of this.

Figure 5 shows an example were LCA seems to perform worse. At 15 meters

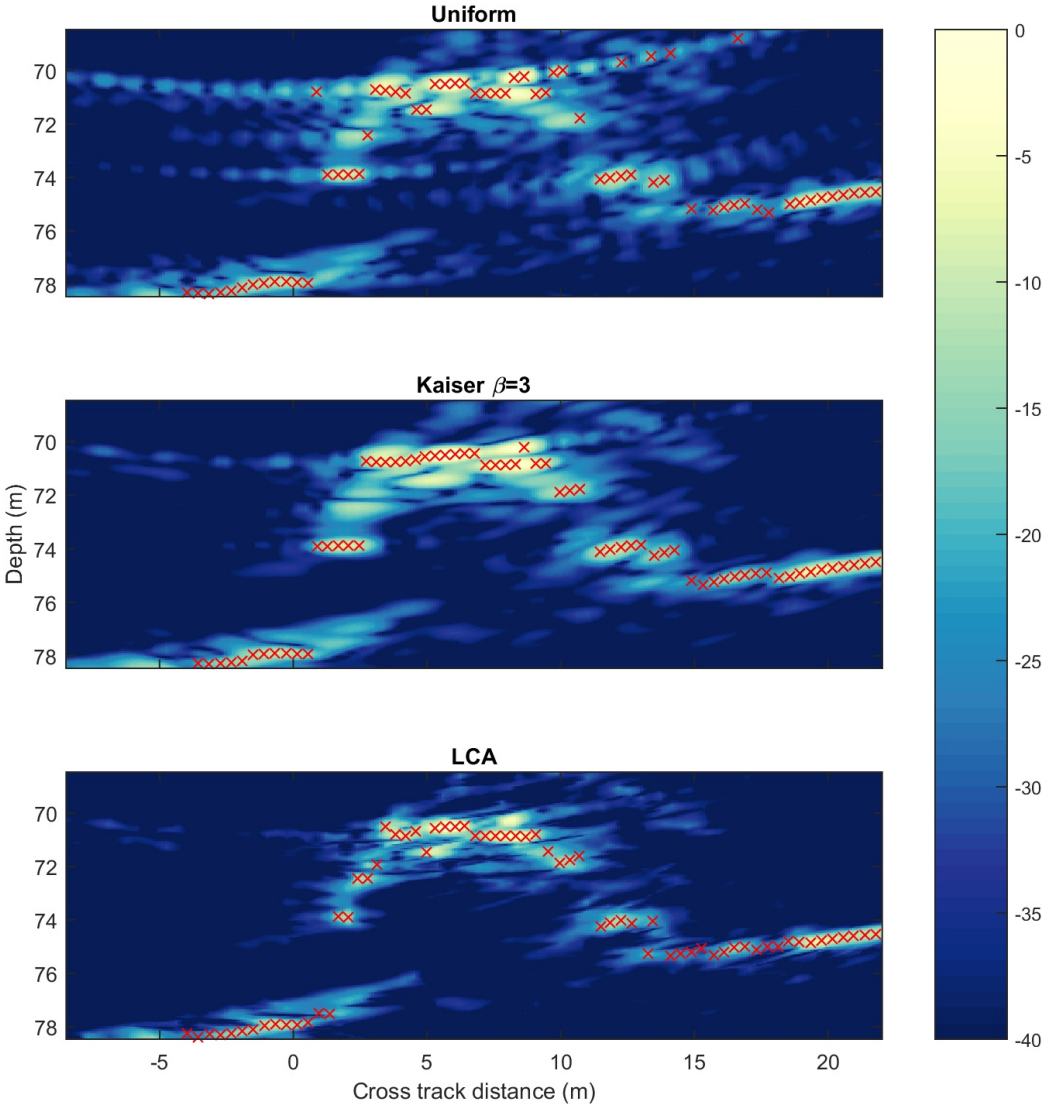

Figure 3: Beam power and bottom detections for different beamforming techniques on measured data, ping 33. Red crosses are amplitude detections. The colormap represent normalized beam power in dB. The strongest beam sample across the three beams is set to 0 dB.

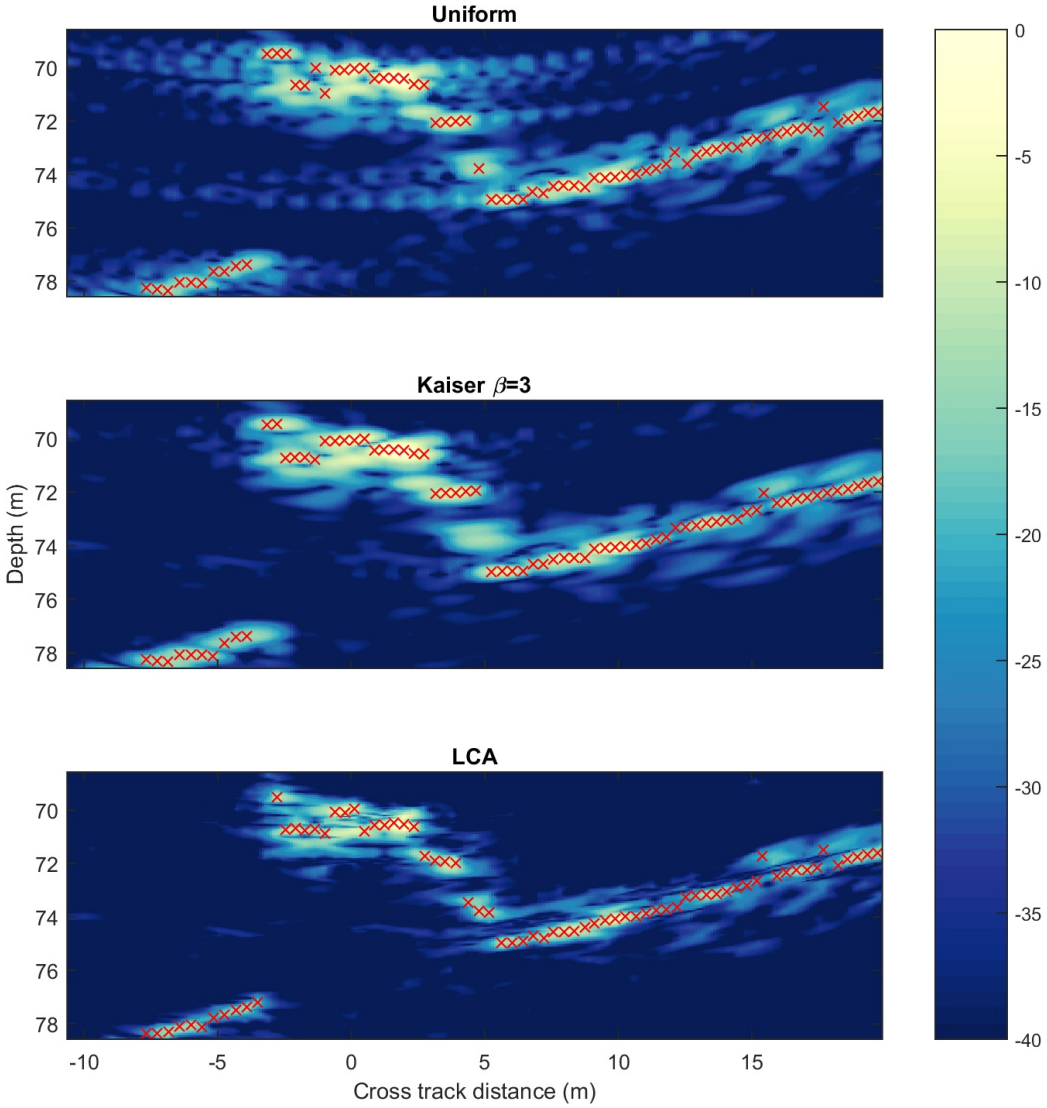

Figure 4: Beam power and bottom detections for different beamforming techniques on measured data, ping 74. Red crosses are amplitude detections. The colormap represent normalized beam power in dB. The strongest beam sample across the three beams is set to 0 dB.

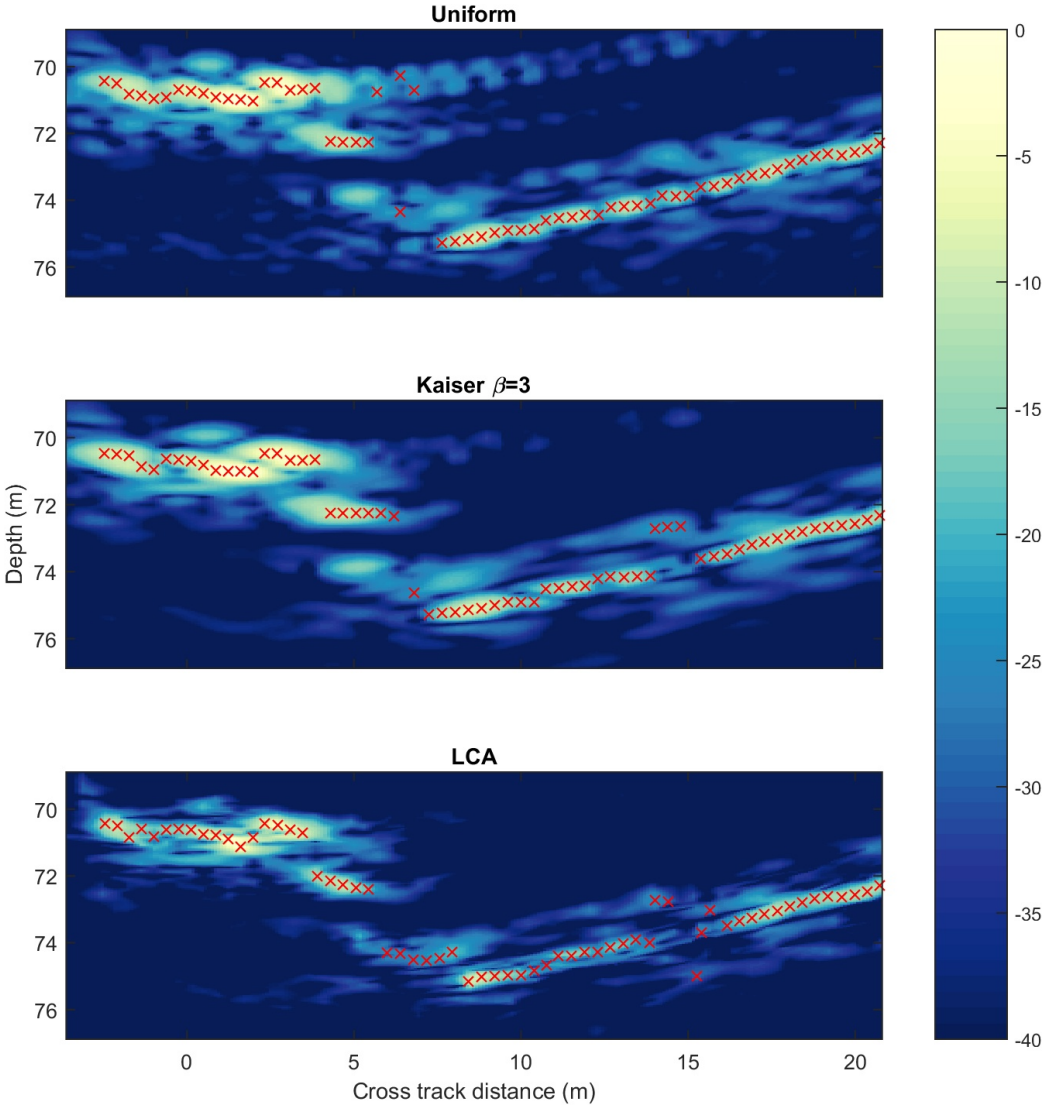

Figure 5: Beam power and bottom detections for different beamforming techniques on measured data, ping 69. Red crosses are amplitude detections. The colormap represent normalized beam power in dB. The strongest beam sample across the three beams is set to 0 dB.

cross track distance we see a two meter vertical spread in the LCA detections while the uniform detections follow a straight line. A few of the kaiser detections are a meter above the line, which seems to be bad but still better than LCA.

A probable explanation for this is that there is a spot in the seabottom with weak backscatter caused by low speckle. LCA choose weights steered towards this spot since it gives lower beam values. Therefore LCA gets very low beam values and badly localized detections, since we have not removed low-amplitude detections. The uniform detections are much better since the bottom lie at almost constant range. Therefore, the weak spot is filled in by sidelobes and we coincidentally get good detections. The wide mainlobe of the kaiser weighted DAS fills in the edges of the soft spot and gives only one location for the misdetections. Therefore, the LCA image may represent the bottom better, although these detections should be discarded. A more sophisticated bottom detector would probably identify this as bad detections and then it will be a separate task to fill the gap.

The examples we have shown are extreme cases that represent the effects we see throughout the dataset. For example, the strong sidelobe arcs for the uniform beams are prevalent in most pings, but usually do not result in the amount of misdetections we saw in Figure 3.

5 Conclusions

Accurate mapping of the seabed using active high frequency sonar is of importance in many applications. In this paper we have considered three different beamformers: Uniformly weighted (or unweighted) DAS, kaiser weighted DAS and LCA. We have compared their performance on data collected by a seabed mapping echosounder of a scene containing a shipwreck. As in our previous work(Lønmo et al., 2015), LCA seems give the best performance.

Uniform DAS gives high-resolution because of a relatively narrow mainlobe but have high sidelobes, which give misdetections and false features in the water column plot. Kaiser weighted DAS avoids the misdetections with lower sidelobes but misses other features and smear out edges because of a wider mainlobe. LCA appear to simultaneously give better resolution than the uniform weighted DAS and better sidelobe supression than kaiser weighted DAS. We see this as less sidelobes in the images, bottom detections that look more like a wreck contour and less like one beam dominating the neighbors, and smaller extension of localized targets.

LCA gives worse detections in some low amplitude areas, while uniform and kaiser weights DAS seem to perform better. However, it seems likely that LCA still gives a more representative image of the bottom, and that a more sophisticated detection algorithm would remove these detections.

Since we lack a true reference to verify this, these conclusions depend on our ability to guess the true structure of the scene. We feel that our interpretations are reasonable, but not infallible. Obtaining and comparing our result with high quality reference data is therefore a high priority for further work.

6 Acknowledgments

We would like to thank Bente Borgundvåg Berg, Jan-Atle Storesund and Kjell Echholt Nilsen for their efforts. They have been vital for data collection, processing and analysis. The colormap used for the ping plots is based on a map from www.ColorBrewer.org.

This work is sponsored by The Research Council of Norway.

References

Blomberg., A. E. A., Austeng, A., Hansen, R., & Synnes, S. (2013). Improving Sonar Performance in Shallow Water Using Adaptive Beamforming. *IEEE Journal of Oceanic Engineering*, *38*(2), 297–307. doi:10.1109/JOE.2012.2226643

Buskenes, J. I., Austeng, A., & Nilsen, C.-I. C. (2011). A Low Complexity Adaptive Beamformer for Active Sonar Imaging. In J. S. Papadakis & L. Bjørnø (Eds.), *Proceedings of the 4rd International Conference & Exhibition on Underwater Acoustic Measurements: Technologies and Results* (pp. 281–286). Greece.

Lønmo, T. I. B., Austeng, A., & Hansen, R. E. (2015). Low Complexity Adaptive Beamforming Applied to Sonar Imaging (Invited). In J. S. Papadakis & L. Bjørnø (Eds.), *Proceedings of the 3rd International Conference and Exhibition on Underwater Acoustics* (pp. 653–658). Crete, Greece. url: http://www.uaconferences.org/docs/Past_proceedings/UACE2015_Proceedings.pdf

Lurton, X. (2010). *An Introduction to Underwater Acoustics: Principles and Applications* (2nd ed.). Springer-Verlag Berlin Heidelberg.

Synnevåg, J.-F., Austeng, A., & Holm, S. (2007). Adaptive Beamforming Applied to Medical Ultrasound Imaging. *IEEE Transactions on Ultrasonics, Ferroelectrics, and Frequency Control*, *54*(8), 1606–1613. doi:10.1109/TUFFC.2007.431

Synnevåg, J.-F., Austeng, A., & Holm, S. (2011). A low-complexity data-dependent beamformer. *IEEE Transactions on Ultrasonics, Ferroelectrics and Frequency Control*, *58*(2), 281–289. doi:10.1109/TUFFC.2011.1805

Van Trees, H. L. (2002). *Optimum Array Processing*. Wiley-Interscience.

Paper III

Lønmo, T. I. B., Austeng, A., & Hansen, R. E. (2019b). Improving Swath Sonar Water Column Imagery and Bathymetry with Adaptive Beamforming. *IEEE Journal of Oceanic Engineering*. Early access. doi:10.1109/JOE.2019.2926863

Improving Swath Sonar Water Column Imagery and Bathymetry with Adaptive Beamforming

Tor Inge Birkenes Lønmo, Andreas Austeng, and Roy Edgar Hansen.

Abstract

Modern swath sonar is a mature technology today and has reached a very high level of sophistication including techniques to increase area coverage rate, data quality, and resolution. There is, however, often a need to explore features at the limit of what is resolvable. It is therefore of interest to consider alternative signal processing techniques for a given physical system. For the traditional Delay-And-Sum (DAS) beamformer there is a tradeoff between angular resolution and sidelobe suppression. Using either the Capon or the Low Complexity Adaptive (LCA) beamformer, the water column edge definition, sidelobe level, and resolution are improved compared to a moderately weighted DAS beamformer. These improvements are similar to recent results for sector-scanning sonar. This leads to improved performance for the amplitude-based center-of-gravity bottom detector. The Capon beamformer performs best, while LCA has a large part of the improvement with higher robustness and easier implementation. We use simulations to show the improvements of the adaptive beamformers from nadir up to 42° across track, and validate the results using field data. The improvements in the water column increase the separation between features and noise and collapse the apparent size of features down to more realistic dimensions. These improvements allow the adaptive beamformers to reveal features that are hidden for the DAS beamformer.

Keywords: *Adaptive beamforming, seabed mapping, bathymetry, swath sonar, low complexity adaptive beamforming, LCA, Capon.*

1 Introduction

Swath sonars are a central tool for exploring the oceans. Among their uses are collecting bathymetric data at large scales (Mayer et al., 2018), water column

(Clarke, 2006, 2017) and backscatter imagery (Lamarche & Lurton, 2018). A common challenge is that the scales of features of interest often are at, or close to, the limit of what can be resolved (Clarke, 2018). Artifacts from beamforming (sidelobes) may also introduce false detections and hide features in the water column (Clarke, 2006). Too large beamwidth may prevent satisfactory target detection at high incidence angles (Pereira & Clarke, 2015). It is therefore of continuous interest to improve the performance of swath sonars.

Current swath sonar processing includes a delay-and-sum (DAS) beamformer and two bottom detection methods: amplitude and phase (split beam interferometry) (Lurton, 2010, Ch. 8.3.3). The driving factor for the amplitude detection uncertainty is the received envelope length (Lurton & Augustin, 2010). It is largely determined by the beamwidth, effective pulse length and seafloor geometry. The DAS beamformers have an inherent tradeoff between beamwidth and sidelobe level (Harris, 1978), while improvements to both are desirable.

The Capon beamformer, also known as the Minimum Variance Distortionless Response (MVDR) beamformer, has for long been used in passive sonar to enhance performance (Cox, Zeskind, & Owen, 1987). It can improve resolution and interference rejection compared to DAS (Van Trees, 2002, Ch. 6). More recently, it has been applied to active sonar (Blomberg, Austeng, & Hansen, 2012; Lo, 2004) and medical ultrasound imaging (Synnevåg, Austeng, & Holm, 2009). The Capon beamformer has been used on swath sonars (Mitchley & Sears, 2014; Pantzartzis, de Moustier, & Alexandrou, 1993; Rønhovde, Yang, Taxt, & Holm, 1999), but robustness concerns and high computational load have limited the adoption (Lurton, 2010, Ch. 5.4.10).

The related robust and computationally inexpensive "Low Complexity Adaptive" (LCA) beamformer has also been proposed in medical ultrasound (Synnevåg, Austeng, & Holm, 2011) and used for sector-scanning and other sonars (Blomberg., Austeng, Hansen, & Synnes, 2013; Buskenes, Hansen, & Austeng, 2017). It provides a large part of the gain of the Capon beamformer while having a computational load and robustness close to DAS (Blomberg. et al., 2013; Buskenes et al., 2017; Synnevåg et al., 2011). Swath sonars have many common features to sector-scanning sonars. It is therefore interesting to investigate if improvements like in (Buskenes et al., 2017) can be achieved for swath sonars, and how they affect bottom detections. Results from preliminary studies indicate that both swath sonar water column imagery and bottom detections can be improved (Lønmo, Austeng, & Hansen, 2015a, 2015b).

In this study, we show that the Capon and LCA beamformers can simultane-

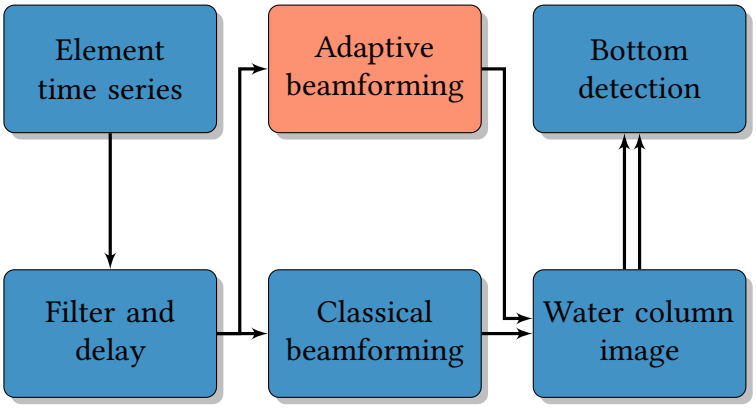

Figure 1: Overview standard and adaptive processing chain. The adaptive beamformers use the same data as the DAS beamformer, and the results from each beamformer are processed in the same way. This ensures that differences can be attributed to the beamformers.

ously improve resolution, edge definition and sidelobe level in the water column image from swath sonars. This reduces bias and variance for amplitude detections and brings better resolution and edge definition. The improved edge definition of the adaptive beamformers is central to these results, and we have adapted the LCA beamformer to take advantage of this. We argue that these gains can improve swath sonar bathymetry from the specular direction until a delayed phase detection transition, and where phase detections fail. We show that the adaptive beamformers may reveal features which are hidden when using the DAS beamformer. We validate the adaptive beamforming techniques on data collected by a state-of-the-art swath sonar.

We initially describe our processing chain and the essentials of our beamformers and detector. Then we describe the simulation method, scenes and results, followed by field results and discussion.

2 Signal processing

We process our data with a standard swath sonar processing chain (Lurton, 2010, Ch 8.3). We vary the beamforming step as described below while keeping all the other parts identical. This is illustrated in Figure 1.

Below we give a brief description of the beamformers we use, swath sonar bottom detection and a comparison of the relevant beamformer properties.

2.1 Classical DAS beamforming

DAS beamforming (Johnson & Dudgeon, 1993) is the standard beamforming method for current swath sonars (Lurton, 2010, Ch 8.3.2). It algorithmically steers the array by delaying the signal from each element such that the signal from the steering direction (far field) or point (near field) add coherently, while others sum incoherently. The delays may be approximated by phase rotation for narrow band signals and small enough steering angles (Johnson & Dudgeon, 1993). The DAS beamformer is typically weighted (also called shaded or tapered) to better suppress interfering signals by lowering the sidelobe level. This reduces resolution and edge definition due to a wider mainlobe (Harris, 1978). The resulting beam time series $b^{(\theta)}(t)$ steered toward the angle θ is given by

$$b^{(\theta)}(t) = \mathbf{w}^H \mathbf{s}^{(\theta)}(t) = \begin{bmatrix} w_1 \\ w_2 \\ \vdots \\ w_{N_{\text{El}}} \end{bmatrix}^H \begin{bmatrix} s_1^{(\theta)}(t) \\ s_2^{(\theta)}(t) \\ \vdots \\ s_{N_{\text{El}}}^{(\theta)}(t) \end{bmatrix}, \tag{8.1}$$

where N_{El} is the number of elements, w_i is the weight for element i and $s_i^{(\theta)}$ is the signal from element i at time t, after it has been delayed toward θ, and $\bullet^H$ indicates the complex conjugate transpose. The steering angle θ is 0 toward nadir and is equal to the incidence angle for a horizontal seafloor. DAS's advantages are speed, simplicity and robustness.

We use Kaiser weights with $\beta = 2.5$ for our DAS beamformer. This weight set has a decent tradeoff between sidelobes and mainlobe. The variations we have observed between differently weighted DAS beamformers are small compared to the differences between DAS and the adaptive beamformers.

2.2 Capon beamforming

The adaptive Capon beamformer (Van Trees, 2002, Ch. 6), (Krim & Viberg, 1996) is known for having better resolution and interference rejection capabilities than the standard DAS beamformer. The key difference between an adaptive beamformer as Capon, and DAS is that the weights $\mathbf{w}_{Capon}^{(\theta)}(t)$ now depend on steering angle and time. This allows for enhanced performance by dynamically adjusting the beampattern to the present signal conditions.

Capon selects the weights by minimizing the variance of the beamformed

signal without distorting signals from the steering direction. For pre-delayed signals this can be expressed as:

$$\mathbf{w}_{Capon}^{(\theta)}(t) = \arg\min_{\mathbf{w}} E\left|\mathbf{w}^H \mathbf{s}^{(\theta)}(t)\right|^2 \tag{8.2}$$

$$= \arg\min_{\mathbf{w}} \mathbf{w}^H R^{(\theta)}(t)\mathbf{w}, \tag{8.3}$$

$$\text{under the constraint that } \sum_{i=1}^{N_{\text{El}}} w_i = 1, \tag{8.4}$$

where $R^{(\theta)}(t) = E\left(\mathbf{s}^{(\theta)}(t)\mathbf{s}^{(\theta)}(t)^H\right)$ is the steered covariance matrix (Krolik & Swingler, 1989). The beam time series can then be obtained by (8.1).

Capon's main drawbacks compared to DAS are potentially lower robustness (Cox et al., 1987) and higher computational demands (Lurton, 2010, Ch. 5.4.10). The main sources of the robustness problems are signal model mismatch and difficulties with estimating the covariance matrix R.

To ensure sufficient robustness we use spatial smoothing (Lo, 2004; Shan, Wax, & Kailath, 1985; Synnevåg et al., 2009) over $N_{\text{El}}/2$ elements, forward-backward averaging (Lo, 2004; Rao & Hari, 1990; Rønhovde et al., 1999) and diagonal loading (Carlson, 1988; Cox, 1973) equal to 5 % of the mean signal energy. The signal statistics may change quickly for our case, so we do not use time averaging (Llort-Pujol, Sintes, Chonavel, Morrison, & Daniel, 2012; Rønhovde et al., 1999). Based on earlier work (Austeng et al., 2008; Buskenes et al., 2017; Synnevåg, Austeng, & Holm, 2007) we consider this to be a relatively robust set of parameters that will work well for our application.

2.3 Low Complexity Adaptive (LCA) beamforming

LCA (Buskenes et al., 2017; Synnevåg et al., 2011) is a relatively new adaptive beamformer, first used in medical ultrasound. With a small weight set, LCA can give a large part of the improvement from Capon without important drawbacks (Buskenes et al., 2017; Synnevåg et al., 2011). It can be viewed as a hybrid between Capon and DAS. LCA, as Capon, minimizes the variance and obeys the distortionless constraint. The difference is that while Capon can select almost any weight, LCA is restricted to a pre-selected weight set $\mathcal{W} = \{\mathbf{w}^1, \mathbf{w}^2, \ldots, \mathbf{w}^{N_{\text{LCA}}}\}$, where N_{LCA} is the number of weights in the set. LCA beamforming may also be interpreted as selecting the apparently best beam value from differently weighted DAS beamformers according to the Capon optimality criteria.

Table 1: Weight parameters for our LCA weight set. The Kaiser β parameter controls sidelobe level and ϕ describe the amount of microsteering compared to the 3 dB beamwidth $\phi_{3dB}(\beta)$ with the given β. Full description in (Buskenes, Hansen, & Austeng, 2017), which proposed this weight set class.

Kaiser β	Microsteering amount ($\phi/\phi_{3dB}(\beta)$)
0 (Rectangular)	$0, \pm 0.9, \pm 1.8$
2.5	$0, \pm 0.9, \pm 1.8$
5	$0, \pm 0.9, \pm 1.8$

The LCA weight set contains standard DAS weights and *microsteered* (Synnevåg et al., 2011) weights. Microsteered weights mimic certain asymmetric beampatterns used by the Capon beamformer, which particularly improves the edge definition (Synnevåg et al., 2011). Microsteering requires that small, additional, delays are applied after beam steering. We apply them by phase rotation.

The pre-selected weight set makes LCA inherently more robust than Capon. As an example, the limited weight set prevents signal cancellation (Synnevåg et al., 2011), which is potentially detrimental for Capon (Van Trees, 2002). This reduces the need for additional constraints on LCA (Synnevåg et al., 2011). In this paper we use LCA without any of the modifications applied to Capon. The LCA weight is selected by:

$$\hat{\mathbf{w}}_{LCA}^{(\theta)}(t) = \underset{\mathbf{w}\in\mathcal{W}}{\arg\min} \left|\mathbf{w}^H \mathbf{s}^{(\theta)}(t)\right|^2. \tag{8.5}$$

Our weight set is described in Table 1. The set was initially selected based on existing examples (Buskenes et al., 2017; Synnevåg et al., 2011), and tuned for swath sonars based on observed performance. The main difference from (Buskenes et al., 2017; Synnevåg et al., 2011) is increased microsteering.

2.4 Bottom detection

Swath sonars may use multiple bottom detection schemes (Lurton, 2010, Ch. 8.3.3). Commonly, amplitude detections are used near specular directions and phase detections are used at higher incidence angles. Amplitude detections are also used when the phase detector fails (Lurton, 2010, Ch. 5.4.10). For example, if there are multiple targets at the same slant range, either within the beam or in a sidelobe that is not sufficiently suppressed.

The location of the transition angle, where the system switches between

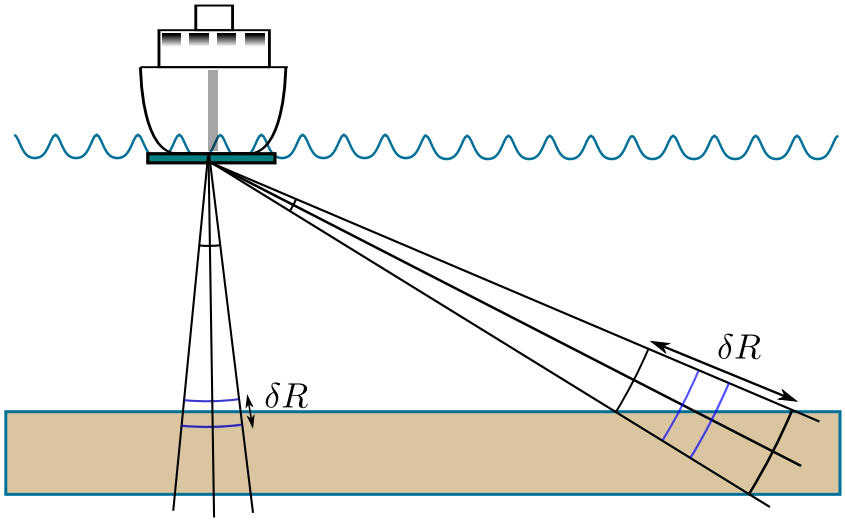

Figure 2: Illustration of pulse- (left) and beam-determined (right) regimes for received envelope length (not to scale). Blue arcs show the effective edges of the pulse (after processing) at a given instant, δR shows the distance corresponding to the received envelope length. At vertical incidence the whole beamwidth is illuminated approximately simultaneously, and the pulse length determines δR. At high incidence angles the pulse length is short compared to the footprint, and the time needed for the pulse to travel across the beam footprint determines δR.

phase and amplitude detections, varies depending on system, signal-to-noise ratio (SNR), scene, detector configuration and transition criteria (Hare, Godin, & Mayer, 1995; Llort-Pujol et al., 2012; Lurton & Augustin, 2010). It may be as low as $\pm 10°$ (Clarke, 2018), or as high as $45°$ (Lurton & Augustin, 2010).

We use a center of gravity (barycenter) detector based on the envelope between the -10 dB points around the peak (Lurton & Augustin, 2010). We use a Hamming (Harris, 1978) shaped averaging filter with same length as the transmitted pulse for selecting the -10 dB points.

For a given swath sonar configuration, the amplitude detection accuracy is determined by the envelope length after processing (Lurton & Augustin, 2010). The envelope length is determined by effective pulse length, beamwidth and seabed geometry (Lurton, 2010, Ch. 8.3.3.2). The typical regimes for a flat seafloor are illustrated in Figure 2. A reduced beamwidth improves amplitude detections, especially at high incidence angles.

Low sidelobe levels are important to avoid false detections with the amplitude detector, which may happen when an echo in a sidelobe is stronger than the

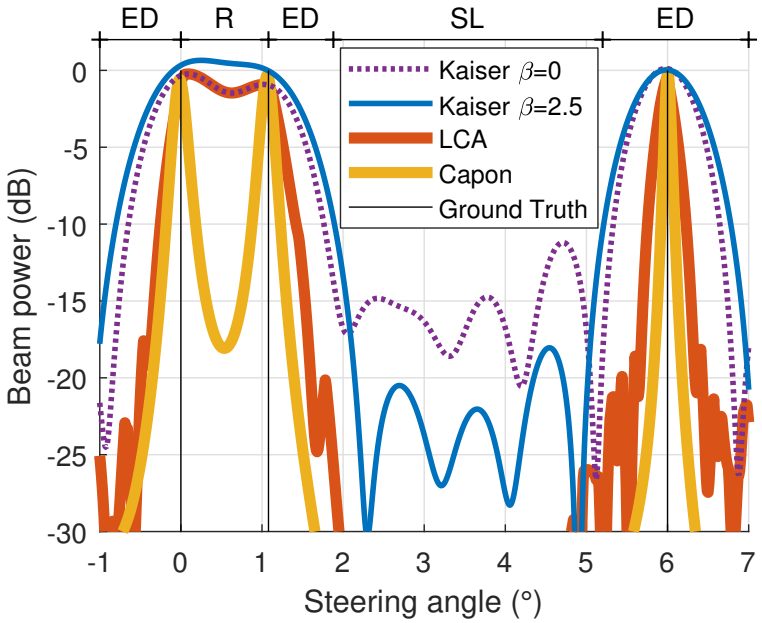

Figure 3: Beamformer steered response for a simplified scenario with 3 equal strength sources and 10 dB SNR. Text above indicates which beamformer property that is most important in each region. R: Resolution, ED: Edge Definition, SL: Sidelobe Level.

seafloor echo. Typical cases where this may be a problem is for strong specular echoes or with large differences in scattering strength across the seafloor (Lurton, 2010, Ch. 8.3.3).

2.5 Comparison of beamformer properties

To prepare for later analysis we provide a comparison of the most important beamformer properties for our study: Resolution, edge definition and sidelobe level.

Figure 3 shows how the DAS, LCA and Capon beamformers work in a simplified case with three equal strength sources and 10 dB SNR. There are one isolated and two closely spaced sources, their directions are shown by the black vertical lines.

Resolution is the ability to separate closely spaced sources. It is illustrated by the region marked "R" in Figure 3. Capon easily resolves the two points, Kaiser $\beta = 0$ DAS and LCA barely resolve the points, while Kaiser $\beta = 2.5$ DAS does not resolve them.

Edge definition describes the steepness of the steered response at the sides of an isolated point or object. For the DAS beamformer, resolution and edge definition are both determined by the mainlobe width. For adaptive beamformers, the two concepts are uncoupled, as the regions marked "ED" in Figure 3 show. We see that although LCA has the same resolution as the best-case ($\beta = 0$) DAS, the edge definition is almost as good as Capon's.

A convenient way to describe the edge definition and resolution improvements is that the adaptive beamformers reduce the *effective beamwidth*. For our purposes the effective beamwidth has essentially the same role for the adaptive beamformers as the beamwidth for DAS, for example in determining amplitude detection accuracy. It is important to note that the effective beamwidth varies across the scene.

Sidelobe level describes how strongly the beamformer suppresses signals from directions different from the steering direction and is illustrated in the sidelobe region marked "SL" in Figure 3. The sidelobe level of the weighted ($\beta = 2.5$) DAS beamformer is lower than the unweighted ($\beta = 0$), illustrating the tradeoff with DAS weighting. The adaptive beamformers have much lower sidelobe levels than both DAS beamformers, in addition to the edge definition and resolution improvements described above.

Real transducers have errors which make the actual signal model different from the one presented earlier. This affects the beamformers, and properties above, to a different degree. For DAS, the mainlobe is very robust against such errors, while the sidelobes are more sensitive (Steinberg, 1976, Ch. 13). In practice, model mismatch effectively limits the lowest attainable sidelobe level.

LCA selects one of a set of DAS beamformers, therefore LCA's sensitivity is linked to DAS's. Resolution and edge definition improvements are linked to the mainlobe of the underlying DAS beamformers, and should therefore be less sensitive to model mismatch than the sidelobe level. Model mismatch can be detrimental for the Capon beamformer if not properly accounted for (Cox, 1973; Li, Stoica, & Wang, 2003).

As this example shows, adaptive beamformers may avoid the tradeoff inherent to DAS and may improve all properties simultaneously. We will use the results from this example to explain the improvements of the adaptive beamformers in the simulated and field examples below.

3 Simulation method

Our simulation program is built around Field II (Jensen, 1996; Jensen & Svendsen, 1992), a point-based simulator well regarded in the medical ultrasound community. Field II can provide element time series for a given set of scatterers and transmit and receive arrays.

We model the seafloor segments as a collection of points with uniform directivity and Gaussian scattering strength. The points are initially distributed on a grid to ensure an even coverage of every resolution cell. Random position changes on the order of a wavelength are added to the point scatterers to emulate a rough seafloor. This assumes a seafloor that is rough compared to the wavelength. The point density is chosen to get fully developed speckle. We have not adjusted the absolute scattering strength to physically meaningful levels since only relative values are important for our analysis.

We model a swath sonar with the standard Mill's cross geometry (Lurton, 2010, Ch. 8.3.2). For faster simulations we replace a long transmit-array with a single element and model the transmit beampattern by limiting the along track extent of the seafloor to $0.7°$. We transmit a 100 μs Hanning (Harris, 1978) shaped pulse with center frequency of 300 kHz. We add Gaussian noise to the simulated element data before doing receiver processing. The element SNR ranges from roughly 20 dB at nadir to around -5 dB at $40°$. We have only seen minor changes in accuracy when adjusting the noise level, and therefore use a constant value. These and the remaining parameters are summarized in Table 2. The parameters were chosen based on (Lurton, 2010) and historical survey data.

4 Simulation results

In this section we introduce simulated results from three scenarios intended to highlight different aspects of beamformer and detector performance relevant for swath sonars. All these results are based on 100 simulated pings. For each ping we perform beamforming and bottom detection for every $0.1°$ between nadir and $40°$. We oversample in angle since adaptive beamformers may attain higher resolution (Åsen, Austeng, & Holm, 2014). The water column plots are incoherently averaged to reduce speckle and better show the performance trend.

Table 2: Simulation parameters

Parameter	Value
Center frequency	300 kHz
Pulse length	100 μs
Pulse type	CW
Pulse shaping	Hanning (Harris, 1978)
Sound speed	1500 m/s
Depth	$\approx$ 40 m (See Figure 4)
Number of elements	128
Element spacing	$\lambda/2$
Attenuation	65 dB/km
Element SNR	$\approx$ -5 to 20 dB
Simulation region	$0.7^\circ \times 120^\circ$

4.1 Flat, stepped seafloor. Step width 5 m, step height 1 m.

The simulated seafloor is shown in Figure 4. This case establishes baseline performance on a flat seafloor while also highlighting performance at sharp edges.

Figure 5a shows the mean water column image for the Kaiser weighted DAS beamformer with $\beta = 2.5$, and the adaptive LCA and Capon beamformers. The adaptive beamformers show a much thinner apparent seafloor, while simultaneously reducing the sidelobe level. The thinning effect is larger at higher steering angles (larger across track distance). Capon produces a somewhat thinner seafloor than LCA.

Figure 6 shows that DAS, LCA and Capon separate most distant seafloor segments by 4.1 dB, 7.7 dB and 22.7 dB respectively. It also shows that both LCA and Capon have a much sharper decay at the outer edges of the segments. Note the similarity to the resolution example in Figure 3.

Figure 5b shows the mean detected depth and root-mean-square depth error (RMSE) for the amplitude detections. The mean depth is similar across all beamformers, but not identical.

We note two subtle differences. The DAS beamformer tends to smooth the edges compared to the adaptive beamformers. In addition, the mean value for the DAS beamformer is somewhat noisier at the highest steering angles.

The RMSE curves in Figure 5b roughly consist of near-linear trends with intermittent peaks for all beamformers. The trends represent the flat-seafloor performance, while the peaks are due to the steps.

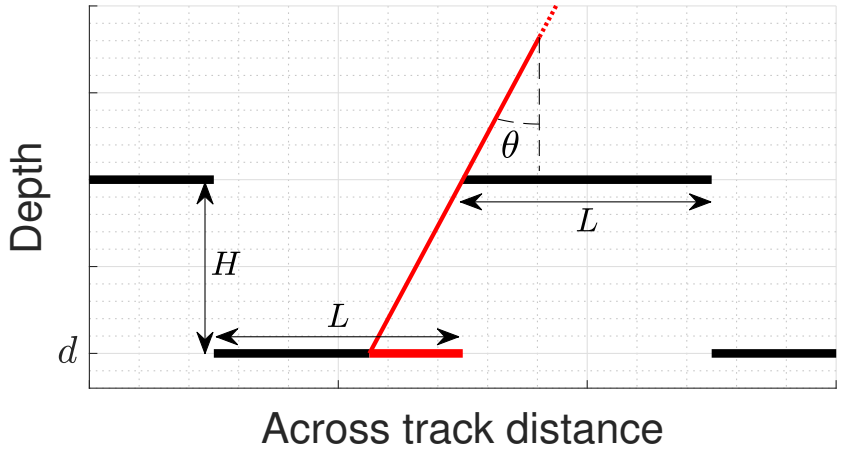

Figure 4: Sketch of part of stepped seafloor (not to scale). Black lines show the areas where points are located. The thin red line shows a beam direction with steering angle θ. Red part of the seafloor is removed due to shadowing, L is the length of each seafloor segment, H is the step height and d is the depth of the lower part of the seafloor. We use $L = 5m$, $H = 1m$, and $d = 40m$.

All beamformers have similar RMSE near nadir. DAS starts to have a barely higher RMSE than the adaptive beamformers after the first peak, a difference that quickly grows as the steering angle increases. LCA starts to have barely higher RMSE than Capon around the third peak. The difference grows with steering angle, but slower than for DAS, so the LCA RMSE trend stays closer to Capon than to DAS.

The main deviation from these trends is the peaks in the RMSE around the steps. The peaks are wider for DAS than for the adaptive beamformers, and LCA has slightly wider peaks than Capon.

LCA also has a rise in RMSE around the peaks near the $30°$ and $40°$ steps. The angles affected correspond to the ranges where echoes from the neighboring seafloor segment interfere. Capon has a similar, but smaller, rise only at the latter step.

4.2 Sinusoidal seafloor. Period 5 m, amplitude 1 m.

This case highlights the beamformer performance on gradually varying seafloors and the effect of different slopes.

Figure 7a shows the mean water column image. As before, the adaptive beamformers show a thinner apparent seafloor, with advantage to Capon, and

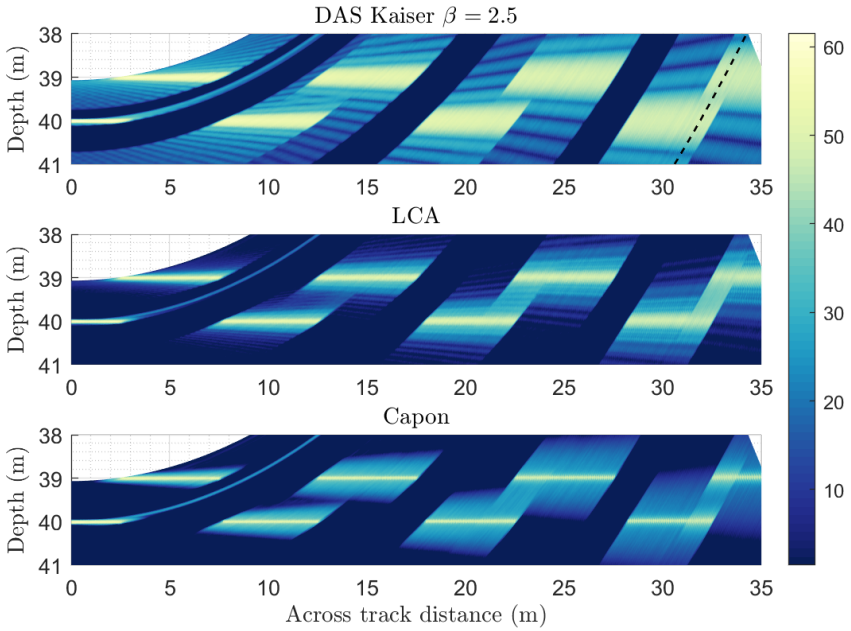

(a)

Figure 5: (Part 1 of 2) (a) Incoherently averaged water column power (dB). Stepped seafloor as sketched in Figure 4 with $L = 5$ m step width and $H = 1$ m step height. Based on 100 simulated pings. Absolute power level is arbitrary. The dashed line to the right of the DAS plot in (a) indicates the location of the cross section in Figure 6. [This figure has a part (b) below.]

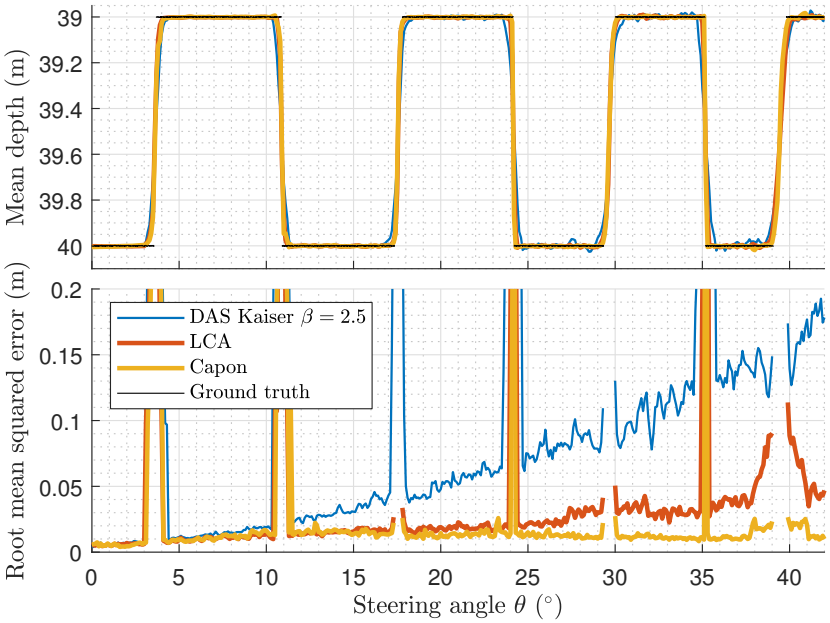

(b)

Figure 5: (Part 2 of 2) (b, top) Mean depth and (b, bottom) RMSE for the detections. When stepping up, as at 30°, a few beams do not hit any seafloor segment and thus have no true depth. These beams have been omitted in the RMSE plot. The RMSE in the high peaks are not representative for the accuracy, due to detections on both the upper and lower segment. However, the width of the peaks indicates the edge definition. [This figure has a part (a) above.]

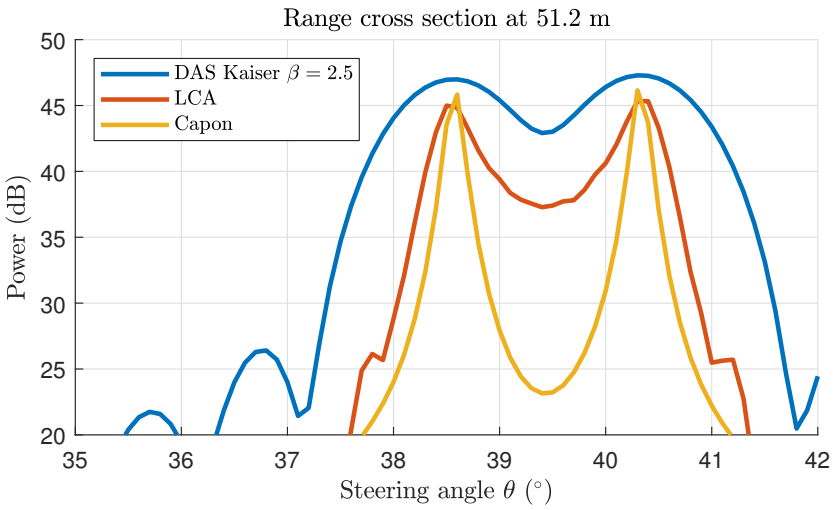

Figure 6: Slant range cross section at the most distant seafloor step of Figure 5a. Location shown by the dashed line in Figure 5a. Note the similarity to the resolution example in Figure 3.

lower sidelobes. However, in this case the difference in apparent seafloor thickness oscillates instead of the gradual increase seen in the previous case. The changes follow the oscillation of the seafloor, with only minor differences at the up-slope and largest differences at the down-slope.

Figure 7b shows the mean detected depth and RMSE for this case. The mean depth is similar for all beamformers. The differences in RMSE also oscillate. They follow the differences in apparent seafloor thickness from Figure 7a. The peaks in the RMSE oscillation are much lower for the adaptive beamformers compared to DAS, and Capon is better than LCA.

4.3 Sinusoidal seafloor. 1 m period , 10 cm amplitude.

This case highlights the beamformer performance close to the DAS resolution limit. The wave dimensions correspond to $\sim 2.5\%$ and $\sim 0.25\%$ of depth, which are at the lower limit of features of interest for swath sonars (Clarke, 2018).

Figure 8a shows the mean water column image. As before, the adaptive beamformers show a thinner apparent seafloor and lower sidelobes. The thinner apparent seafloor allows the adaptive beamformers to reveal the sinusoidal seafloor structure, which is hard to see with the DAS beamformer.

Figure 8b shows the mean detected depth and RMSE. The detections are

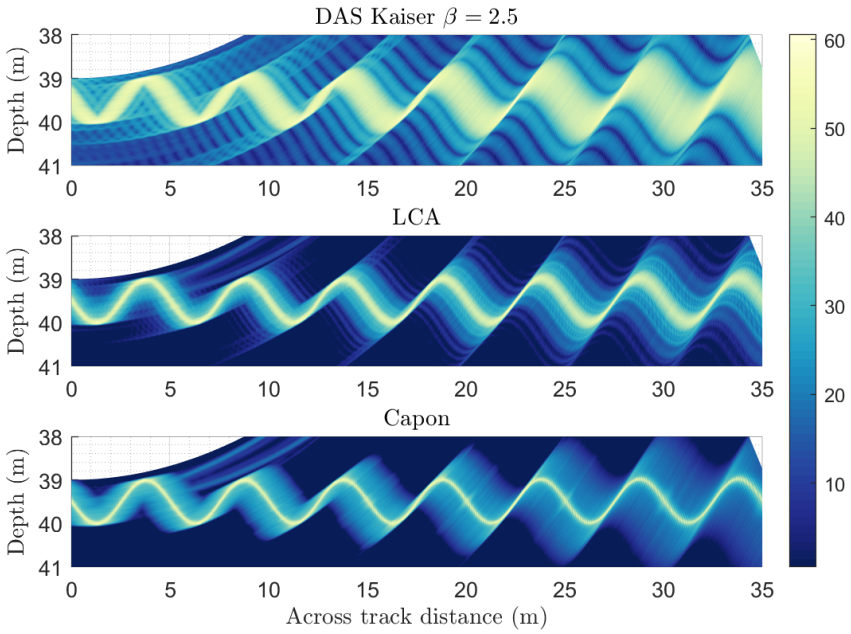

(a)

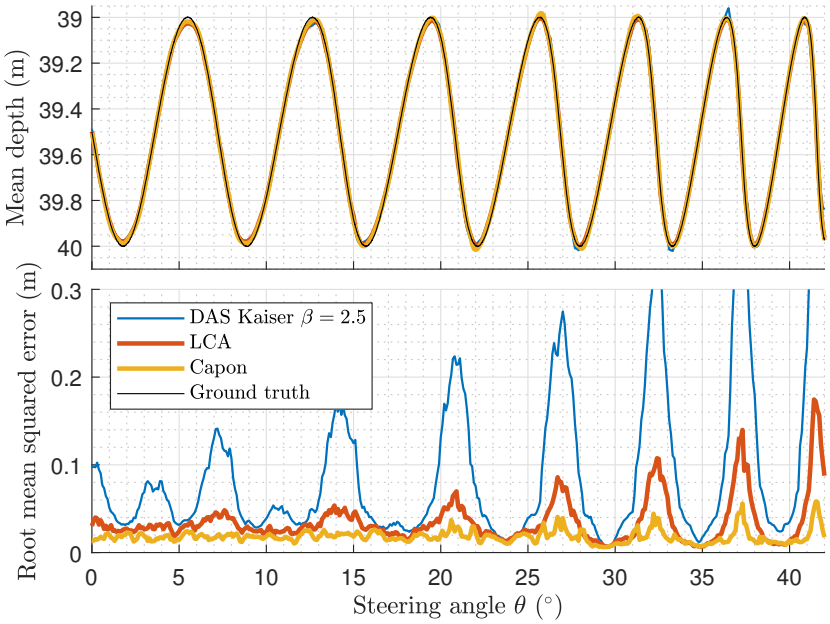

(b)

Figure 7: (a) Incoherently averaged water column power (dB), (b, top) mean depth and (b, bottom) RMSE for the detections. Sinusoidal seafloor with 5 m period and 1 m peak-to-peak amplitude. Based on 100 simulated pings. Absolute power level is arbitrary.

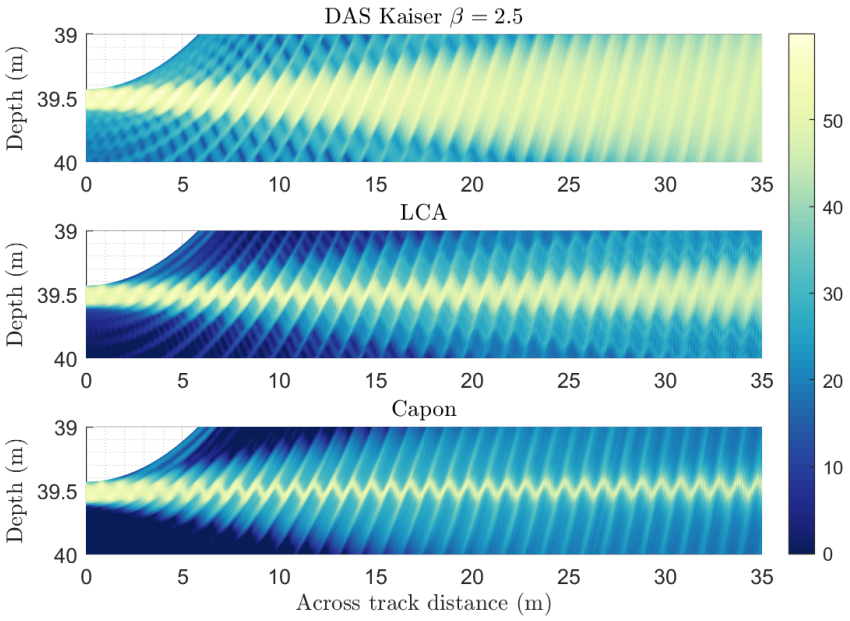

(a)

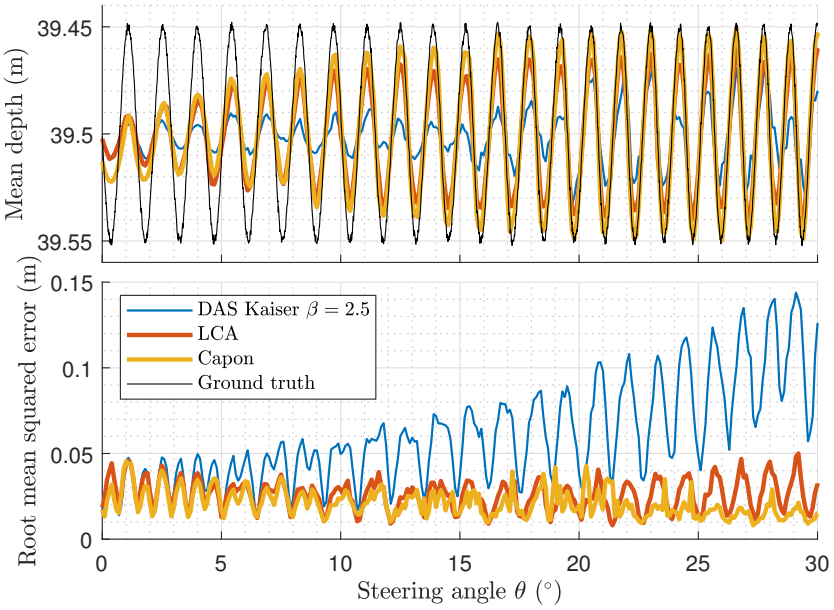

(b)

Figure 8: (a) Incoherently averaged water column power (dB), (b, top) mean depth and (b, bottom) RMSE for the detections. Sinusoidal seafloor with 1 m period and 10 cm peak-to-peak amplitude. Based on 100 simulated pings. Absolute power level is arbitrary. Figure 9 shows the effect of these improvements at a glance. Note that the axis limits differ from the previous figures.

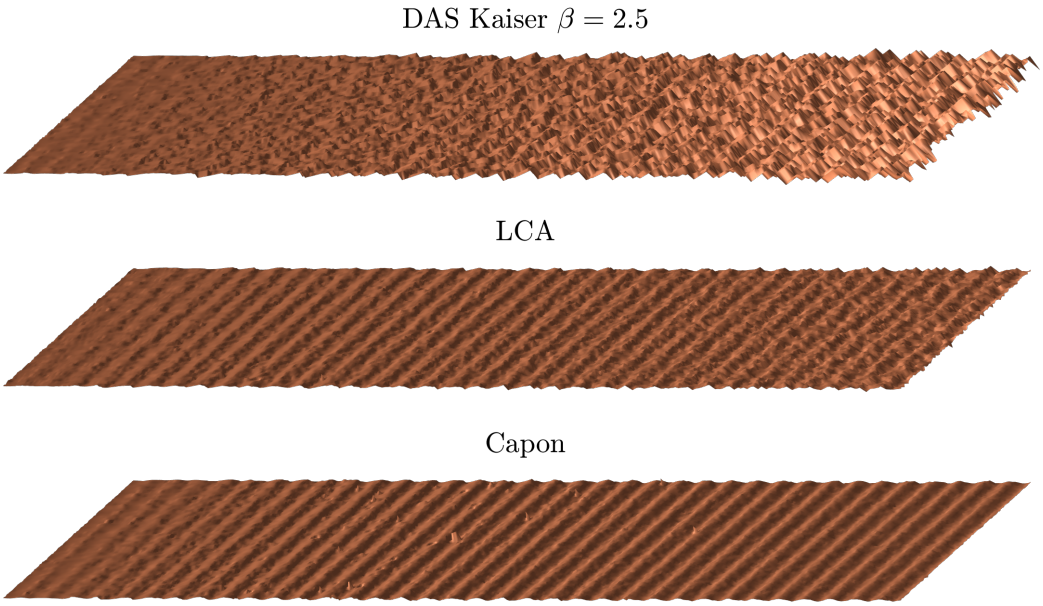

Figure 9: Sun-illuminated plot of stacked detections from 100 simulated pings over a sinusoidal seafloor with period 1 m and peak-to-peak amplitude 10 cm. Nadir is to the left, the right edge is at $42°$ steering angle. Same data as in Figure 8. The sinusoidal seafloor structure is clearly visible with LCA and Capon, while hard to see with DAS. Capon has a few outliers, which we believe a more advanced detector would avoid.

biased toward the average depth for all beamformers, however the bias is quickly reduced for the adaptive beamformers as the steering angle increases. Capon converges to lower bias than LCA. Similarly, the RMSE is lower for the adaptive beamformers after about $3°$ steering angle with an advantage to Capon at the highest angles. Capon also has lower bias and somewhat lower RMSE in the immediate neighborhood of nadir.

Figure 9 shows the effect of the detection improvements at a glance. The wave pattern on the seabed is largely hidden by the DAS beamformer and clearly shown by the adaptive beamformers. It is barely visible for all beamformers near nadir.

Capon has larger outliers than LCA in Figure 9. We found them to be artefacts due to a lack of threshold filtering in our amplitude detector.

5 Field results

To complement and validate our simulated results, we have used the same beamformers on field data collected with a swath sonar comparable to the one simulated. Data courtesy of the Canadian Hydrographic Service. Collected August 2016 near Sidney, BC, Canada .

5.1 The wreck of HMCS Mackenzie

(a)

Figure 10: (Part 1 of 3) (a): HMCS Mackenzie while in service. HMCS Mackenzie now serves as an artificial reef and the red box indicates the area imaged. (b, c, d): Water column power (dB) for DAS and the adaptive beamformers respectively. The water column images show parts of the rear mast, cables attached to the mast, deck and likely a davit (lower left part of deck). The wreck is surrounded by what we expect to be marine organisms. The dotted red ellipses show two regions with high density of them. Absolute power level is arbitrary. Photo by PH2 M. Correa, U.S. Navy, via Wikipedia:HMCS Mackenzie. Data courtesy of the Canadian Hydrographic Service.

Figure 10 shows the water column image of a ping over the wreck of HMCS Mackenzie. It illustrates many of the effects observed in the simulations and shows how the different beamformers perform on complicated scenes. Wrecks are also often targets of particular interest and are cases where the water column image may be needed to supplement the bathymetric detections (Wyllie, Weber, & Armstrong, 2015).

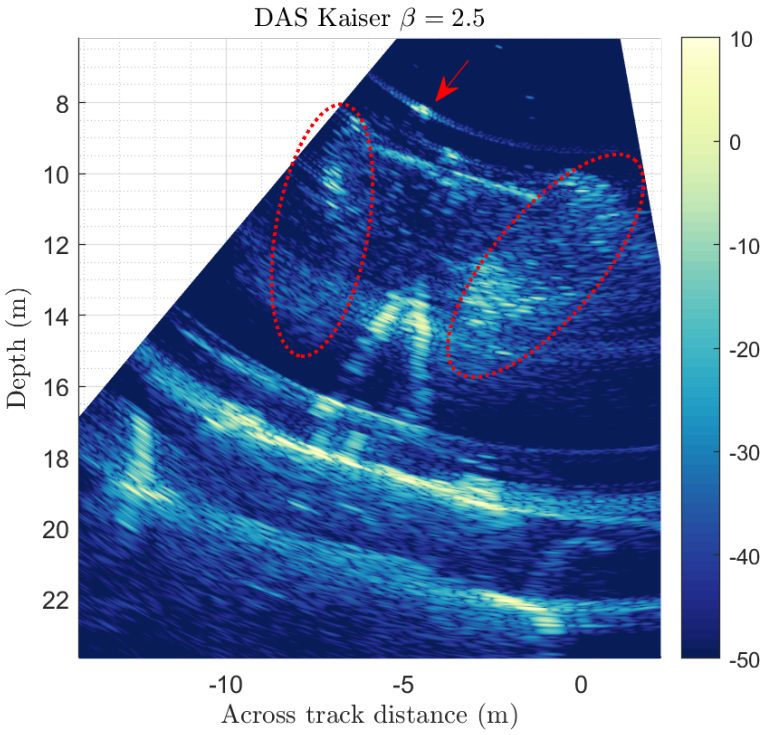

(b)

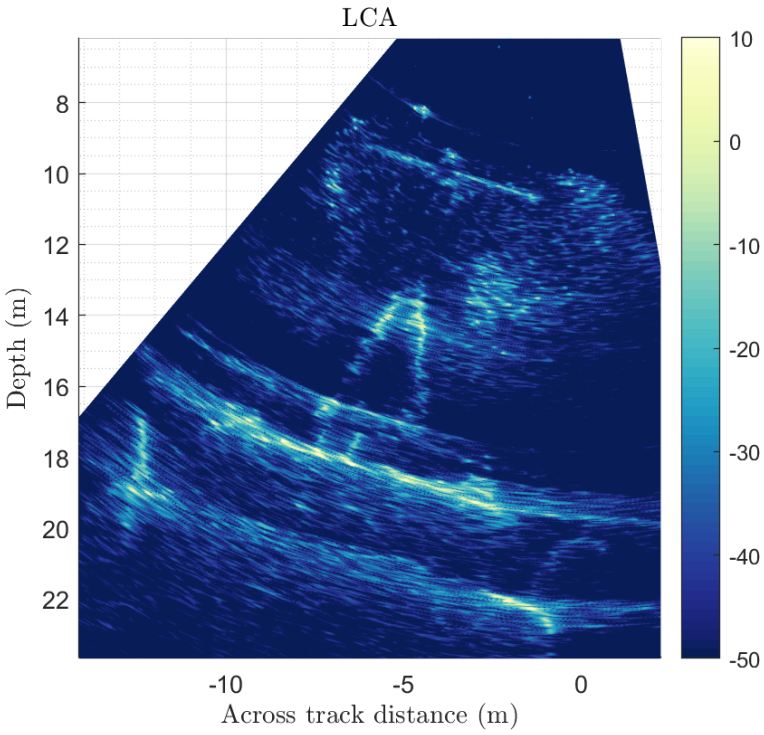

(c)

Figure 10: (Part 2 of 3) Caption with part 1.

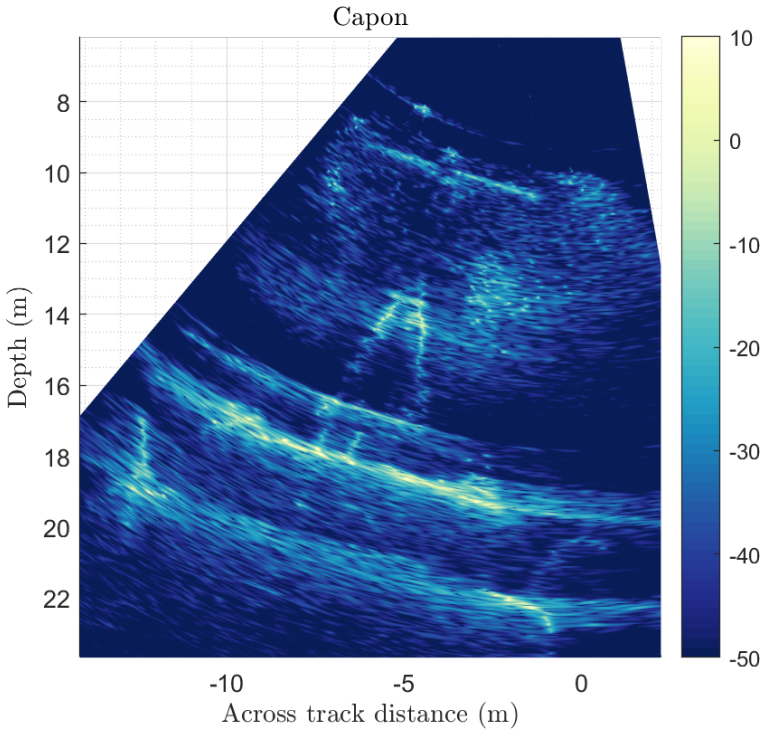

(d)

Figure 10: (Part 3 of 3) Caption with part 1.

In contrast to the simulated water column plots, Figure 10 is not averaged, and therefore shows speckle effects. The ping shows parts of the rear mast, deck and presumably a davit. The wreck is surrounded by what we expect to be marine organisms, particularly in the regions marked by the dotted red ellipses.

The adaptive beamformers reduce the apparent width for many features in the water column down to more realistic dimensions. This effect is largest for features with limited angular extent, like the davit. The difference in apparent thickness for the deck is much smaller.

The sidelobe level is reduced by the adaptive beamformers as for the simulated data. For example, at both sides of the deck and around the point-like features indicated by a red arrow in the DAS plot of Figure 10.

The appearance of the marine organisms is similar with DAS and Capon, although Capon has more well-defined points. It appears somewhat patchier and has a lower average level with LCA.

5.2 Smooth seafloor with boulder

Figure 11 shows excerpts of the water column image over a smooth seafloor with a boulder and accompanying amplitude detections. The few point targets in the water column are expected to be fish.

As before we see lower sidelobes and a thinner apparent seafloor for the adaptive beamformers. The apparent size of the fish is reduced, and they are better separated from the background.

The detections for the adaptive beamformers form a smoother curve than the detections from DAS, especially at larger across track distances. Figure 12 shows a sun-illuminated view of the detections around this ping. It shows that the smoother curve manifests as less noisy bathymetry for the adaptive beamformers.

The boulder appears to be better defined in the water column with the adaptive beamformers, and there are visible differences in the detections shown in Figure 11 and 12. However, without ground truth we cannot reliably decide which beamformer is the most accurate.

6 Discussion

First we connect the results to the properties we saw in section 2.5. Then we discuss the consequences of the improvements.

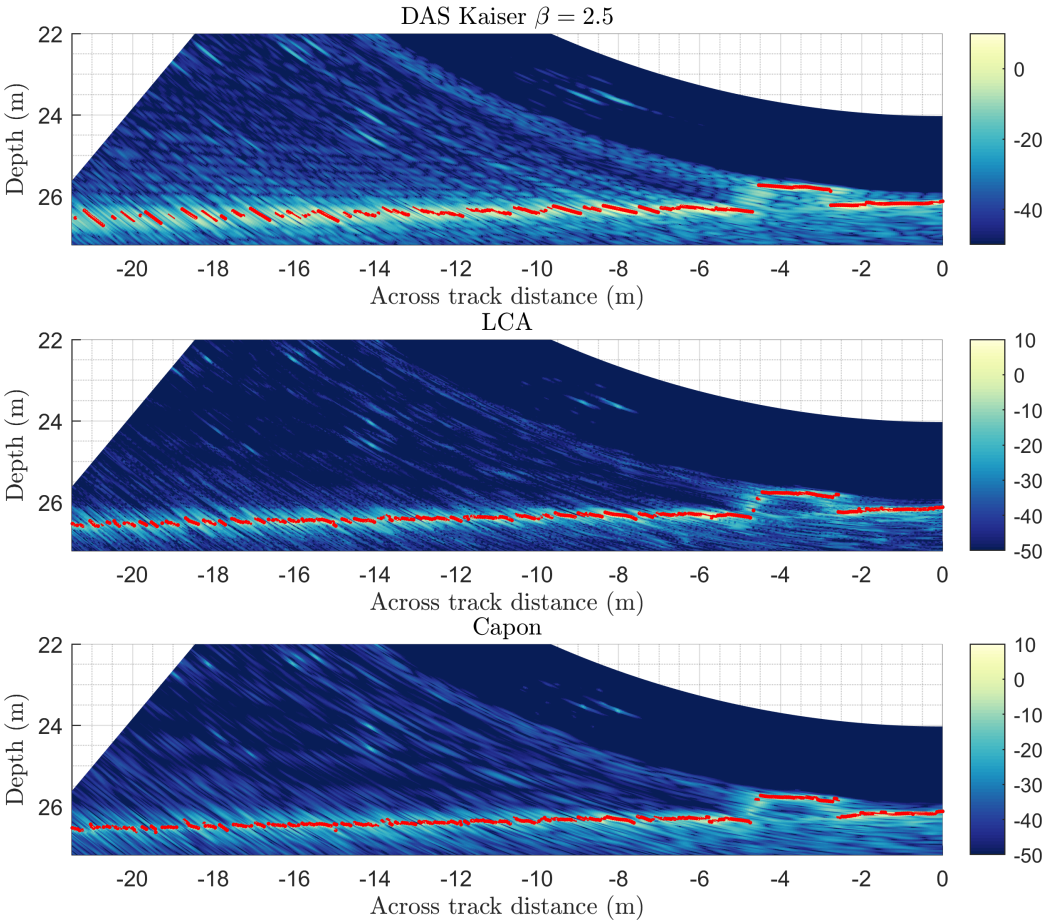

Figure 11: Water column power (dB), one ping over a boulder with presumed fish in water column. Red dots are amplitude bottom detections. Absolute power level is arbitrary. Field data courtesy of the Canadian Hydrographic Service.

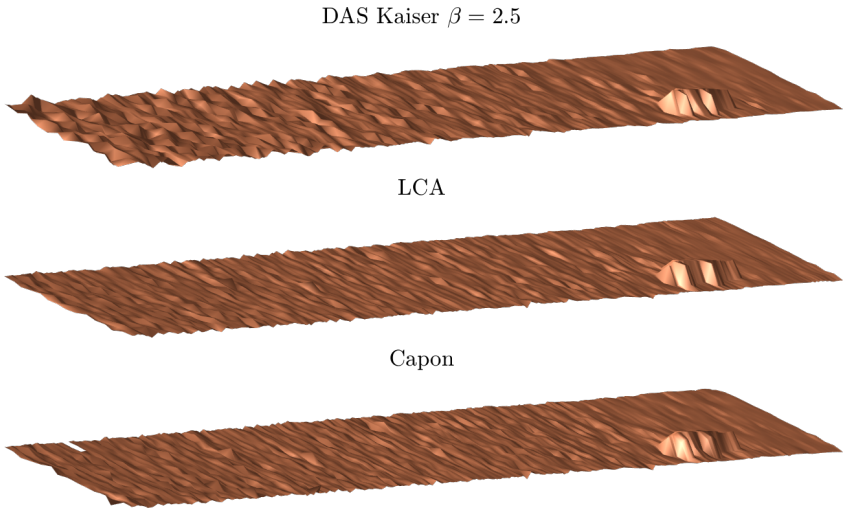

Figure 12: Sun-illuminated bathymetry of boulder area. Correspond to data from 15 pings with steering angles between $0°$ and $40°$. Vessel track is along the short edge to the right. Mean depth is 26.3 m. Plot made by stacking detections along-track based on the ship's average speed, disregarding other vessel motion. Weather during data collection was calm. One clear outlier has been removed for Capon. Field data courtesy of the Canadian Hydrographic Service.

6.1 Edge definition

The narrowing of the seafloor with the adaptive beamformers is largely due to edge definition improvements. At the highest steering angles in Figure 5a the pulse illuminates only a small area compared to the beamwidth. For each instant, the received signal is like the edge definition example in Figure 3, and the smaller effective beamwidth of the adaptive beamformers narrows the apparent seafloor width by a large amount. For normal incidence, the pulse length determines the length of the echo, and therefore also the apparent seafloor thickness (Lurton, 2010, Ch. 8.3.3). As the adaptive beamformers operate in the across track angular domain, they cannot improve this, and the performance is similar to DAS. The gradually growing advantage of the adaptive beamformers follows from the continuous transitions between these two extremes. A couple of deviations from the gradual trend are due to resolution. These are discussed in the next section.

The extent of the narrowing oscillates in Figure 7a since the effect described above for Figure 5a is linked to the incidence angle, not the steering angle. The sinusoidal shape changes the incidence angle and therefore the narrowing by the adaptive beamformers. Similar arguments explain most of the narrowing in the

remaining examples.

The amplitude detection accuracy is determined by the envelope length after processing (Section 2.4). Since the apparent seafloor is narrower, the envelope is shorter, and the RMSE is improved. Consequently, the scale of the RMSE improvement follows the extent of the narrowing in the water column.

The shorter envelopes also imply more independent amplitude detections, and therefore better bathymetric resolution. This is because shorter envelopes mean smaller footprints of the detection windows, and consequently shorter separation until a detection with no common footprint can be formed.

The adaptive beamformers also improve the edge definition of detected objects. This can be seen by the faster transitions of the mean value and narrower RMSE peaks in Figure 5b.

As microsteering is the main contributor to edge definition for LCA, microsteered weights are essential for the improved performance.

6.2 Resolution

Resolution has the largest influence at the most distant step in Figure 5, where the seafloor segments are relatively close compared to the beamwidth. The cross section in Figure 6 shows that LCA resolves the segments slightly better than DAS, while Capon resolves them much better. With the results from the previous section, we have verified that LCA has edge definition similar to Capon and resolution similar to DAS, as observed in Figure 3.

Figure 5b shows that this causes higher RMSE for LCA. The extra flexibility allows Capon to largely suppress the echo from the interfering seafloor segment, without major changes in performance.

In a similar way, we expect resolution effects to explain the slight rise in RMSE for LCA around the step at 30° steering angle, and the better bias and RMSE for Capon near nadir in Figure 8b.

6.3 Sidelobe level

Water column images from both simulated and field data show that the adaptive beamformers lower the sidelobe level compared to DAS. Since the adaptive beamformers simultaneously improve resolution and edge definition, it means that they avoid the tradeoff of DAS.

The sidelobe levels for all beamformers appear worse in the field examples than the simulated examples. One cause of this difference is that the field water column image has not been averaged, therefore we see the peaks instead of the average level. We believe model mismatch is the dominant factor for the remaining difference. This will limit the achievable sidelobe level for LCA and Capon.

6.4 Significance of the improvements

Figure 8a and Figure 9 show that the adaptive beamformers may reveal seabed and water column features that are hidden or barely visible with the DAS beamformer. As seafloor features of interest often are at the limit of achievable resolution (Clarke, 2018) this can increase the areas available for surface surveys. It may provide more information from each survey or, in edge cases, reduce the need for expensive AUV or ROV surveys.

For the general case, the better defined features and the lower sidelobes of the adaptive beamformers will ease the interpretation of the image. This includes localizing features, estimating sizes and separating real features from artifacts.

The observed improvements in RMSE show that the adaptive beamformers may improve amplitude detection accuracy significantly compared to DAS. This does not matter if other error sources like transducer alignment dominate (Clarke, 2003; Hare, 1995). However, for a well aligned and integrated system, detector accuracy matters (Clarke, 2018). The accuracy gain in practice will also be limited by phase detection accuracy, when applicable.

Since the RMSE improvements are larger at higher angles, we expect larger gains in accuracy for cases where the amplitude-phase detection transition happens at high angles. An expected effect of this is that the peak depth uncertainty, typically occurring at the transition (Lurton & Augustin, 2010), is reduced.

The highest potential for improvements is after the transition angle in cases where the phase detector fails. Both since the RMSE differences are larger at higher angles, and since this tends to happen at objects which may be more interesting. In these cases, like in section 4.1, the adaptive beamformers may reduce the RMSE greatly and resolve the object(s) better. If the DAS amplitude detection uncertainty would be too high, the detections may be rejected. For those cases, the adaptive beamformers may prevent missing data. Note that other solutions to the missing data problem have been proposed (Kraeutner & Bird, 1999; Pereira & Clarke, 2015).

Since the amplitude detection accuracy is improved, this must be accounted for when modelling the bathymetric uncertainty (Hare, 2001; Mohammadloo, Snellen, & Simons, 2018). For DAS the beamwidth is central for modeling the amplitude detection uncertainty (Hare, 2001; Lurton, 2003). For the adaptive beamformers the effective beamwidth and other parameters change depending on the received signal. Modelling amplitude detection accuracy for adaptive beamformers will therefore be more complex and need to account for new factors, which are out of scope for this paper. However, due to the simple signal condition, the edge definition example in Figure 3 should show the best-case effective beamwidth for the adaptive beamformers. A best-case accuracy estimate may therefore be calculated by using the effective beamwidth from such a case in the existing modelling methods.

The lower sidelobe level should reduce the frequency of false detections.

LCA and Capon show similar performance improvements in the field as in the simulations. This suggests that they are robust enough for practical use. However, the lower sidelobe level improvement in the field indicates that reducing model mismatch, e.g. via calibration, may enable further improvements.

The adaptive beamformers operate across track and thus do not improve along track density, which may be a limiting factor for object detection (Clarke, 2018).

6.5 A note about backscatter

Backscatter processing relies on a number of corrections tailored to the DAS beamformer (Lurton & Lamarche, 2015). The adaptive beamformers may change backscatter statistics (Li & Stoica, 1996; Synnevåg et al., 2011) and may therefore require different processing. Existing backscatter performance can be preserved by continuing to use DAS for backscatter, restricting LCA and Capon to bathymetry and water column imagery. This is particularly easy with LCA, since the required DAS beams are computed as part of the LCA computation.

7 Conclusions

In this work, we have considered three different beamformers for swath sonar processing: the traditional delay-and-sum (DAS) beamformer, the Low Complexity Adaptive (LCA) beamformer; and the adaptive Capon beamformer. We have found that the adaptive beamformers LCA and Capon improve amplitude bottom detection accuracy and water column imaging for swath sonars compared to the

Table 3: Summary of observed performance for the adaptive beamformers LCA and Capon versus weighted DAS (Kaiser $\beta = 2.5$).

	Performance vs DAS	
Property	LCA	Capon
Resolution	Better	Much better
Edge definition	Much better	Much better
Sidelobe level	Better	Better
Amplitude detection accuracy		
– near specular	Similar/Better	Similar/Better
– far from specular	Much better	Much better
– around objects	Much better	Much better
Computational load	Higher	Much higher
Implementation complexity	Higher	Much higher
Phase detection accuracy	Further study needed	
Backscatter	Further study needed	

traditional DAS beamformer. Table 3 summarizes the most important properties for the three beamformers.

LCA and Capon improve the resolution and edge definition of features in the water column, both in simulated and field data, while simultaneously reducing the sidelobe level. This can allow the adaptive beamformers to reveal features hidden for DAS. Edge definition causes most of the improvements, with similar performance for both LCA and Capon. This means that high levels of micro-steering are very important for LCA performance. Capon has the best resolution. The adaptive beamformers effectively reduce the angular extent of many water column features to a more realistic size. The extent of the improvement depends on the effect of reducing the beamwidth.

The narrower features in the water column give shorter detection envelopes for the adaptive beamformers, which improve amplitude detection accuracy and resolution. We expect this to be a net benefit from near nadir until the extended phase detection transition, and when phase detections fail. In the latter case, the adaptive beamformers may prevent holes in the bathymetric data.

Capon's better performance compared to LCA comes at the cost of a higher computational load and implementation complexity. Existing backscatter and phase detection performance can be preserved by running the current DAS beamformer in parallel with the adaptive beamformer.

Acknowledgments

We thank the staff at the Center for Coastal and Ocean Mapping/Joint Hydrographic Center at the University of New Hampshire for support and many insightful discussions during and after the first author's research visit. Special thanks to A. Lyons, J.H. Clarke, G. Rice, T. Weber, G. Masetti and V. Schmidt. J.H. Clarke was central for acquiring the field data for this paper. G. Rice provided the Pydro par.py module which was helpful during data processing (Rice, 2017). We also thank Kongsberg Maritime AS for assistance and feedback, and acknowledge the helpful comments from the reviewers. We thank the Canadian Hydrographic Service for the use of field data.

References

Åsen, J. P., Austeng, A., & Holm, S. (2014). Capon beamforming and moving objects-an analysis of lateral shift-invariance. *IEEE Transactions on Ultrasonics, Ferroelectrics, and Frequency Control*, *61*(7), 1152–1160. doi:10.1109/TUFFC.2014.3014

Austeng, A., Bjastad, T., Synnevåg, J.-F., Masoy, S.-E., Torp, H., & Holm, S. (2008). Sensitivity of minimum variance beamforming to tissue aberrations. In *IEEE Ultrasonics Symposium 2008*. doi:10.1109/ultsym.2008.0258

Blomberg, A. E. A., Austeng, A., & Hansen, R. E. (2012). Adaptive Beamforming Applied to a Cylindrical Sonar Array Using an Interpolated Array Transformation. *IEEE Journal of Oceanic Engineering*, *37*(1), 25–34. doi:10.1109/JOE.2011.2169611

Blomberg., A. E. A., Austeng, A., Hansen, R., & Synnes, S. (2013). Improving Sonar Performance in Shallow Water Using Adaptive Beamforming. *IEEE Journal of Oceanic Engineering*, *38*(2), 297–307. doi:10.1109/JOE.2012.2226643

Buskenes, J. I., Hansen, R. E., & Austeng, A. (2017). Low Complexity Adaptive Sonar Imaging. *IEEE Journal of Oceanic Engineering*, *42*(1). doi:10.1109/JOE.2016.2565038

Carlson, B. (1988). Covariance matrix estimation errors and diagonal loading in adaptive arrays. *IEEE Transactions on Aerospace and Electronic Systems*, *24*(4), 397–401. doi:10.1109/7.7181

Clarke, J. E. H. (2003). Dynamic Motion and Residuals in Swath and Sonar Data: Ironing out the Creases. *International Hydrographic Review*, *4*(1), 6–23. url: https://journals.lib.unb.ca/index.php/ihr/article/view/20600

Clarke, J. E. H. (2006). Applications of multibeam water column imaging for hydrographic survey. *The Hydrographic Journal*, *120*, 3–15. url: http://www.omg.unb.ca/omg/papers/HJ_water_column_JHC.pdf

Clarke, J. E. H. (2017). Coherent refraction "noise" in multibeam data due to oceanographic turbulence. In *Proceedings of the U.S. Hydrographic Conference 2017*, Galveston, Texas, USA.

Clarke, J. E. H. (2018). The Impact of Acoustic Imaging Geometry on the Fidelity of Seabed Bathymetric Models. *Geosciences*, *8*(4), 109. doi:10.3390/geosciences8040109

Cox, H. (1973). Resolving power and sensitivity to mismatch of optimum array processors. *The Journal of the Acoustical Society of America*, *54*(3), 771–785. doi:10.1121/1.1913659

Cox, H., Zeskind, R. M., & Owen, M. M. (1987). Robust adaptive beamforming. *IEEE Transactions on Acoustics, Speech and Signal Processing*, *35*(10), 1365–1376. doi:10.1109/TASSP.1987.1165054

Hare, R. (1995). Depth and Position Error Budgets for Multibeam Echosounding. *The International Hydrographic Review*, *72*(2), 37–69.

Hare, R. (2001). *Error Budget Analysis for US Naval Oceanographic Office (NAVOCEANO) Hydrographic Survey Systems*. University of Southern Mississippi, Hydrographic Science Research Center (HSRC). Final Report for Task 2, FY 01.

Hare, R., Godin, A., & Mayer, L. (1995). *Accuracy estimation of Canadian Swath (multibeam) and Sweep (multi-transducer) sounding systems*. Canadian Hydrographic Service.

Harris, F. (1978). On the use of windows for harmonic analysis with the discrete Fourier transform. *Proceedings of the IEEE*, *66*(1), 51–83. doi:10.1109/PROC.1978.10837

Jensen, J. A. (1996). Field: A Program for Simulating Ultrasound Systems. In *Medical & Biological Engineering & Computing* (Vol. 34, pp. 351–353). url: http://field-ii.dk/documents/jaj_nbc_1996.pdf

Jensen, J. A., & Svendsen, N. B. (1992). Calculation of pressure fields from arbitrarily shaped, apodized, and excited ultrasound transducers. *IEEE Transactions on Ultrasonics, Ferroelectrics, and Frequency Control*, *39*(2), 262–267. doi:10.1109/58.139123

Johnson, D. H., & Dudgeon, D. E. (1993). *Array signal processing: Concepts and techniques*. Prentice Hall.

Kraeutner, P. H., & Bird, J. S. (1999). Beyond interferometry, resolving multiple angles-of-arrival in swath bathymetric imaging. In *Proc. OCEANS '99 MTS/IEEE. Riding the Crest into the 21st Century* (Vol. 1, 37–45 vol.1). doi:10.1109/OCEANS.1999.799704

Krim, H., & Viberg, M. (1996). Two decades of array signal processing research: the parametric approach. *IEEE Signal Processing Magazine*, *13*(4), 67–94. doi:10.1109/79.526899

Krolik, J., & Swingler, D. (1989). Multiple broad-band source location using steered covariance matrices. *IEEE Transactions on Acoustics, Speech, and Signal Processing*, *37*(10), 1481–1494. doi:10.1109/29.35386

Lamarche, G., & Lurton, X. (2018). Introduction to the Special Issue "Seafloor backscatter data from swath mapping echosounders: from technological development to novel applications". *Marine Geophysical Research*, *39*(1-2), 1–3. doi:10.1007/s11001-018-9349-4

Li, J., & Stoica, P. (1996). An adaptive filtering approach to spectral estimation and SAR imaging. *IEEE Transactions on Signal Processing*, *44*(6), 1469–1484. doi:10.1109/78.506612

Li, J., Stoica, P., & Wang, Z. (2003). On robust Capon beamforming and diagonal loading. *IEEE Transactions on Signal Processing*, *51*(7), 1702–1715. doi:10.1109/TSP.2003.812831

Llort-Pujol, G., Sintes, C., Chonavel, T., Morrison, A. T., & Daniel, S. (2012). Advanced Interferometric Techniques for High-Resolution Bathymetry. *Marine Technology Society Journal*, *46*(2), 9–31. doi:10.4031/mtsj.46.2.4

Lo, K. (2004). Adaptive Array Processing for Wide-Band Active Sonars. *IEEE Journal of Oceanic Engineering*, *29*(3), 837–846. doi:10.1109/joe.2004.833096

Lønmo, T. I. B., Austeng, A., & Hansen, R. E. (2015a). Interference rejection by Low Complexity Adaptive Beamforming. In *Proceedings of the Institute of Acoustics* (Vol. 37). Institute of Acoustics, Bath, United Kingdom. url: http://www.proceedings.com/27961.html

Lønmo, T. I. B., Austeng, A., & Hansen, R. E. (2015b). Low Complexity Adaptive Beamforming Applied to Sonar Imaging (Invited). In J. S. Papadakis & L. Bjørnø (Eds.), *Proceedings of the 3rd International Conference and Exhibition on Underwater Acoustics* (pp. 653–658). Crete, Greece. url: http://www.uaconferences.org/docs/Past_proceedings/UACE2015_Proceedings.pdf

Lurton, X. (2003). Theoretical Modelling of Acoustical Measurement Accuracy for Swath Bathymetric Sonars. *International Hydrographic Review*, *4*(2), 17–30. New Series. url: https://journals.lib.unb.ca/index.php/ihr/issue/view/1555

Lurton, X. (2010). *An Introduction to Underwater Acoustics: Principles and Applications* (2nd ed.). Springer-Verlag Berlin Heidelberg.

Lurton, X., & Augustin, J.-M. (2010). A Measurement Quality Factor for Swath Bathymetry Sounders. *IEEE Journal of Oceanic Engineering*, *35*(4), 852–862. doi:10.1109/JOE.2010.2064391

Lurton, X., & Lamarche, G. (Eds.). (2015). *Backscatter measurements by seafloor-mapping sonars: Guidelines and Recommendations*. GeoHab Backscatter Working Group. url: http://geohab.org/wp-content/uploads/2013/02/BWSG-REPORT-MAY2015.pdf

Mayer, L., Jakobsson, M., Allen, G., Dorschel, B., Falconer, R., Ferrini, V., … Weatherall, P. (2018). The Nippon Foundation—GEBCO Seabed 2030 Project: The Quest to See the World's Oceans Completely Mapped by 2030. *Geosciences*, *8*(2), 63. doi:10.3390/geosciences8020063

Mitchley, M., & Sears, M. (2014). Searching for seafloor massive sulfides: A quantitative review of high-resolution methods in deep sea sonar bathymetry for mining applications. *Marine Geophysical Research*, *35*(2), 157–174. doi:10.1007/s11001-014-9219-7

Mohammadloo, T. H., Snellen, M., & Simons, D. G. (2018). Multi-beam echosounder bathymetric measurements: Implications of using frequency modulated pulses. *The Journal of the Acoustical Society of America*, *144*(2), 842–860. doi:10.1121/1.5050816

Pantzartzis, D., de Moustier, C., & Alexandrou, D. (1993). Application of high-resolution beamforming to multibeam swath bathymetry. In *Proc. OCEANS '93* (Vol. 2, pp. 77–82). doi:10.1109/OCEANS.1993.326070

Pereira, D. L. d. S., & Clarke, J. E. H. (2015). Improving shallow water multibeam target detection at low grazing angles. In *U.S. Hydrographic Conference 2015*, National Harbor, Maryland U.S.A. url: http://www.omg.unb.ca/omg/papers/DouglasPereira_and_JHC_USHC2015_Paper.pdf

Rao, B. D., & Hari, K. V. S. (1990). Effect of spatial smoothing on the performance of MUSIC and the minimum-norm method. *IEE Proceedings (F-Radar and Signal Processing)*, *137*(6), 449–458. doi:10.1049/ip-f-2.1990.0065

Rice, G. (2017). Pydro par.py module V0.3.8. Computer software. Available from https://nauticalcharts.noaa.gov/data/tools-apps.html.

Rønhovde, A., Yang, L., Taxt, T., & Holm, S. (1999). High-resolution beamforming for multibeam echo sounders using raw EM3000 data. In *OCEANS '99 MTS/IEEE. Riding the Crest into the 21st Century* (Vol. 2, pp. 923–930). doi:10.1109/OCEANS.1999.804997

Shan, T.-J., Wax, M., & Kailath, T. (1985). On spatial smoothing for direction-of-arrival estimation of coherent signals. *IEEE Transactions on Acoustics, Speech and Signal Processing*, *33*(4), 806–811. doi:10.1109/TASSP.1985.1164649

Steinberg, B. D. (1976). *Principles of aperture and array system design: Including random and adaptive arrays*. John Wiley & Sons.

Synnevåg, J.-F., Austeng, A., & Holm, S. (2007). Adaptive Beamforming Applied to Medical Ultrasound Imaging. *IEEE Transactions on Ultrasonics, Ferroelectrics, and Frequency Control*, *54*(8), 1606–1613. doi:10.1109/TUFFC.2007.431

Synnevåg, J.-F., Austeng, A., & Holm, S. (2009). Benefits of minimum-variance beamforming in medical ultrasound imaging. *IEEE Transactions on Ultrasonics, Ferroelectrics, and Frequency Control*, *56*(9), 1868–1879. doi:10.1109/TUFFC.2009.1263

Synnevåg, J.-F., Austeng, A., & Holm, S. (2011). A low-complexity data-dependent beamformer. *IEEE Transactions on Ultrasonics, Ferroelectrics and Frequency Control*, *58*(2), 281–289. doi:10.1109/TUFFC.2011.1805

Van Trees, H. L. (2002). *Optimum Array Processing*. Wiley-Interscience.

Wyllie, K., Weber, T. C., & Armstrong, A. (2015). Using multibeam echosounders for hydrographic surveying in the water column: Estimating wreck least depths. In *Proceedings of the US Hydrographic Conference*, National Harbor, MD: International Hydrographic Organization. url: https://scholars.unh.edu/ccom/17/